

DELIVERY AND ACTIVATION OF CONTRAST AGENTS FOR MAGNETIC
RESONANCE IMAGING

Thesis by

Matthew John Allen

In Partial Fulfillment of the Requirements

For the Degree of

Doctor of Philosophy

California Institute of Technology

Pasadena, California

2004

(Defended December 9, 2003)

© 2004

Matthew John Allen

All Rights Reserved

This thesis is dedicated to my Mom for being my first and greatest teacher. She taught me by example to never stop learning and showed me the true importance of family. A source of unconditional and perpetual love and support, I am deeply sorrowed not to be able to share this experience with her.

In loving memory of Yvonne Theresa Allen

Acknowledgements

The work described in this thesis would not have been possible without help from many people. First, I thank my advisor, Tom Meade. Tom enabled me to follow my ideas wherever they led, even back and forth across the boundaries of chemistry and biology. His ability to provide space, funding, and intellectual support is surpassed only by his ceaseless positive perspective. There was rarely a conversation in his office that I didn't leave inspired and excited to further my research. Tom is an excellent writer, and the writing skills that I acquired from him are invaluable. I would especially like to thank Tom for being understanding of difficult family situations. If I had to start graduate school again, I would choose Tom as an advisor without hesitation.

My second advisor, Scott Fraser, gave me numerous valuable suggestions during our discussions. I appreciate all of the reference letters you wrote for me. Thank you to the rest of my committee: John Bercaw, John Richards, and Harry Gray. It has been an honor to have such a renowned group of scientists on my committee.

Thanks to everyone in the Meade group for never letting my graduate career become dull. Your ideas, support, and suggestions are greatly appreciated. Thanks to everyone who proofread my thesis chapters: Joe Duimstra, Amanda Eckerman, Frank Femia, Ellen Kohlmeier, Jody Major, Elise Schultz, and Brad Ulrich. I am grateful to everyone who housed me during my homeless week—Frank, Keith MacRenaris, and Lauren Urbanczyk. Lauren, you definitely have the nicest couch. Many of the cell experiments described in this thesis would not have been possible without the help of Keith MacRenaris. I won't forget the common-law members of A+ office—Keith and Paul Lee. You guys provided non-stop entertainment in the form of witty and not-so-

witty conversation. Thank you, Jiyoun Lee, for introducing me to ham-n-jam sandwiches. My experiences would not have been as meaningful without the other members of the Meade group: Kylie Barker, Steve Bull, Paul Enders, Ying Song, Alisha Taylor, and Peijiao Wang.

Several good friends have left the Meade group during my tenure. Angie Louie taught me cell culture techniques and constructively critiqued my writing. I thank Brian Johnson for the tour of Heidelberg, our extreme bouts with nature, and the many trips to AM/PM. I'm glad you didn't die in the desert. Carlo Quinonez gave me many good ideas and suggestions in the lab and memorable trips to Tijuana. I thank Jeremiah Miller for innumerable good times including swimming, lifting weights, and trips to Pat's Liquor store. My experience would not have been the same without J. C. Olsen, Jeff Smith, and C. J. Yu.

Many friends outside of the Meade group have enriched my academic and social well-being. Thanks to Dr. Tongyou Ji and P.N. Venkatasubramanian (Venkat) at the Northwestern Research Park for many helpful suggestions and magnet time. I thank Susan Schofer for countless running of the five-mile loop. My friends Lily Ackerman, Chip Kent, and Libby Mayo greatly enriched my time at Caltech. Thank you to everyone at the biological imaging center for your support and suggestions. I thank David Koos for his help with two-photon laser microscopy and Brent Segal for his helpful tips on solid-phase synthesis. Without the organizational miracles achieved by Mary Flowers on a daily basis, research in the imaging center would come to a grinding halt. Thanks to Ben Vesper for cell-sitting and Dianne de Haseth for helping me navigate the Northwestern administration. It would be impossible for anyone to graduate without

Dian Buchness, who deserves special thanks, particularly for helping me while on detached duty.

Importantly, I thank my family who are always a constant source of support. My parents, John and Yvonne, and brother, Chris, were always there for me, whether I needed help moving, a visit from a familiar face, or a phone call. My in-laws, Al and Judy Kelsch, gave me an occasional quiet escape with very good food. I especially thank my wife, Carrie, who is my best friend. She helped me through difficult times and made good times even better.

Abstract

Magnetic Resonance Imaging (MRI) has become a powerful tool for noninvasive imaging of living specimens. Magnetic resonance contrast agents containing the paramagnetic ion gadolinium(III) are used to enhance regions, tissues, and cells that are magnetically similar but histologically distinct. To increase the effectiveness of contrast agents, agents responsive to biological phenomena and directed to specific regions need to be developed. These two improvements are related in that many biologically significant molecules are located in specific locations. Therefore, the design, synthesis, and testing of advanced contrast agents are described.

Many interesting biological targets for imaging reside inside the cell membrane. As the current generation of contrast agents is strictly extracellular, a method of intracellular delivery is required in the development of MRI contrast agents. I have developed cationic, polyarginine-oligomers to deliver gadolinium(III)-based contrast agents into the interior of cells. Delivery was confirmed and studied using methods including inductively coupled plasma-mass spectrometry, MRI, and two-photon laser microscopy to image lanthanide-based MRI contrast agents.

A second approach focused on the synthesis of a series of contrast agents designed to cross the blood brain barrier and label A β -plaques associated with Alzheimer's disease. These agents were found to permeate cell membranes, and the intracellular properties of these agents are compared to the polyarginine agents. Finally, attempts towards the creation of an advanced MRI contrast agent that is chemically activated by matrix metalloproteinases are described.

Table of Contents

Acknowledgements	iv
Abstract	vii
Table of Contents	viii
List of Figures, Schemes, and Tables	xiii
Abbreviations	xx
Chapter 1: Introduction	1
I. Introduction	2
A. Magnetic Resonance Imaging and Nuclear Spin Relaxation Processes	2
B. Classes of Contrast Agents	14
II. Contrast Agents for Diagnosis	15
A. Cancer	15
1. Gadolinium(III) DTPA and Its Derivatives	15
2. Manganese(II) and Iron Oxide Agents	19
B. Non-Cancer Diseases	20
1. Blood Pool-Related Diseases	20
2. Diseases of the Gastrointestinal Tract	22
3. Skeletal System Diagnosis	22
4. Other Diseases	23
III. Targeted Delivery of Contrast Agents	24
A. Contrast Agent Delivery	24
1. Gadolinium(III)-Containing Agents	24
2. Iron Oxide Agents	25

B.	Penetrating the Blood Brain Barrier	26
IV.	Imaging Biochemical Events	26
A.	Enzymatically Activated Contrast Agents	27
B.	Contrast Agents to Detect Biologically Significant Molecules	32
C.	pH Sensitive Agents	42
V.	Conclusions and Outlook	50
VI.	Scope of Thesis	50
VII.	References	53
Chapter 2: Synthesis, Visualization, and Delivery Properties of Polyarginine-		
Labeled Magnetic Resonance Imaging Contrast Agents		64
I.	Introduction	65
II.	Results	67
A.	Synthesis and Physical Characterization	67
B.	Cell Studies	72
1.	Proliferation and Viability Assays	72
2.	Two-Photon Laser Microscopy	73
3.	T_1 Studies	75
4.	Concentration Effects	77
5.	Incubation Time	79
6.	Washout Studies	79
7.	Cell Type Specificity	81
C.	MR Imaging	83

III.	Discussion	86
	A. Physical Characterization	86
	B. Cell Studies	87
	1. Proliferation and Viability Assays	87
	2. Two-Photon Laser Microscopy	87
	3. T_1 Studies	90
	4. Concentration Effects	91
	5. Incubation Time and Washout Studies	93
	6. Cell Type Specificity	94
	C. MR Imaging	94
IV.	Conclusion	94
V.	Experimental Procedures	95
VI.	References	103
Chapter 3: An MR Contrast Agent to Cross Cell Membranes, the Blood Brain		
	Barrier, and Label A β Plaques	106
I.	Introduction	107
II.	Results	111
	A. Synthesis	111
	B. Partition Coefficients	111
	C. Relaxivities	114
	D. UV-Visible and Fluorescence Spectroscopy	114
	1. UV-Visible Absorption	114

2. Fluorescence Spectroscopy	114
E. Dynamic Light Scattering	118
F. Cell Studies	119
1. Viability Assays	119
2. Concentration Effects	119
3. Incubation Time	123
4. Washout Studies	123
5. Blood Brain Barrier Model	126
G. Brain Slices	129
III. Discussion	132
A. Synthesis and Physical Properties	132
1. Relaxivities	133
2. Aggregate Sizing	134
3. UV-Visible and Fluorescence Spectroscopy	138
B. Cell Studies	139
1. Viability Assays	139
2. Concentration Effects	139
3. Incubation Time and Washout Studies	140
4. Blood Brain Barrier Model	140
C. Comparison with Polyarginine Cell Culture Properties	142
D. Brain Slices	143
IV. Conclusion	144
V. Future Work	144

VI.	Experimental Procedures	146
VII.	References	151
Chapter 4: Towards a Matrix Metalloproteinase Sensitive Contrast Agent		154
I.	Introduction	155
II.	Results and Discussion	157
	A. Design and Synthesis	157
	B. Determination of q Values	162
	C. Aspartic Acid Model Complexes	164
	D. Proposed Binding of Amide Carbonyl	169
III.	Conclusion	172
IV.	Future Directions	172
V.	Experimental Procedures	174
VI.	References	182

List of Figures

Figure 1.1	Schematic of hydrogen nuclei before and after being placed in a magnetic field \mathbf{B}_0 . Top: Nuclei are randomly oriented before exposure to \mathbf{B}_0 , then align with and precess about \mathbf{B}_0 at the Larmor frequency, ω_L , after placement in \mathbf{B}_0 . Bottom: Slightly more spins occupy the lower energy state leading to a net magnetization vector, \mathbf{M} .	4
Figure 1.2	Schematic depicting the behavior of the net magnetization vector, \mathbf{M} , upon exposure to an RF pulse. The RF pulse generates a magnetic field \mathbf{B}_1 that causes \mathbf{M} to flip away from the z -axis and revolve about \mathbf{B}_0 in an xy -plane.	5
Figure 1.3	MRI images of the brain: (a) T_1 -weighted image; (b) proton-density weighted image; (c) T_2 -weighted image. Image reproduced with permission from Reference 1.	8
Figure 1.4	Positive-contrast enhancement in a brain lesion obtained by using a T_1 -weighted sequence and a T_1 contrast agent: (a) pre-contrast; (b) post-contrast—the bright ring is the area enhanced with contrast agent. Image reproduced with permission from Reference 1.	9
Figure 1.5	Schematic depicting the interactions of water molecules with a gadolinium(III) based contrast agent. The five variables shown have an influence on r_1 .	13
Figure 1.6	Common MRI ligands used to coordinate paramagnetic metal ions.	16
Figure 1.7	MRI contrast agent activated by β -galactosidase.	29
Figure 1.8	DTPA-based carbonic anhydrase sensitive contrast agent (ligand only).	30
Figure 1.9	Contrast agent sensitive to TAFI.	31
Figure 1.10	Contrast agent that detects DNA cleaving agents.	33
Figure 1.11	CLIO-based contrast agent that is sensitive to the presence of proteases.	34
Figure 1.12	Contrast agents sensitive to the presence of iron ions.	35
Figure 1.13	Contrast agent sensitive to the presence of calcium(II).	37

Figure 1.14	Contrast agent that differentiates between oxygenated and deoxygenated hemoglobin (ligand only).	38
Figure 1.15	Contrast agent that detects specific DNA sequences.	40
Figure 1.16	Contrast agent specific for zinc(II).	41
Figure 1.17	CEST contrast agent (ligand only) sensitive to <i>L</i> -lactate.	43
Figure 1.18	Schematic representation of a liposome based radical-responsive MRI contrast agent.	44
Figure 1.19	Contrast agent sensitive to pH based on a polyion complex composed of a mixture of two polymers.	45
Figure 1.20	Contrast agent sensitive to pH based on a squaric ester containing polymer (ligand only).	46
Figure 1.21	Contrast agent sensitive to pH based on a phosphate containing DOTA derivative (ligand only).	48
Figure 1.22	Contrast agent sensitive to pH based on amphiphilic molecules (ligand only).	49
Figure 1.23	Contrast agent sensitive to pH based on CEST effects (ligand only).	51
Figure 2.1	Schematic of hypothesized mechanism of trans-membrane polyarginine delivery. Inset: Chemical structure of the putative bidentate hydrogen-bonding interacting proposed between the guanidine headgroup of arginine and the phosphates present in lipid bilayers.	68
Figure 2.2	Two-photon laser microscopy image ($\lambda_{EX} = 750$ nm) of NIH/3T3 cells, A: untreated control where signal is due to autofluorescence of the cells, B: cells incubated with 11 for one hour and rinsed prior to imaging, and C: cells incubated with 9 for one hour and rinsed prior to imaging.	74
Figure 2.3	Results of T_1 study of NIH/3T3 cells incubated with 0.3 mM 4 , 5 , 6 , and gadolinium(III) DO3A (1,4,7-tris-carboxymethyl-1,4,7,10-tetraazacyclododecane). After incubation cells were rinsed with DPBS. T_1 values were measured at 60 MHz and 37 °C. The graph depicts the percent change in T_1 from untreated NIH/3T3 cells. Error bars represent one standard deviation.	78

- Figure 2.4** Demonstration of the dependence of uptake of **4-6** on incubation concentration. After incubation, NIH/3T3 cells were rinsed with DPBS, treated with trypsin, dissolved in nitric acid, and analyzed with ICP-MS. The graphs show uptake per cell plotted against incubation concentration. Error bars represent one standard deviation. 80
- Figure 2.5** Washout rate of **4-6** from NIH/3T3 cells as a function of the number of rinses. Cells were incubated for one hour and then medium was changed. After each rinse period the medium was removed and analyzed using ICP-MS. Long incubation times were 24, 48, 72, and 96 hours. Short incubation times were 1, 3, 6, and 10 hours. Error bars represent one standard deviation. 82
- Figure 2.6** Cell type specificity for **7-9**. Cells were incubated with compound for one hour and rinsed with DPBS, treated with trypsin, dissolved in nitric acid, and analyzed with ICP-MS. The graph shows uptake per cell for each cell type plotted against complex. Incubation concentration of **7-9** was constant within each group of cells, but was not constant from compound to compound. Error bars represent one standard deviation. 84
- Figure 2.7** T_1 -weighted spin-echo MR images of NIH/3T3 cells at 9.4 T. Images were obtained using a spin-echo pulse sequence with TR 500 ms, echo delay time (TE) 16 ms: (A) NIH/3T3 cells incubated with **4**, (B) Untreated NIH/3T3 cells, (C) Deionized water in a capillary tube as a spatial marker. The scale bar represents 1.2 mm. 85
- Figure 2.8** Schematic demonstrating the difference between the absorption of one and two photons of light leading to fluorescence in single-photon or two-photon laser microscopy, respectively. 88
- Figure 2.9** Molecular orbital diagram for europium(III) and gadolinium(III) demonstrating the large energy difference needed to excite gadolinium(III) (273 nm) versus europium(III) (375 nm). Figure modified from reference 7. 89
- Figure 2.10** Schematic of ICP-MS: Liquid samples are sent through a nebulizer, atomized by the argon plasma, and detected using a mass spectrometry setup. 92

Figure 3.1	Chemical structures of compounds that bind to A β plaques: Congo Red, Chrysamine G, Thioflavin S, BSB, and styrylbenzenes.	110
Figure 3.2	Dianionic (1), monoanionic (2), and neutral (3) versions of the amyloid targeting MRI contrast agent.	112
Figure 3.3	Excitation and emission spectra for 1-3 .	117
Figure 3.4	A representative autocorrelation function from dynamic light scattering of 1 in MOPS buffer.	120
Figure 3.5	Dynamic light scattering results showing the size of aggregates at various concentrations in 10% Pluronic F-127 and MOPS buffer.	121
Figure 3.6	Dynamic light scattering results showing the size of aggregates at various concentrations in 10% Pluronic F-127.	122
Figure 3.7	Demonstration of the dependence of uptake of 1 on incubation concentration. After incubation, NIH/3T3 cells were rinsed with DPBS, treated with trypsin, dissolved in nitric acid, and analyzed with ICP-MS. The graph shows uptake per cell plotted against incubation concentration. Error bars represent one standard deviation.	124
Figure 3.8	Demonstration of the dependence of uptake of 1 on incubation time. After incubation, NIH/3T3 cells were rinsed with DPBS, treated with trypsin, dissolved in nitric acid, and analyzed with ICP-MS. The graph shows uptake per dish plotted against incubation concentration. Error bars represent one standard deviation.	125
Figure 3.9	Washout rate of 1 from NIH/3T3 cells as a function of the number of rinses. Cells were incubated for one hour and then medium was changed. After each rinse period the medium was removed and analyzed using ICP-MS. Long incubation times were 24 and 48 hours. Short incubation times were 1, 3, and 6 hours. Error bars represent one standard deviation.	127

Figure 3.10	Schematic of cell culture well and insert used in BBB model experiment. The base of the insert is a 0.45 mm filter coated with type 1 rat tail collagen. bMVEC-B cells formed a monolayer over the filter. Contrast agent was added to the insert, and samples of medium were taken from the bottom chamber and analyzed for gadolinium content using ICP-MS.	128
Figure 3.11	Results of BBB model experiment testing the ability of compounds 1-3 , and 6 to permeate the BBB. The graphs depict the concentration of gadolinium that had crossed the BBB model versus time. Cells were incubated with 3 mM compound in modified EBM-2 medium (top) and modified EBM-2 medium saturated with Pluronic F-127 (bottom).	130
Figure 3.12	Fluorescence microscopy images of brain slices exposed to complexes 1 and 2 . Top: Sections of hippocampus (left) and midbrain (right) from a PDAPP mouse that were treated with 1 . Bottom: Sections of a PDAPP mouse brain that were treated with 1 (left) or 2 (right).	131
Figure 3.13	Schematic of the proposed explanation for the high relaxivity values caused by an increase in t_r resulting from aggregation. The hydrophobic region of the agents aggregate leaving the hydrophilic chelates exposed to water. The formation of the large aggregate would slow the molecular tumbling rate and lead to increased relaxivity values.	135
Figure 3.14	Structure of Pluronic F-127.	137
Figure 3.15	bMVEC-B cells day 3-4 after confluence. Stained with anti ZO-1, showing tight junctions (bright green). Blue is the nuclear stain DAPI.	141
Figure 4.1	Structure of β -galactosidase responsive contrast agent (Top), and MRI of capillary tubes containing the contrast agent and either active or inactive enzyme (Bottom).	158
Figure 4.2	Structure of proposed MMP responsive MRI contrast agent.	159
Figure 4.3	Model complexes representing MMP responsive contrast agent before and after exposure to MMP-7.	161

Figure 4.4	Vibrational quenching of europium(III) emissive state by water. An offset has been applied so that the lowest vibrational level of OH/OD is shown at the same energy as the highest level of the ground-state manifold of the europium(III) ion. No anharmonicity is assumed in the vibrational ladder, with $\nu_{\text{OH}} = 3405 \text{ cm}^{-1}$ and $\nu_{\text{OD}} = 2520 \text{ cm}^{-1}$. Figure modified from reference 7.	165
Figure 4.5	Sample fluorescence decay measurements used to determine values of q . Top graph: Fluorescence lifetime decay measurement in H_2O at 594 nm. Bottom graph: Fluorescence lifetime decay measurement in D_2O at 594 nm. Right: Sample calculation to determine value of q .	167
Figure 4.6	Chemical structures of a series of aspartic acid modified europium(III) chelates.	168
Figure 4.7	Proposed binding of peptide modified DOTA.	171
Figure 4.8	Structure of target bridged complex in which a caspase cleavable peptide is held over the free coordination sites of gadolinium(III). Upon exposure to caspase the peptide should be cleaved allowing for water access to the gadolinium(III) ion and a subsequent increase in q .	173

List of Schemes

Scheme 2.1	Synthesis of polyarginine containing lanthanide chelates: (a) (1) Piperidine, DMF (2) Fmoc-R(Pbf)-OH, HATU, DMF, DIPEA; (b) (1) Piperidine, DMF (2) DOTA(tris- <i>t</i> -bu ester), HATU, DMF, DIPEA (3) 95% TFA, 2.5% H_2O , 2.5% TIS; (b) $\text{Eu}(\text{OH})_3$ or $\text{Gd}(\text{OH})_3$ in water at 80 °C for 12 hours.	69
Scheme 3.1	Synthetic route to the dianionic (1), monoanionic (2), and neutral (3) versions of A β targeting MRI contrast agents.	113
Scheme 3.2	Proposed synthesis of a contrast agent conjugated to styrylbenzene via a dithiol linker for extending intracellular lifetime. (a) <i>N</i> -succinimidyl-3-(2-pyridyldithio)propionate, 0.1 M pH 7.4 phosphate buffer, DMSO; (b) $\text{Gd}(\text{OH})_3$, 80.2 °C; (c) (1) NaNO_2 , HCl, 0 °C, (2) KS_2COEt , 65 °C, (3) 0.3 NaOH, 65 °C.	145

Scheme 4.1	Synthesis of europium(III) chelates modified with peptides: (a) i. Piperidine, DMF, ii. DOTA(tris- <i>t</i> -bu ester), HATU, DMF, DIPEA, iii. TFA cleavage cocktail; (b) Eu(OH) ₃ , H ₂ O, Δ.	163
-------------------	---	-----

List of Tables

Table 2.1	Relaxivity values and octanol-water partition coefficients measured for 4 , 5 , and 6 . Relaxivity measured at 59.97 MHz, and 37 °C in 10 mM MOPS, 100 mM NaCl, 20 mM NaHCO ₃ , and 4 mM NaH ₂ PO ₄ at pH 7.41. Values for partition coefficients are plus or minus one standard deviation.	71
Table 2.2	Results of T_1 study of NIH/3T3 cells incubated with 0.3 mM 6 , 10 , and untreated cells. After incubation cells were rinsed with either fresh modified DME medium or DPBS. T_1 values were measured at 60 MHz and 37 °C. Units for T_1 are s.	76
Table 3.1	Physical properties of 1-3 including molecular charge, $P_{\text{oct/wat}}$, and r_1 in pH 7.41 MOPS buffer and 10% Pluronic F-127.	115
Table 3.2	UV-visible and fluorescence properties of 1-3 including molar absorptivity (ϵ) in 10% Pluronic F-127 and MOPS buffer, fluorescence quantum yield, λ_{EM} , and λ_{EX} .	116
Table 4.1	Values of q measured for the peptide-contrast agent conjugates 1-6 .	166
Table 4.2	Values of q measured for the aspartic acid-contrast agent conjugates 16-18 .	170

Abbreviations

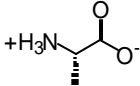
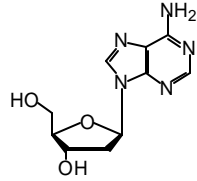
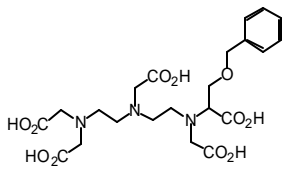
Abbreviation	Name
AD	Alzheimer's disease
APP	amyloid precursor protein
ASL	analytical services laboratory
ATCC	American type culture collection
BBB	blood brain barrier
BCS	bovine calf serum
bMVEC-B	primary bovine brain microvascular endothelial cells
CEST	chemical exchange saturation transfer
CLIO	cross-linked iron oxide
CT	computed tomography
DME	Dulbecco's modified Eagle's
DMEM	Dulbecco's modified Eagle's medium
DPBS	Dulbecco's phosphate buffered saline
EMEM	Eagle's minimal essential medium
ESI	electrospray ionization
FBS	fetal bovine serum
GI	gastrointestinal
HIV	human immunodeficiency virus
HSA	human serum albumin
ICP-MS	inductively coupled plasma mass spectrometry
LCDIO	long-circulating dextran coated iron oxide

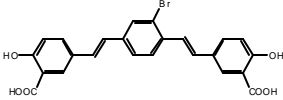
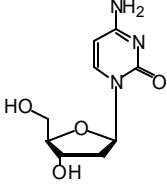
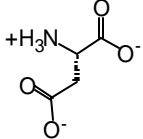
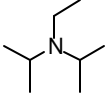
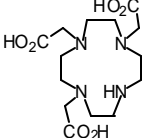
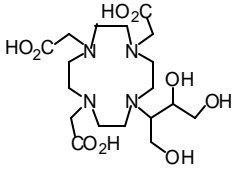
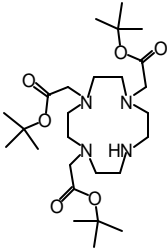
Abbreviation	Name
MAB	monoclonal antibody
MALDI-TOF	matrix-assisted laser desorption ionization time of flight
MDCK	canine kidney epithelial cells
MION	magnetic iron oxide nanoparticle
MMP	matrix metalloproteinase
MR	magnetic resonance
MRamp	magnetic resonance signal amplification
MRI	magnetic resonance imaging
NIH/3T3	mouse fibroblast cells
PAMAM	polyamidoamine
PBS	phosphate buffered saline
PET	positron emission tomography
PD	platelet derived
PPMAL	protein/peptide microanalytical laboratory
RAW 264.7	mouse macrophage cells
RF	radiofrequency
RIME	receptor-induced magnetization enhancement
SPECT	single photon emission computerized tomography
SPIO	superparamagnetic iron oxide
TE	echo delay time
TPLM	two-photon laser microscopy
TR	recycle time

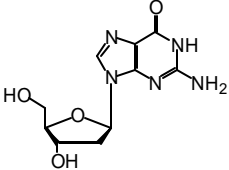
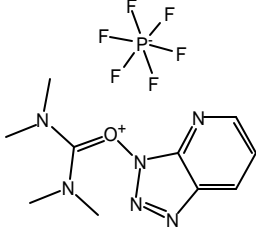
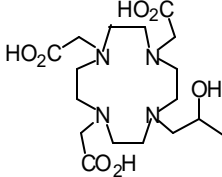
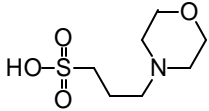
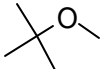
Abbreviation	Name
USPIO	ultrasmall superparamagnetic iron oxide
UV	ultraviolet

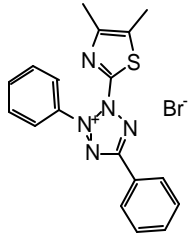
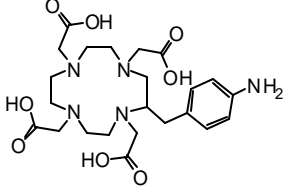
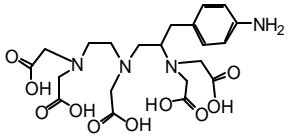
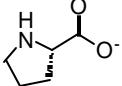
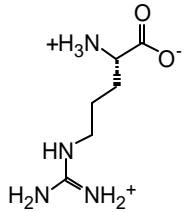
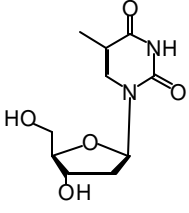
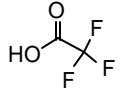
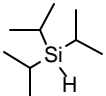
Symbol	Definition
A	UV-Vis absorption
B_0	magnetic field vector
B_1	RF generated field
c	the molal concentration of contrast agent
e	molar absorptivity
?	fluorescence quantum yield
g	the electron g-factor
g_I	the nuclear gyromagnetic ratio
h	Planck's constant
?	Refractive index
I	spin quantum number equal to $\frac{1}{2}$ for the hydrogen atom
I	integrated area under the fluorescence emission peak
k_{D_2O}	rate of luminescence decay in D_2O
k_{H_2O}	rate of luminescence decay in H_2O
I_{EM}	maximum emission wavelength
I_{EX}	maximum excitation wavelength
M	net magnetization vector

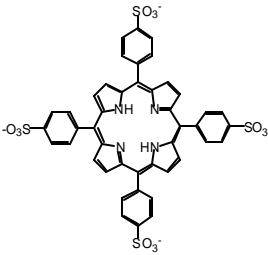
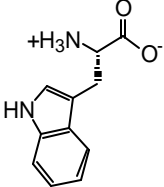
Symbol	Definition
m_B	the Bohr magneton
$P_{\text{oct/wat}}$	octanol-water partition coefficient
q	the number of bound water molecules per paramagnetic ion
r_{GdH}	the electron spin – proton distance
S	the spin of the paramagnetic ion
T_{1e}	the longitudinal electron spin relaxation time of the metal ion
T_{2e}	the transverse electron spin relaxation time of the metal ion
t_m	the mean lifetime of water molecules in the innersphere environment
t_r	the rotational correlation time or the reorientational correlation time of the metal-proton vector
ω_I	the nuclear Larmor frequency
ω_L	the Larmor frequency
ω_S	the electron Larmor frequency

Abbreviation(s)	Name	Structure
A (Ala)	alanine	
A	adenine	
BOPTA	3-benzyloxy-2-[(2-[(2-(biscarboxymethyl-amino)ethyl)carboxymethyl-amino]ethyl)carboxymethylamino]-propionic acid	

Abbreviation(s)	Name	Structure
BSB	<i>(trans,trans)</i> -1-bromo-2,5-bis-(3-hydroxycarbonyl-4-hydroxy)styrylbenzene	
C	cytosine	
D (Asp)	aspartic acid	
DIPEA	diisopropylethylamine	
DMF	dimethylformamide	
DMSO	dimethylsulfoxide	
DO3A	1,4,7,10-tetraazacyclododecane-1,4,7-trisacetic acid	
DO3AB	1,4,7,10-tetraazacyclododecane-1-(2,3-dihydroxy-1-hydroxymethylpropyl)-4,7,10-trisacetic acid	
DO3A(tris- <i>t</i> -Bu ester)	1,4,7-tris- <i>tert</i> -butoxycarbonylmethyl-1,4,7,10-tetraazacyclododecane	

Abbreviation(s)	Name	Structure
G	guanine	
G (Gly)	glycine	$+\text{H}_3\text{N}-\text{CH}_2-\text{COO}^-$
HATU	<i>O</i> -(7-azabenzotriazol-1-yl)-1,1,3,3-tetramethyluronium hexafluorophosphate	
HPDO3A	1,4,7,10-tetraazacyclododecane-1-hydroxypropyl-4,7,10-trisacetic acid	
L (Leu)	leucine	$+\text{H}_3\text{N}-\text{CH}(\text{CH}_2\text{CH}(\text{CH}_3)_2)-\text{COO}^-$
M (Met)	methionine	$+\text{H}_3\text{N}-\text{CH}(\text{CH}_2\text{CH}_2\text{S}-\text{CH}_3)-\text{COO}^-$
MOPS	3-(<i>N</i> -morpholino)propane sulfonic acid	
MTBE	methyl <i>tert</i> -butyl ether	

Abbreviation(s)	Name	Structure
MTT	3-(4,5-dimethylthiazolyl-2)-2,5-diphenyl-tetrazolium bromide	
<i>p</i> -NH ₂ -Bz-DOTA	2- <i>p</i> -aminobenzyl-1,4,7,10-tetraazacyclododecane-1,4,7,10-tetraacetic acid	
<i>p</i> -NH ₂ -Bz-DTPA	<i>p</i> -aminobenzyl diethylenetriamine pentaacetic acid	
P (Pro)	proline	
R (Arg)	arginine	
T	thymine	
TFA	trifluoroacetic acid	
TIS	triisopropylsilane	

Abbreviation(s)	Name	Structure
TPPS	5,10,15,20-tetrakis(<i>p</i> -sulfonatophenyl)-porphyrin	
W (Trp)	tryptophan	

Chapter 1

Introduction

The text of this chapter was taken in part from the following manuscripts:

Allen, M.J.; Meade, T.J. *Met. Ions Biol. Syst.* Vol. 42, Marcel Dekker Inc., New York, in press.

Introduction

This chapter focuses on the wide range of chemical and biological applications that exist for magnetic resonance imaging (MRI) contrast agents. It begins with an introduction of how MRI and contrast agents function followed by a review of both clinical and experimental uses for MRI contrast agents. A description of the targeted delivery of contrast agents including how they bind to and accumulate in specific biological tissues is then presented. Finally, the new class of bio-activatable MRI contrast agents is described. These agents respond to biological phenomena by altering the intensity of observed signal in a conditional fashion.

Magnetic Resonance Imaging and Nuclear Spin Relaxation Processes

MRI has become an extremely important tool for clinical diagnosis of disease and for noninvasive imaging of three-dimensional opaque objects. MRI is based on the same principles as NMR spectroscopy. The work in this thesis deals exclusively with the hydrogen nucleus, as does the majority of MRI, so the following description of MRI pertains to the hydrogen nucleus. This explanation is easily extended to encompass other nuclei with nuclear spin quantum numbers equal to $\frac{1}{2}$. For an introduction into the use of other nuclei in MRI, see chapter one of *The Chemistry of Contrast Agents in Medical Magnetic Resonance Imaging* edited by Merbach and Toth.¹

The nucleus of the hydrogen atom has a nuclear spin angular momentum. Nuclear spin angular momentum is a purely quantum mechanical property. The nuclear spin can be described as a vector (\mathbf{I}) that can be quantified using **Equation 1.1** in which h is Planck's constant, and I is the nuclear spin quantum number equal to $\frac{1}{2}$ for the hydrogen atom. If placed in an external magnetic field, \mathbf{B}_0 , the nuclear spin of a

hydrogen nucleus will precess about \mathbf{B}_0 at the Larmor frequency, ω_L , in a discrete direction relative to \mathbf{B}_0 (**Figure 1.1**). With a spin of $\frac{1}{2}$, only two directions are quantum mechanically allowed for the hydrogen nucleus. These two directions correspond to energy levels of the nucleus. A nucleus can change energy states, but in order to move to a higher energy level, energy in the form of electromagnetic radiation needs to be supplied. Electromagnetic radiation in the radiofrequency (RF) range, of frequency $(h/2p)\omega_L$, is of the correct energy to initiate this excitation.

$$\text{Equation 1.1: } |\mathbf{I}| = \frac{h}{2p} \sqrt{I(I+1)}$$

On a bulk scale, proton nuclear spins are distributed between the two allowed states according to a Boltzmann distribution, which is dependent on temperature and the energy difference between the allowed states. For hydrogen, the two energy states are spin ‘up’ (low energy) and spin ‘down’ state (high energy). The Boltzmann distribution shows that slightly more spins occupy the lower energy state leading to a net magnetization vector, \mathbf{M} , that is the sum of all of the spins. RF pulses can be applied to generate a magnetic field perpendicular to \mathbf{B}_0 . This RF generated field, \mathbf{B}_1 , causes the spins to flip away from the z -axis and gain x - and y -components (**Figure 1.2**). Conventionally, the magnetic field \mathbf{B}_0 is aligned with the z -axis. This precessing about the z -axis in an xy -plane generates a detectable alternating RF field.

At the end of the applied RF pulse, the \mathbf{B}_1 field ceases to exist and the nuclear spins return to their ground state by interacting with the surrounding environment through a process called relaxation. As the spins realign with \mathbf{B}_0 , the current produced by rotation

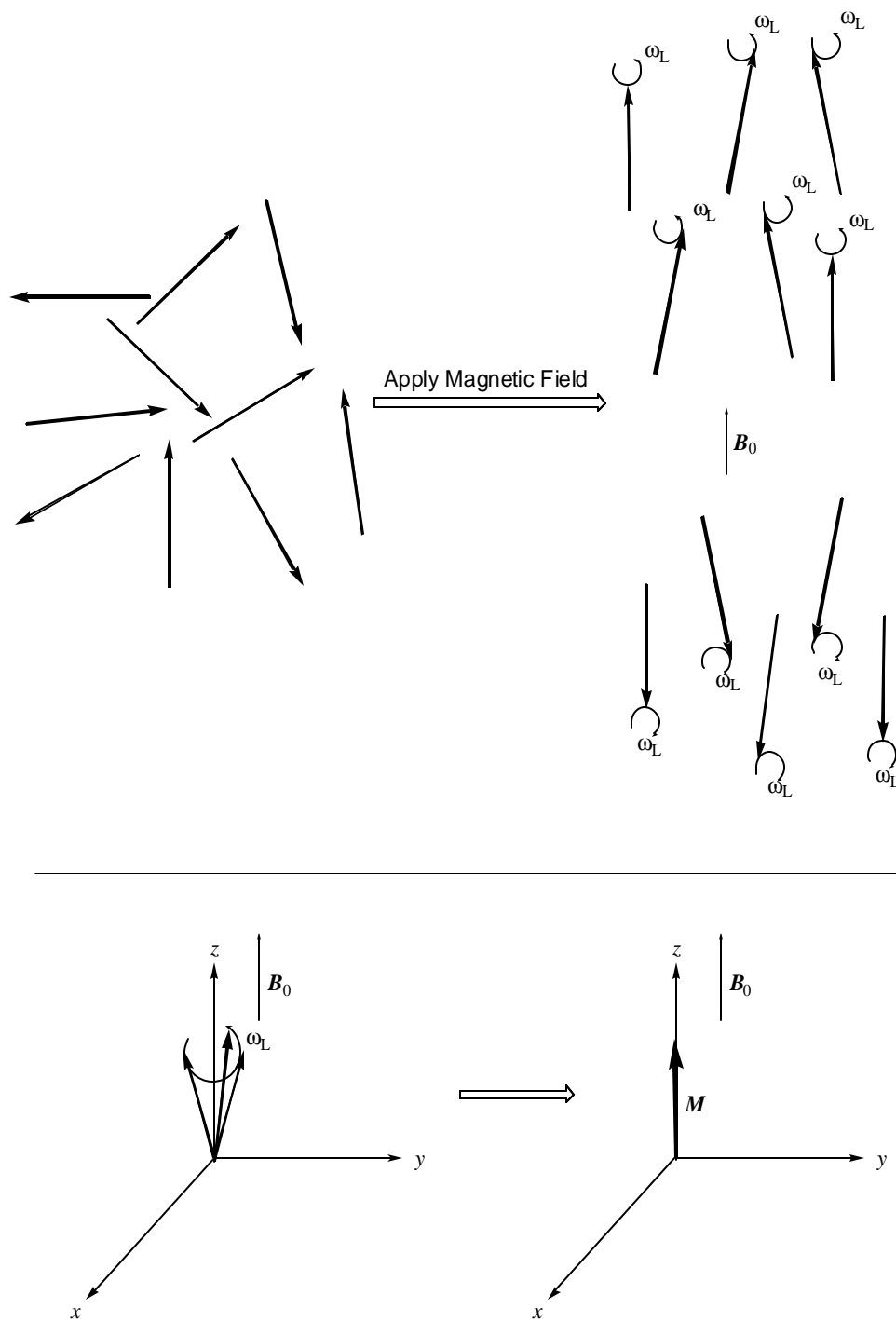


Figure 1.1: Schematic of hydrogen nuclei before and after being placed in a magnetic field B_0 . Top: Nuclei are randomly oriented before exposure to B_0 , then align with and precess about B_0 at the Larmor frequency, ω_L , after placement in B_0 . Bottom: Slightly more spins occupy the lower energy state leading to a net magnetization vector, M .

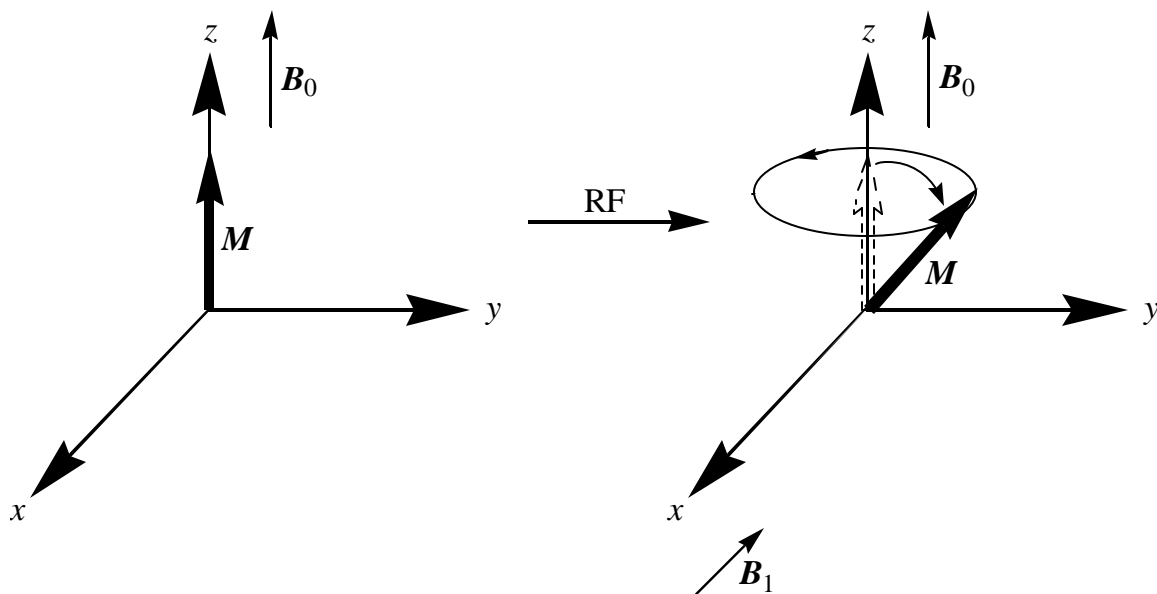


Figure 1.2: Schematic depicting the behavior of the net magnetization vector, M , upon exposure to an RF pulse. The RF pulse generates a magnetic field B_1 that causes M to flip away from the z -axis and revolve about B_0 in an xy -plane.

in the xy -plane diminishes. The time necessary for disappearance of this current can be measured and is termed the relaxation time. Relaxation times of a sample are measured and used to produce an image in MRI.

Relaxation is described in two parts: spin-lattice relaxation and spin-spin relaxation. In spin-lattice relaxation, the z -component of \mathbf{M} returns to equilibrium as characterized by a time constant T_1 ; while in spin-spin relaxation, the x - and y -components of \mathbf{M} return to zero with a time constant T_2 . Spin-lattice and spin-spin relaxation are often referred to as T_1 and T_2 relaxation, respectively.

T_1 relaxation occurs due to magnetic field fluctuations at the Larmor frequency brought about by the random motions of molecules in the surrounding medium (lattice). These molecules in motion each have magnetic moments, and the movement of these moments leads to a magnetic 'noise' that encompasses a broad frequency range including the Larmor frequency. Magnetic noise at the Larmor frequency will stimulate transition to the lower energy state.

T_2 relaxation occurs via fluctuations of a magnetic field caused by the random motion of molecules resonating at the same frequency. Fluctuation in the individual proton spins leads to a loss of phase coherence in the xy -plane with no net loss of energy from the system. Spin-spin relaxation is additionally affected by dephasing arising from bulk inhomogeneities in \mathbf{B}_0 .

Biological samples for MRI are large and inhomogeneous. In order to create an image of these heterogeneous samples, spatial information is encoded into the signal using time-varying magnetic gradients that alter the magnetic field strength, which allows

for mapping of spatial positions to frequencies. Mathematical transformations are performed to produce images from the spatially encoded data.^{1,2}

Contrast in MR images is achieved based on differences in T_1 , T_2 , and proton density within a sample. Using different RF pulse sequences, image intensity can be weighted with respect to T_1 , proton density, or T_2 (**Figure 1.3**). Inherent contrast can be improved with the use of paramagnetic contrast agents (**Figure 1.4**). Most contrast agents reduce T_2 and T_1 . Agents are classified as T_1 if they shorten T_1 more than T_2 , and T_2 if they affect T_2 more than T_1 . The ability to reduce T_1 and T_2 relaxation times is described by the concentration normalized relaxivity values r_1 and r_2 , respectively. Work with T_1 agents is presented in Chapters 2–4 of this thesis, so a detailed description of only T_1 agents will be presented. For more information on T_2 contrast agents see chapter two in *The Chemistry of Contrast Agents in Medical Magnetic Resonance Imaging*.¹

Contrast agents contain paramagnets, which have one or more unpaired electrons; the most common agents contain the lanthanide ion gadolinium(III). Because the work described in this thesis deals exclusively with gadolinium(III)-based contrast agents, the following theoretical description of relaxivity will pertain solely to gadolinium(III)-containing contrast agents. Paramagnetic relaxation of water protons originates from dipole-dipole interactions between the nuclear spins of the hydrogen nuclei of water molecules and the fluctuating local magnetic field caused by the spins of the unpaired electrons. The effect is a decrease in T_1 that falls off strongly with distance.

Detailed theory about the relaxivity properties of paramagnetic contrast agents is contained in the Solomon-Bloembergen equations. Observed T_1 is due to a combination of the T_1 intrinsic to the diamagnetic sample and the T_1 caused by the presence of a

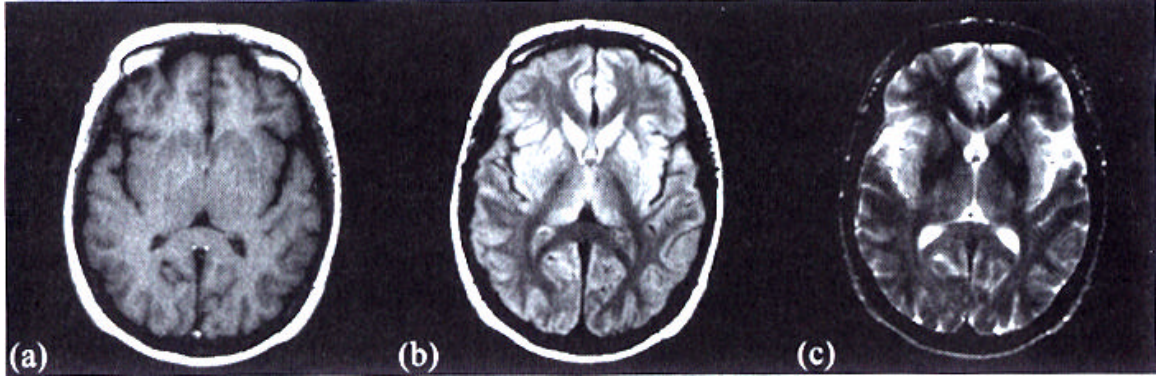


Figure 1.3: MRI images of the brain: (a) T_1 -weighted image; (b) proton-density weighted image; (c) T_2 -weighted image. Image reproduced with permission from Reference 1.

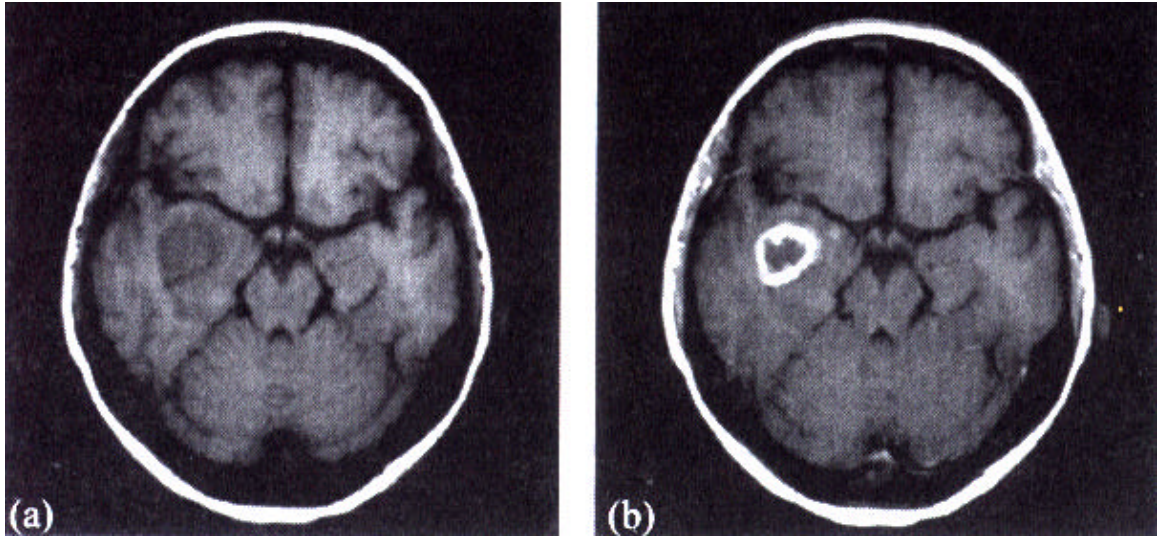


Figure 1.4: Positive-contrast enhancement in a brain lesion obtained by using a T_1 -weighted sequence and a T_1 contrast agent: (a) pre-contrast; (b) post-contrast—the bright ring is the area enhanced with contrast agent. Image reproduced with permission from Reference 1.

paramagnetic species (**Equation 1.2**). The term $1/T_{1p}$ can be written as the product of the relaxivity, r_1 , and the concentration of the contrast agent, $[Gd]$ (**Equation 1.3**). This term is composed of an inner sphere and an outer sphere term (**Equation 1.4**). The inner sphere term describes the relaxation of the hydrogen nuclei of water molecules directly bound to the paramagnetic ion, while the outer sphere term accounts for interactions between paramagnetic ions and closely diffusing water molecules. The relaxation of current clinically approved agents is due to approximately 60% inner sphere and 40% outer sphere effects.¹ Inner sphere effects can be modified whereas outer sphere effects cannot easily be affected.

$$\text{Equation 1.2: } \frac{1}{T_{1obs}} = \frac{1}{T_{1d}} + \frac{1}{T_{1p}}$$

$$\text{Equation 1.3: } \frac{1}{T_{1obs}} = \frac{1}{T_{1d}} + r_1[Gd]$$

$$\text{Equation 1.4: } r_1 = r_1^{IS} + r_1^{OS}$$

The inner sphere term can be broken down further as in **Equation 1.5**, where c is the molal concentration of contrast agent, q is the number of bound water molecules per paramagnetic ion, t_m is the mean lifetime of water molecules in the inner sphere environment, and $1/T_{1m}$ is the longitudinal proton relaxation rate. The term $1/T_{1m}$ is composed of a dipole-dipole term and a scalar term (**Equation 1.6**). The scalar term becomes negligible at magnetic field strengths above 10 MHz. Since most clinical and

experimental MR images are acquired at field strengths higher than 10 MHz, the scalar term is not an important factor in proton relaxation, thus $1/T_{1m}$ is essentially determined by the $1/T_1^{DD}$ term. The dipole-dipole term is modulated by reorientation of the nuclear spin vectors with respect to the electron spin vector, changes in orientation of electron spin, and the rate of water exchange. This term is described in **Equation 1.7** where γ_I is the nuclear gyromagnetic ratio, g is the electron g -factor, m_B is the Bohr magneton, r_{GDH} is the electron spin – proton distance, S is the spin of the paramagnetic ion, ω_S is the electron Larmor frequency, ω_I is nuclear Larmor frequency, and t_c is the correlation time described by **Equation 1.8**. The t_c term is composed of t_m ; the rotational correlation time that is the reorientational correlation time of the metal-proton vector, t_r ; and the longitudinal and transverse electron spin relaxation times of the metal ion, T_{1e} and T_{2e} , respectively.

$$\text{Equation 1.5: } \frac{1}{T_1^{IS}} = \frac{cq}{55.5} \left(\frac{1}{(T_{1m} + t_m)} \right)$$

$$\text{Equation 1.6: } \frac{1}{T_{1m}} = \frac{1}{T_1^{DD}} + \frac{1}{T_1^{SC}}$$

$$\text{Equation 1.7: } \frac{1}{T_1^{DD}} = \frac{2}{15} \left(\frac{g_I^2 g^2 m_B^2}{r_{GDH}^6} \right) S(S+1) \left(7 \frac{t_{c2}}{1 + \omega_S^2 t_{c2}^2} + 3 \frac{t_{c1}}{1 + \omega_I^2 t_{c1}^2} \right)$$

$$\text{Equation 1.8: } \frac{1}{t_{ci}} = \frac{1}{t_r} + \frac{1}{T_{ie}} + \frac{1}{t_m}, i = 1, 2$$

The theory of T_1 contrast agents demonstrates that numerous parameters affect relaxivity (**Figure 1.5**). The parameters q , r_{GdH} , t_m , t_r , and T_{1e} can be adjusted by altering the chemical environment around the paramagnetic ion.³ By increasing the value of q , the relaxivity of the agent will increase. Increasing q above two will most likely result in increased toxicity due to decreased stability of the complex. A decrease in r_{GdH} will lead to an increase in relaxivity. Decreasing the term t_m will allow more water molecules to be affected by the gadolinium(III) ion resulting in an increase in relaxivity. If the value of t_m is decreased too much, the relaxivity of a complex will begin to decrease because the lifetime of the water molecules bound to the gadolinium(III) ion will not be long enough to influence the relaxation of the protons of the water molecule. By optimizing the value of t_r or T_{1e} , the relaxivity of the contrast agent will be increased. There is an interdependence of the terms t_m , t_r , and T_{1e} . For most small molecule gadolinium(III) complexes, t_r is the limiting of the three variables. As the value of t_r becomes optimized the variables t_m and T_{1e} begin to influence the relaxivity of the contrast agents. These parameters can be exploited to create activatable contrast agents that are discussed later in this chapter, and the use of a q modulating contrast agent is examined as a means to detect protease activity using MRI in Chapter 4.

Since the development of MRI in the 1970s, technological advances have led to increases in both the speed and resolution of MRI.⁴ Superconducting magnets have made higher signal-to-noise ratios and superior image resolutions possible compared with resistive or permanent magnets. Modern computers and advances in coil technology have improved image quality and decreased acquisition times. Today scans are routinely obtained in minutes (single slices in seconds) with the same spatial resolution as X-ray

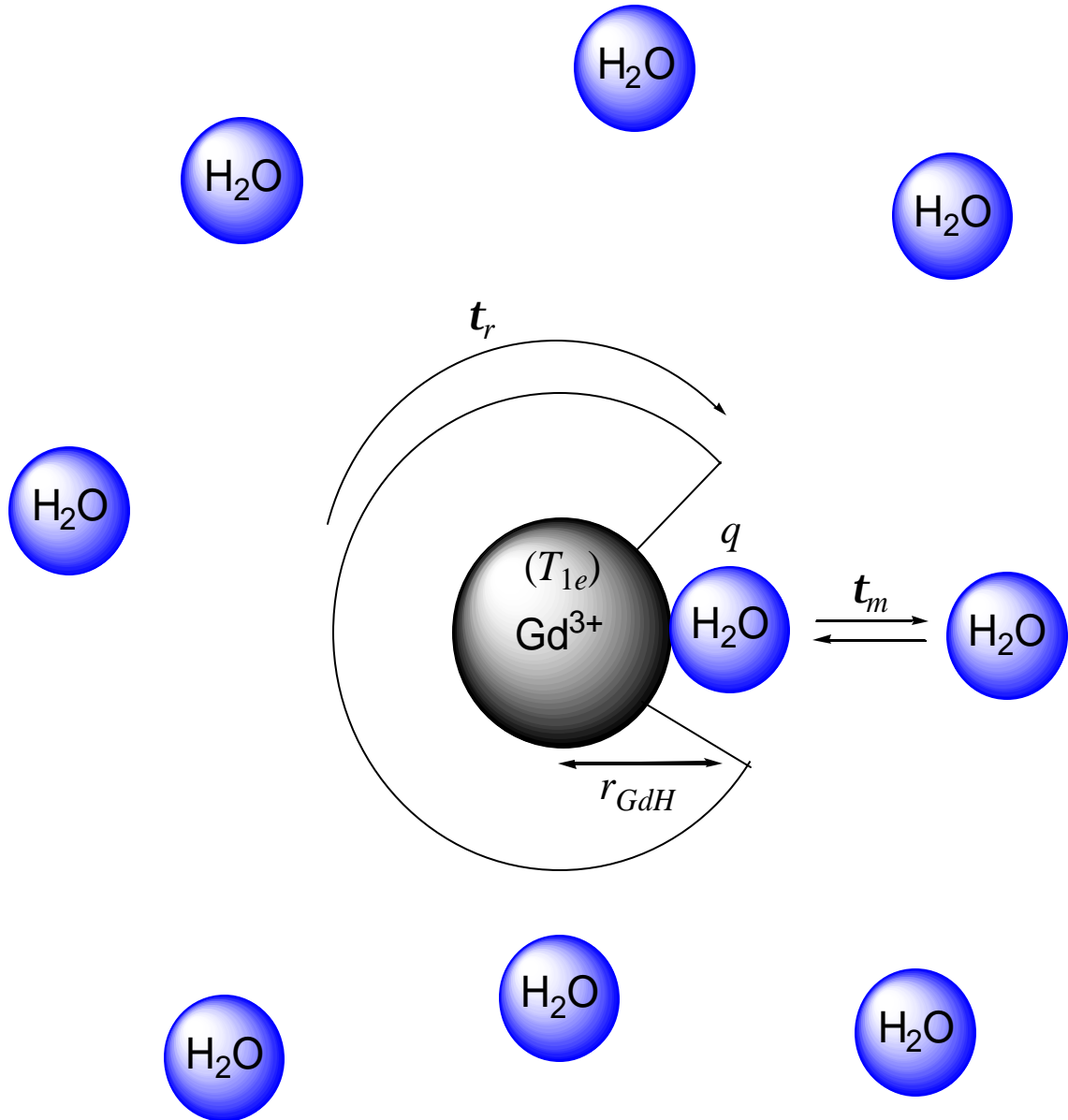


Figure 1.5: Schematic depicting the interactions of water molecules with a gadolinium(III)-based contrast agent. The five variables shown have an influence on r_1 .

computed tomography (X-ray CT), approximately 1 mm.⁵ Where higher fields are employed, resolution on the order of cells ($\sim 10 \mu\text{m}$) has been reported.⁶ Due to high resolution and the noninvasive ability to image opaque samples, MRI is becoming one of the primary imaging modalities in modern medicine.⁷

Classes of Contrast Agents

MRI can distinguish between various parts of a specimen based on differences in T_1 , T_2 , and water concentration. However, when intrinsic contrast is low, contrast agents improve image quality. In MR images derived from changes in T_1 , regions that are associated with a contrast agent (nearby water molecules) have increased signal intensity compared to regions not associated with a contrast agent. The inverse is true for T_2 -weighted images. Regions associated with a superparamagnetic center (such as an iron oxide particle) have reduced signal intensity in an MR image compared to areas without contrast agents. The T_2 shortening caused by superparamagnetic particles arises from the local magnetic field inhomogeneities associated with the large magnetic moments of these particles.

Many types of molecules enhance contrast in MRI. While both organic and inorganic radicals can be MRI contrast agents, this discussion is restricted to metal containing agents. The lanthanide ion gadolinium(III) is generally chosen as the metal atom for contrast agents because it has a high magnetic moment ($\mu^2 = 63 \text{ BM}^2$), and has the most unpaired electrons of any stable ion.⁸ Transition metal ions such as high spin manganese(II) and iron(III) are candidates due to their high magnetic moments and five unpaired electrons.⁵ Free metal ions can be toxic to biological systems, thus suitable ligands or chelates must be used to bind the metal ions to form nontoxic complexes. The

chelators prevent uptake of the free metal ions by biological systems. Common ligands used to coordinate paramagnetic metal ions are shown in **Figure 1.6**.

Further, a number of other paramagnetic metal-based substances are contrast agents. These materials include free transition metal ions such as copper(II) chloride, manganese(II) chloride, and ferric ammonium citrate.^{9,10} Linear polymers and dendrimers conjugated to metal chelates as well as liposomes containing paramagnetic ions are used as MR contrast agents.¹¹⁻¹⁴ Superparamagnetic iron oxide nanoparticles are frequently used as T_2 enhancing contrast agents.^{15,16} Finally, lanthanide polyoxometalates (e.g. $K_9GdW_{10}O_{36}$),¹⁷ clays and zeolites containing paramagnets,¹⁸ and nanoparticles containing gadolinium ions^{19,20} can be used to enhance MR contrast.

Contrast Agents for Diagnosis

Cancer

The development of new contrast agents, improved pulse sequences, and hardware is evolving MRI into one of the leading modalities for cancer diagnosis. Numerous MRI contrast agents aid the successful diagnosis of malignant tumors while others hold potential for improving the efficiency and accuracy of cancer diagnosis.

Gadolinium(III) DTPA and Its Derivatives

A commonly used, clinically approved MRI contrast agent is the gadolinium(III) complex of diethylenetriaminepentaacetic acid (DTPA, gadopentetate dimeglumine, or MagnevistTM). The stability constant for demetallation (K_{Gd}) for gadolinium(III) DTPA is very high ($\log K_{Gd} = 22.4$), and the water-soluble complex is stable and nontoxic. It is an extracellular contrast agent that accumulates in tissue by perfusion-dominated

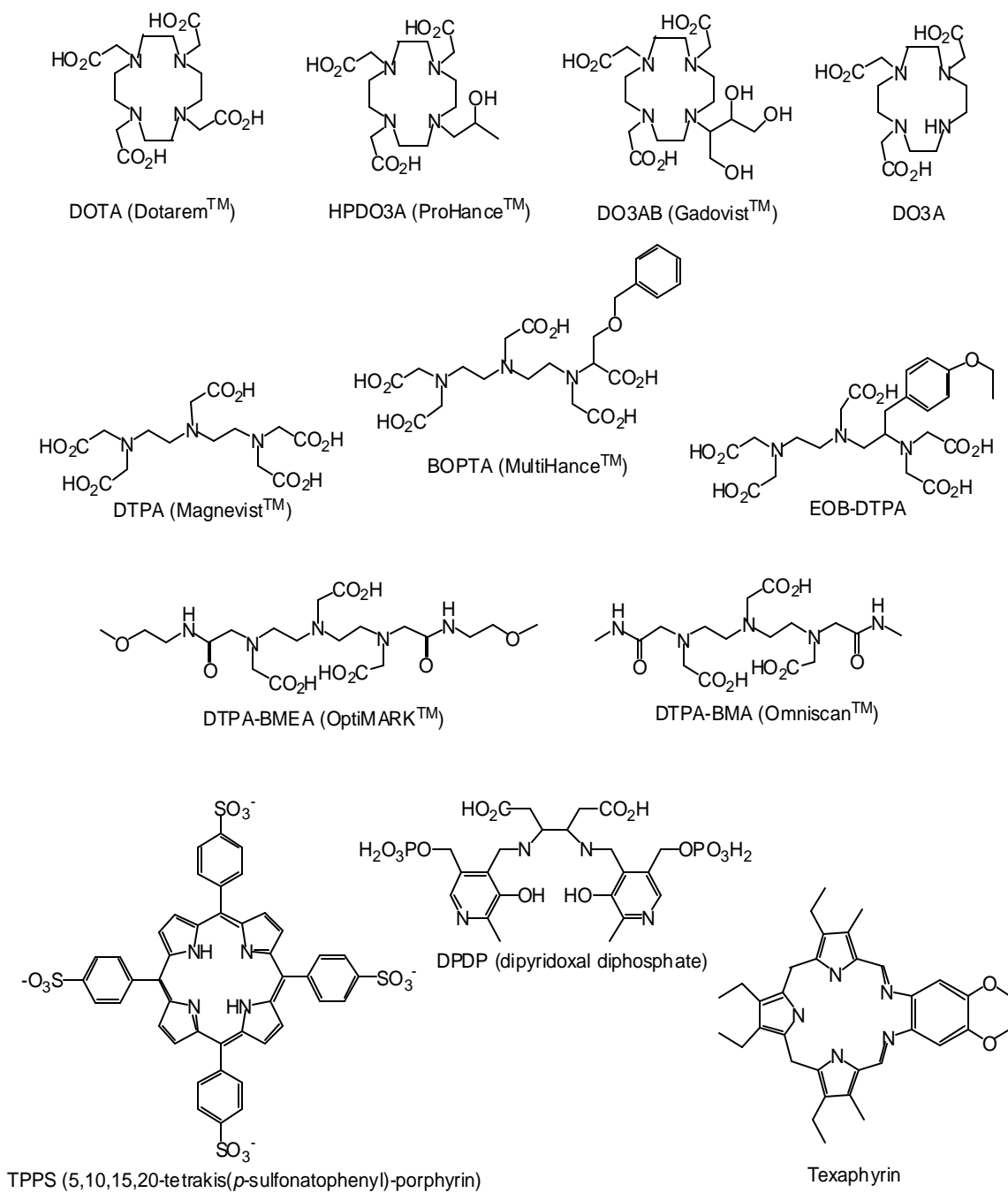


Figure 1.6: Common MRI ligands used to coordinate paramagnetic metal ions.

processes. Gadolinium(III) DTPA enhanced MRI assists in diagnosis and monitoring of treatment response for many types of cancer.

Breast cancer is a major cause of death among women, and X-ray mammography is the method of choice for early cancer screening. While this technique is rapid and cost-effective, it may result in a missed fraction of cancers as high as nine percent, and there are concerns that repeated radiation exposure resulting from frequent mammographic screening may induce cancer.^{21,22} MRI has been tested as an alternative to mammography because of its sensitivity and lack of ionizing radiation. Gadolinium(III) DTPA has been used to screen premenopausal women for breast cancer.²³ It has been used to follow the treatment of breast cancer before and after chemotherapy and can reveal tumor recurrence with a sensitivity of nearly 100% and a specificity greater than 90%.^{24,25} The use of gadolinium(III) DTPA in MRI can differentiate between benign and malignant breast tumors based on the contrast agent uptake rate.^{26,27} A correlation between gadolinium(III) DTPA signal enhancement and microvessel density was used to visualize angiogenesis.²⁸ By employing a dedicated breast coil to maximize spatial resolution, MRI using gadolinium(III) DTPA for diagnosing breast cancer is more sensitive than mammography and has the potential to eliminate unnecessary biopsies.^{22,29}

Hepatocellular carcinoma is the most common primary malignancy of the liver. Gadolinium(III) DTPA has been shown to differentiate between hepatocellular carcinoma and cavernous hemangioma, the most common benign tumor of the liver.³⁰ During treatment for hepatic tumors, gadolinium(III) DTPA can be used to monitor the progress and effects of therapy.³¹

Gadolinium(III) DTPA is used for the identification of patients at risk for recurrence of certain cancers and to predict disease free survival in osteosarcoma.³² A qualitative measurement of tumor vascular physiology can be acquired using gadolinium(III) DTPA which may help to evaluate the prognosis and treatment of lung cancer.³³ Finally, gadolinium(III) DTPA has been used to diagnose pulmonary arterial angiosarcomas, the most common primary tumor of the heart and great vessels, and to distinguish them from central pulmonary embolisms.³⁴

Gadolinium(III) DTPA-BMA (gadodiamide or OmniscanTM) improves the imaging of hepatocellular carcinoma and hydronephrosis in rats by increasing differences in vascularity, blood flow, and permeability.³⁵ It has been used in the diagnosis of pancreatic tumors.³⁶ Gadoxetic acid (gadolinium(III) EOB-DTPA) can detect hepatic lesions better than unmodified gadolinium(III) DTPA.³⁷ Recently, the simultaneous application of iron oxide microspheres and gadolinium(III) DTPA made it possible to characterize tumors in terms of gross histopathologic features as well as the vasculature spatial distribution and physiologic function.³⁸ In another study using both superparamagnetic iron oxide particles and gadolinium(III) DTPA, colorectal tumors (the second most common malignant tumors in the United States, Europe, and Japan) were accurately staged.³⁹

Linear polymers and dendrimers modified with gadolinium chelates have potential as diagnostic contrast agents. Dynamic micro-MRI with the dendrimer based contrast agent DAB-Am64-(1B4M-Gd)₆₄ is useful in the evaluation of hepatic micrometastatic tumors as small as 0.3 mm diameter in mice.⁴⁰ Ovarian cancer, which has the highest mortality rate of all gynecological malignancies in the United States, was

shown to be detectable using a PAMAM dendrimer containing gadolinium(III) chelates and folic acid functional groups.⁴¹ Finally, gadolinium(III) DTPA attached to a linear polymer has been used as a blood pool agent which can differentiate between benign and malignant breast tumors in dogs.⁴²

Manganese(II) and Iron Oxide Agents

Manganese-containing porphyrins have had success in the visualization of tumors because these complexes tend to localize in tumors. The proposed mechanism via which porphyrins accumulate in tumors is through selective uptake by benzodiazepine receptors abundant in tumor cells but not in normal cells.⁴³ Mangafodipir trisodium (MnDPDP) was shown to be useful in establishing the diagnosis of acinar cell carcinoma, a rare pancreatic exocrine neoplasm.⁴⁴ MnDPDP, which specifically labels liver tumors over healthy liver tissue, helps determine if surgery on hepatic tumors is a viable option.⁴⁵⁻⁴⁷ The manganese porphyrin, ATN-4T, accumulates in subcutaneous tumors in rabbits while rapidly clearing from surrounding tissues to yield images with enhanced tumor intensity.⁴⁸ HOP-8P, a manganese porphyrin complex demonstrated sustained tumor enhancement of squamous cell carcinoma in mice.⁴⁹

The use of superparamagnetic iron can assist in distinguishing various internal structures (tumor, edema, neovascularization) and makes it possible to follow early stages of tumor development.⁵⁰ Success has been had when using various iron oxide particles to detect cancer in the lymph nodes. AMI-7227 particles have been shown useful in assessing the spread of malignancy to the lymph nodes in the pelvis.⁵¹ Long-circulating dextran coated iron oxide (LCDIO) enhanced lymph node imaging considerably improves the noninvasive diagnosis of locoregional cancer spread in mice.⁵² Ultrasmall

(~50 nm diameter) iron oxide particles (USPIO) improved diagnosis of metastatic axillary lymph nodes compared with precontrast MRI.⁵³

Iron oxide nanoparticles have shown promise in the diagnosis of liver cancer.^{54,55} It is estimated that 25% of all patients with liver metastases can be cured with surgery if detected early by imaging.⁵⁶ AMI-25, a superparamagnetic iron oxide particle coated with dextran, is taken up by healthy liver but not tumors.⁵⁷ It has been shown to be effective in diagnosing 90% of hepatocellular carcinoma⁵⁸ with an ability to differentiate between benign and malignant tumors with a sensitivity of 88% and a specificity of 89%.⁵⁹ Reovist is a superparamagnetic iron oxide (SPIO) particle that improves diagnostic confidence and detection of focal liver lesions.⁶⁰

Iron oxide nanoparticles have assisted the diagnosis of other types of cancer. Squamous cell carcinoma of the esophagus, which is one of the most aggressive malignant tumors of the digestive tract, has been specifically detected in rats using magnetite particles coated with anti-EGFR MAbs as a contrast agent.⁶¹ The USPIO particle Code 7227 has shown potential to be an MRI contrast agent for bone tumors in rabbits.⁶² Magnetic-dextran nanocapsules can be useful in the detection and characterization of various splenic tumors.⁵⁷ Small unilamellar vesicles sterically stabilized with polyethylene glycol were shown to differentiate between colon carcinoma cells and healthy tissue in rats.⁶³

Non-Cancer Diseases

Blood Pool-Related Diseases

Contrast agent enhanced MRI has improved the diagnosis of a number of diseases other than cancer. For example, agents used to image the blood pool assist in the

evaluation of heart disease and can provide minimally invasive angiography, image angiogenesis, measure organ blood volume, and identify hemorrhage.¹¹ There are a few examples of gadolinium(III) DTPA assisting with imaging of the circulatory system. The agent has a uniform distribution across ventricular epicardium when intrapericardially administered to pigs.⁶⁴ Patients with angina that have normal coronary arteries often exhibit regional accumulation of gadolinium(III) DTPA.⁶⁵ Finally, a derivative of gadolinium(III) DTPA (OmniscanTM) can help image the carotid artery.⁶⁶

Liposomes loaded with gadolinium-containing chelates have potential as blood pool agents.⁶⁷ Modification of the surface of these liposomes with polyethylene glycol leads to longer blood retention times.¹¹ Dendrimers containing gadolinium(III) DTPA are suitable blood pool contrast agents because large molecular weights slow their clearance from the blood.⁶⁸ In addition to dendrimers, linear polymers conjugated to gadolinium(III) chelates have large molecular weights making them suitable blood pool agents. For example, a carboxymethyl dextran polymer linked to gadolinium(III) 1,4,7,10-tetraazacyclododecane-N,N',N'',N'''-tetraacetic acid (DOTA) with an amino spacer has been shown to be a blood pool agent in pigs and depicted infarcted myocardium.⁶⁹ Further, dysprosium(III) DTPA bis(methylamide) has assisted in characterization of myocardial perfusion defects as a T_2 enhancing agent.⁷⁰

Various iron oxide nanoparticles are suitable contrast agents for MRI angiography.^{71,72} Superparamagnetic iron oxide particles have been shown to accumulate in human atherosclerotic plaques which indicates potential for noninvasive assessment of active atherosclerotic disease.⁷³ Iron oxide nanoparticles have been used to visualize

macrophages after cerebral ischemia in rats and to differentiate reperfused myocardium from acutely ischemic tissue.^{74,75}

Diseases of the Gastrointestinal Tract

Imaging of the gastrointestinal (GI) tract is an area aided by MRI contrast agents. In order to successfully image the GI a contrast agent must possess the following properties: little or no absorption by the stomach or intestines, complete excretion, the absence of motion or susceptibility artifacts, affordability, and uniform marking of the GI tract.⁷⁶ Gadolinium(III) DTPA has been used to depict the lumen of the digestive organs in rats and diagnose and classify fistulas *in ano*.^{77,78} It is effective in the primary diagnosis of Crohn's disease and in differentiating nonactive from active forms of the disease.^{79,80} Gadolinium(III) DOTA has been used to examine the movement of material exiting the stomach and for diagnosis of delayed gastric emptying.^{81,82} Zeolites containing gadolinium have been shown to be an inexpensive, non-toxic alternative to X-ray and barium salts for imaging of the GI tract.⁸³⁻⁸⁵ Further, hectorite clay that has undergone ion exchange with gadolinium ions has been used as an oral contrast agent for GI tract imaging.⁸⁶ Superparamagnetic iron oxide agents have been used to image the GI tract and assess ulcerative colitis.^{36,87,88} Finally, monodisperse sulphonated styrene-divinylbenzene latex particles with supported ferrite gives good MRI contrast in rats with no observed susceptibility artifact.⁸⁹

Skeletal System Diagnosis

Contrast agent enhanced MRI is a valuable resource in the study of diseases related to the skeletal system. MRI is the method of choice for diagnosing rheumatoid and osteoarthritis⁹⁰ because gadolinium(III) chelates can detect rheumatoid arthritis

earlier than X-ray.⁹¹⁻⁹⁴ Imaging of the cerebrospinal fluid compartment of rats was accomplished by intrathecal injecting of gadolinium(III) DTPA,⁹⁵ while MRI discography aided by gadolinium(III) DTPA or a mixture of gadolinium(III) DTPA and the dendrimer based contrast agent Gadomer-17 may be an acceptable substitute for the imaging of disc pathology.^{96,97}

Other diseases

Gadolinium(III) DTPA can be used to stage and differentiate the two types of pancreatitis without radiation or renal damage.^{98,99} Gadodiamide enhanced MRI is useful for early diagnosis of Nelson's syndrome.¹⁰⁰ The kidneys are the most important organs that maintain homeostasis. Gadolinium(III) DTPA enhanced MRI can be used to examine kidney function and monitor progress in kidney transplant patients.^{90,101} The dendrimer G4D-(1B4M-Gd)₆₄ has been used for in vivo observation of damage to the kidneys and is a potentially useful contrast agent for renal screening post trauma or after harmful therapies such as chemotherapy or radiation therapy.¹⁰² Contrast agent enhanced MRI has been used to image the lymph nodes using micelles¹⁰³ and liposomes¹⁰⁴ containing gadolinium(III) DTPA as well as dextran coated iron oxide particles.^{105,106} To image the liver and diagnose diseases such as cirrhosis, several metal-based contrast agents have been used. These include iron oxide nanoparticles,¹⁰⁷⁻¹⁰⁹ liposomes containing gadolinium(III) HPDO3A,¹¹⁰ MnDPDP,¹¹¹ and a modified gadolinium(III) DTPA conjugate of polylysine.¹¹² OmniscanTM has been used to study thrombosis in rats,¹¹³ and MION particles have been used to help quantitatively evaluate pigmented choroidal melanoma in rabbits and can be a noninvasive method of eye imaging.¹¹⁴

Targeted Delivery of Contrast Agents

As can be seen from the previous section, MRI contrast agents can be used to aid in the diagnosis of many diseases; however, the agents described thus far have the limitation of being non-site specific. The inability to localize selectively in a desired area lessens the diagnostic potential of these agents. The first step toward improving the diagnostic capability of contrast agents is to make them target specific and accumulate in desired biological locations. A summary of attempts towards this goal will be divided into gadolinium and iron oxide based contrast agents; however, this chapter cannot address every aspect of the growing area of contrast agent delivery. For more on this topic see reviews by Weissleder et al.¹¹⁵ and Okuhata.¹¹⁶

Contrast Agent Delivery

Gadolinium(III)-Containing Agents

Many attempts have been made to deliver gadolinium(III) chelates to specific biological targets. An aminoxy-functionalized DTPA derivative that is tumor specific has been synthesized by taking advantage of the fact that tumor cells overexpress sialic acid residues.¹¹⁷ A DOTA derivative conjugated to the HIV-Tat peptide has the ability to be internalized into many different cell lines unlike unmodified chelates that are not internalized into cells.¹¹⁸ Liposomes containing gadolinium were conjugated to mouse antibodies and successfully targeted to ICAM-1, an endothelial leukocyte receptor upregulated on cerebral microvasculature during experimental autoimmune encephalitis.¹¹⁹ Polylysine labeled with gadolinium(III) DTPA and transferrin can image cells expressing the transferrin receptor.¹²⁰ Further, this polymer has been modified with an anti-CEA F(ab')₂ immunoconjugate to image colorectal carcinoma.¹²¹ Dendrimers

labeled with gadolinium(III) DTPA have been conjugated to folate and used to successfully image tumor cells which are expressive of the high-affinity folate receptor in mice.^{122,123} Specific, noninvasive imaging of angiogenesis in rabbits was accomplished using an antibody to the angiogenesis marker endothelial integrin $\alpha_v\beta_3$ conjugated to gadolinium containing liposomes¹²⁴ and perfluorocarbon-nanoparticles.¹²⁵

Iron Oxide Agents

Iron oxide nanoparticles have been developed into targeted contrast agents. Similar to DOTA, magnetic nanoparticles have been functionalized with the HIV-Tat peptide, and cells internalize the resulting agents in a similar fashion to their gadolinium(III)-containing counterparts.^{126,127} Recently, Annexin V (a protein that binds to phosphatidylserine) labeled nanoparticles have been used to image apoptosis.^{128,129} Phosphatidylserine moves from the interior to the exterior of a cell membrane when a cell undergoes apoptosis. This agent is potentially useful for in vivo imaging of apoptosis resulting from diseases involving excessive apoptosis such as heart failure, transplant rejection, or aplastic anemia. In another case, human transferrin was covalently coupled to an USPIO particle and used to detect tumors in rats due to the specificity of transferrin-mediated endocytosis in the tumor cells.¹³⁰

Cross-linked iron oxide (CLIO) particles labeled with anti-human E-selectin (CD62E) F(ab')₂ fragments were used to image E-selectin expression which occurs on endothelial cell surfaces.¹³¹ The agent was successful in vitro and if successful in vivo, holds the potential to detect early signs of tumor angiogenesis, arthritis, and atherosclerosis. SPIO particles were coated with monoclonal antibodies directed against epidermal growth factor receptors, which are overexpressed in esophageal squamous cell

carcinoma.¹³² This agent was used successfully in a rat model of esophageal cancer, one of the most malignant and hard to treat tumors known.

Penetrating the Blood Brain Barrier

The blood brain barrier (BBB) is one of the most challenging physical hurdles when designing contrast agents intended for the brain. The BBB contains various mechanisms for minimizing the flow of material into and out of the brain.^{5,133} This barrier prevents most passive diffusion except by extremely small molecules such as water and ethanol. Electric charge, lipid solubility, and molecular weight can be used to help predict whether or not a molecule will cross the BBB.¹³⁴

Brain tumors have a fenestrated BBB and diseases such as multiple sclerosis have episodes that involve temporary weakening of the BBB. Gadolinium(III) DTPA,^{133,135} gadolinium(III) BOPTA,¹³⁶ and MION particles^{137,138} have all been used to image these BBB breakdowns. In addition, a method used to image rat brains has been the injection of superparamagnetic iron oxide particles directly into the brain.^{139,140} Further, manganese(II) chloride can map active regions of the brain because the manganese(II) ion enters excitable cells through voltage-gated calcium channels.⁹ One recent development in the delivery of contrast agents into the brain involves the conjugation of putrescine (an endogenously occurring polyamine that is known to increase BBB permeability) to an **Ab** peptide linked to gadolinium(III) DTPA. This agent successfully crossed the BBB as predicted.¹⁴¹

Imaging Biochemical Events

Targeted contrast agents may greatly improve the accuracy and scope of diagnostic imaging. Another class of contrast agents that will significantly affect the

field of MRI is activatable agents. Activatable agents are relatively new; however, this class of agents offers the potential for potent diagnostic tools.

The agents described thus far share the common property of enhancing MRI images at all times. Conversely, activatable agents possess two distinct states. One state is *off* and corresponds to low contrast enhancement, while the other state, the *on* state, corresponds to high contrast enhancement. An activatable agent can be *switched* from one state to the other by the occurrence of a metabolic or physiological event. The design of this new class of agents exploits the fundamental means by which a paramagnetic species affects the intensity of an image acquired by MRI.

Some *switches* used to activate gadolinium(III) agents are variables in the Solomon-Bloembergen equations and include q , t_r , and t_m , which were described earlier in this chapter. Increasing q or t_r or decreasing t_m to an optimal value leads to a decrease in T_1 resulting in higher contrast enhancement. Another class of activatable lanthanide based agents makes use of a chemical exchange saturation transfer (CEST) event as the *switch*. Finally, activation of iron oxide agents is due to the enhanced anisotropy caused by the dipolar coupling between nearby crystals of aggregated USPIO. This enhanced anisotropy leads to a dramatic decrease in T_2 .

Enzymatically Activated Contrast Agents

The first example of an enzymatically activated contrast agent was prepared by Meade and coworkers (**Figure 1.7**).^{142,143} This agent is activated in the presence of *b*-galactosidase and is a gadolinium(III) chelate modified with galactopyranoside such that water access to the gadolinium(III) is restricted. When the environment of the agent becomes rich in *b*-galactosidase, the galactopyranoside is cleaved thereby allowing water

to access the gadolinium(III) and increasing q . This increase in q increases the relaxivity of the contrast agent.

Anelli and coworkers have synthesized a DTPA derivative which can detect carbonic anhydrase (**Figure 1.8**).¹⁴⁴ The gadolinium complex contains a sulfonamide group in place of one of the carboxylic acid arms of the DTPA, helping it to selectively target the enzyme carbonic anhydrase. Upon binding to the enzyme, the relaxivity increases significantly (approximately five fold at 40 MHz). This increase in relaxivity is due to an increase in t_r caused by binding to the large enzyme.

Nivorozhkin and coworkers prepared an agent that is sensitive to the presence of human carboxypeptidase B (a thrombin-activatable fibrinolysis inhibitor (TAFI)), which has been implicated in thrombotic disease (**Figure 1.9**).¹⁴⁵ TAFI cleaves a trylisine masking group attached to the agent exposing an aromatic functional group. This aromatic group has a high binding affinity for human serum albumin (HSA). The contrast agent binds HSA leading to an increase in t_r resulting in an increase in relaxivity. This event is known as a receptor-induced magnetization enhancement (RIME). The trylisine chain makes this agent a pro-RIME agent because the trylisine chain inhibits interaction with HSA.

Bogdanov and coworkers prepared a peroxidase activatable agent.¹⁴⁶ This agent consists of a gadolinium(III) chelate linked to benzene-1,2-diol that acts as a monomer. In the presence of peroxide, the monomers are oligomerized yielding a threefold increase in relaxivity due to an increase in t_r . This MRI signal amplification (MRamp) can detect peroxidase concentration in vitro and has been used to detect E-selectin expression on

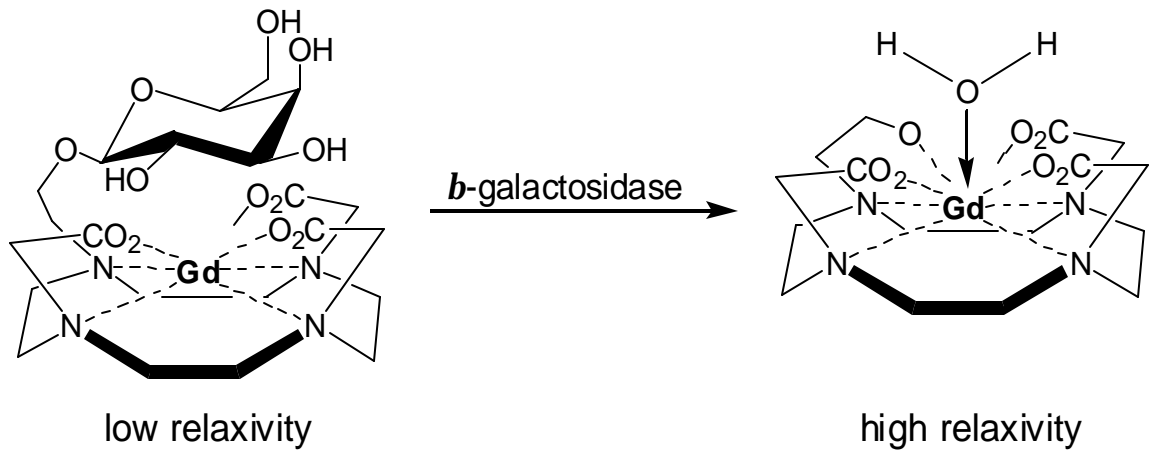


Figure 1.7: MRI contrast agent activated by β -galactosidase.¹⁴²

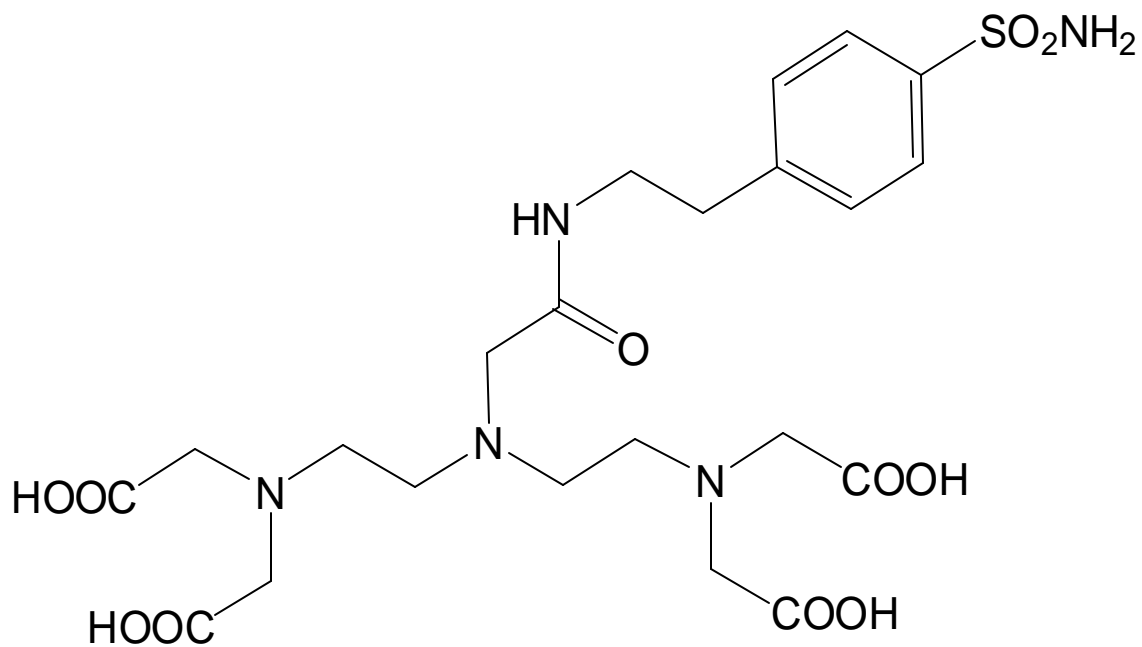


Figure 1.8: DTPA-based carbonic anhydrase sensitive contrast agent (ligand only).¹⁴⁴

human endothelial cells in cell culture by imaging the high local enzymatic activity of antibody-bound peroxidase associated with the plasma membrane of these cells.

Perez and coworkers have utilized the difference in relaxivity between solitary CLIO particles and those in close proximity to other CLIO particles to detect DNA-cleaving agents (**Figure 1.10**).¹⁴⁷ Two strands of complementary DNA are each conjugated to a CLIO particle. When the complementary strands bind, the CLIO particles from each strand come into close proximity to each other. Upon cleavage of the double strand by a DNA-cleaving agent, the two CLIO particles become separated leading to a detectable change in relaxivity.

Utilizing a similar mechanism, Zhao and coworkers have developed a protease sensitive MRI contrast agent (**Figure 1.11**).¹⁴⁸ With this agent, the strong interaction between biotin and avidin is exploited. A molecule of biotin is conjugated to each side of a peptide that is cleaved by proteases. CLIO particles coated with avidin are exposed to the bi-biotinylated peptides. In the presence of protease specific for the peptide, the CLIO particles will not aggregate; however, in the absence of protease, aggregation of the CLIO particles will occur resulting in an increase in relaxivity. Currently this agent has only been used in vitro.

Contrast Agents to Detect Biologically Significant Molecules

Iron is a key element in biology and in many enzymes. An iron-sensitive contrast agent was synthesized by Aime and coworkers by functionalizing DTPA with salicylate moieties as shown in **Figure 1.12**.¹⁴⁹ Upon addition of iron(III), the gadolinium(III) DTPA-salicylate complexes bind to the iron ions via the salicylate functional groups. This binding yields an increase in t_r and relaxivity. Recently, using a similar approach,

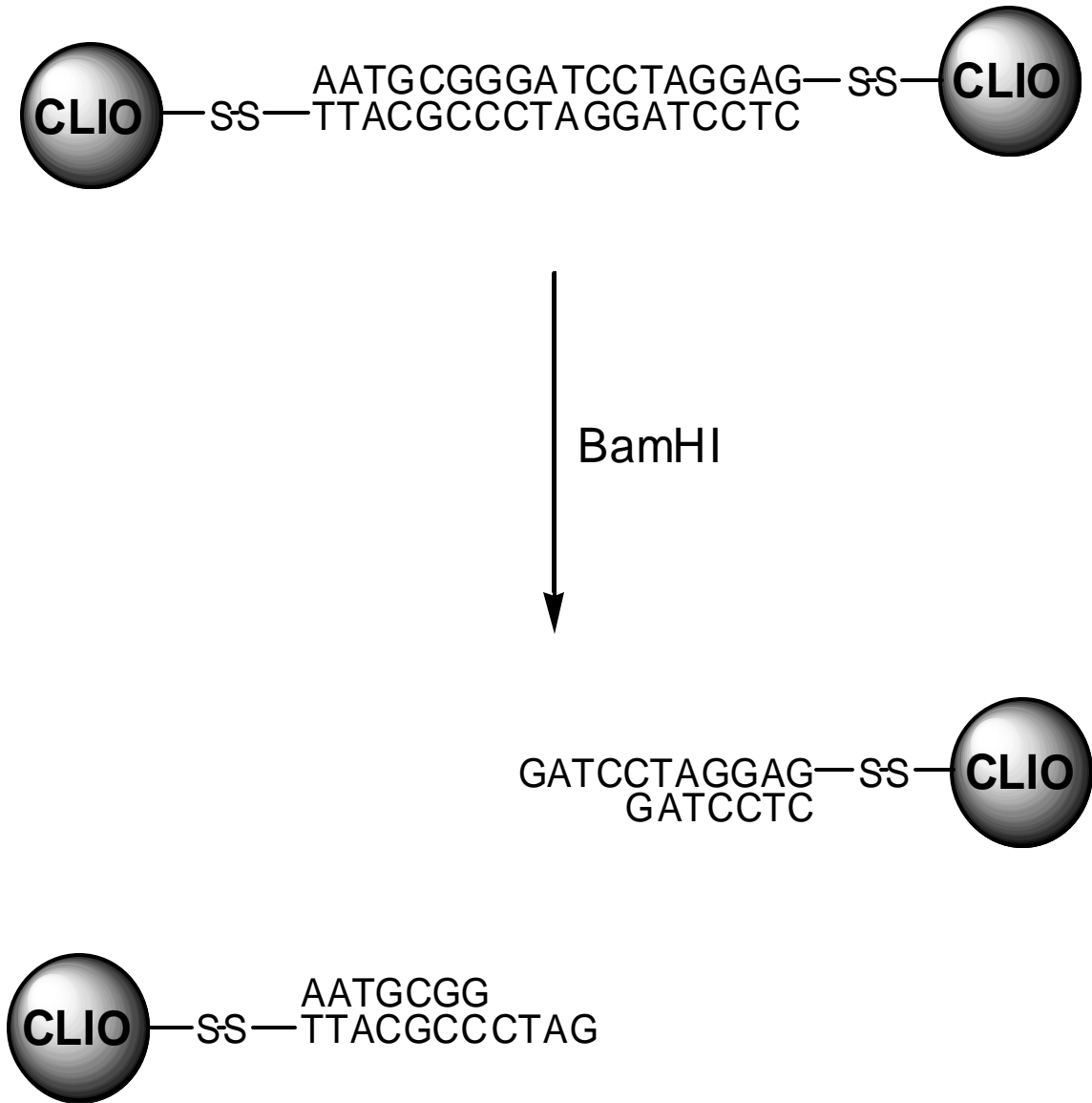


Figure 1.10: Contrast agent that detects DNA cleaving agents.¹⁴⁷

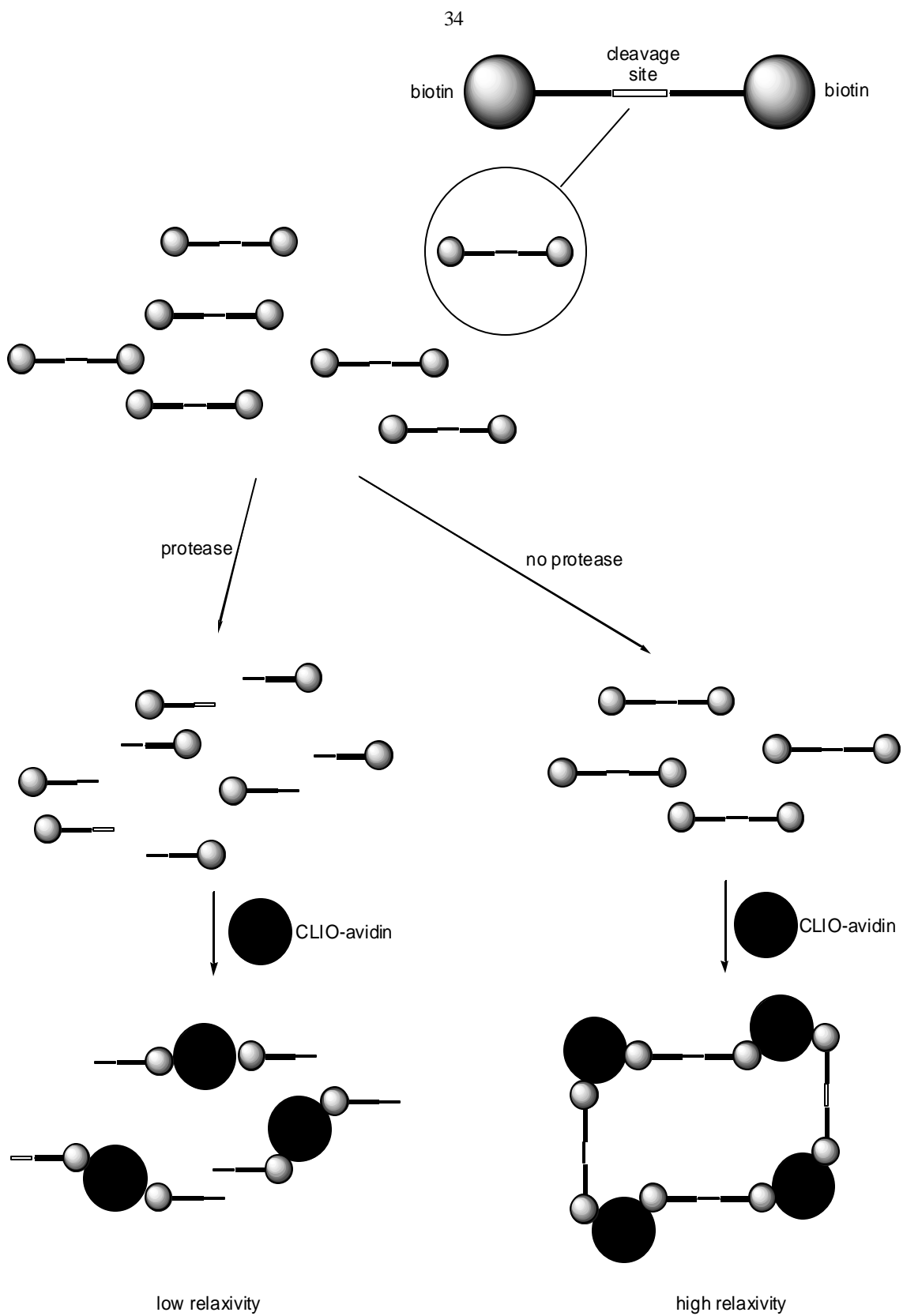


Figure 1.11: CLIO-based contrast agent that is sensitive to the presence of proteases.¹⁴⁸

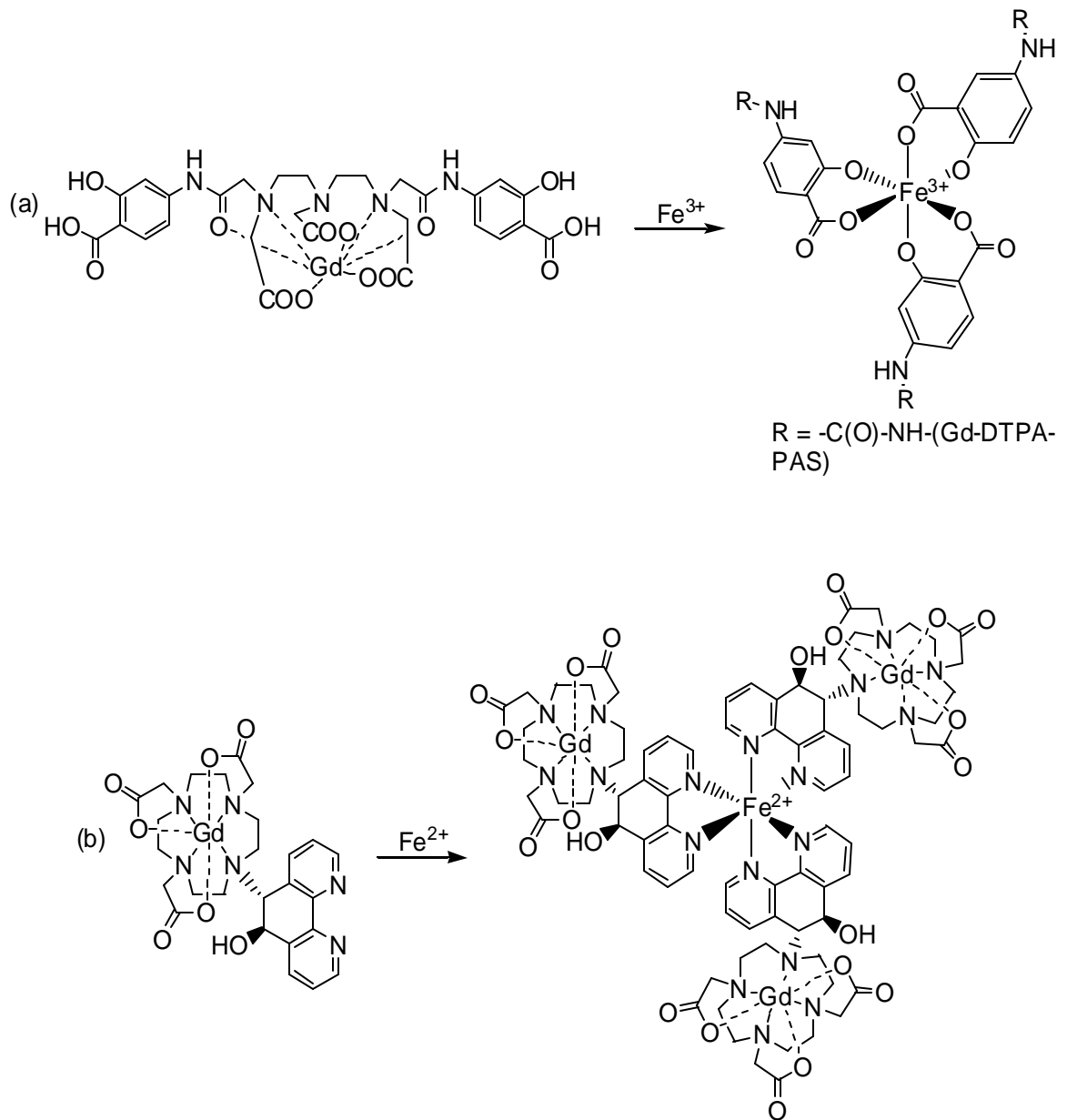


Figure 1.12: Contrast agents sensitive to the presence of iron ions.^{149,150}

another iron-sensitive contrast agent was designed.¹⁵⁰ This time, DOTA was conjugated to the ligand 5,6-dihydrophenanthroline. Self-assembly around iron(II) ions leads to an increase in t_r and a subsequent increase in relaxivity from 5.1 to 12.5 mM⁻¹s⁻¹.

An important intracellular secondary messenger of signal transduction is calcium(II). Changes in the cytosolic concentration of calcium(II) trigger changes in cellular metabolism and are responsible for cell signaling and regulation. Li and coworkers have developed a contrast agent that can specifically detect calcium ions (**Figure 1.13**).^{151,152} This agent is a gadolinium-based and possesses two limiting conformational states with regard to calcium(II) concentration. In the absence of calcium(II), the aromatic aminoacetates of the ligand interact with the two gadolinium(III) ions. In the presence of calcium(II), the aromatic iminoacetates rearrange to bind calcium(II) thereby allowing water to bind directly to gadolinium(III). This increase in q yields an increase in relaxivity.

A DTPA-based gadolinium contrast agent that differentiates between oxygenated and deoxygenated hemoglobin was created by Aime and coworkers (**Figure 1.14**).¹⁵³ The complex contains two boronic acid moieties that enable it to bind to hemoglobin. There is a threefold difference in relaxivity between when the agent is bound to oxygenated versus deoxygenated hemoglobin. This difference is attributed to the different binding states that the agent has with hemoglobin in each of the two states.

The partial pressure of dioxygen is relevant in various pathological conditions including strokes and tumors. Aime and coworkers have developed a dioxygen pressure responsive contrast agent based on manganese porphyrins.¹⁵⁴ The porphyrin complex is encapsulated into poly-*b*-cyclodextrins to prevent dimerization and to increase t_r . At low

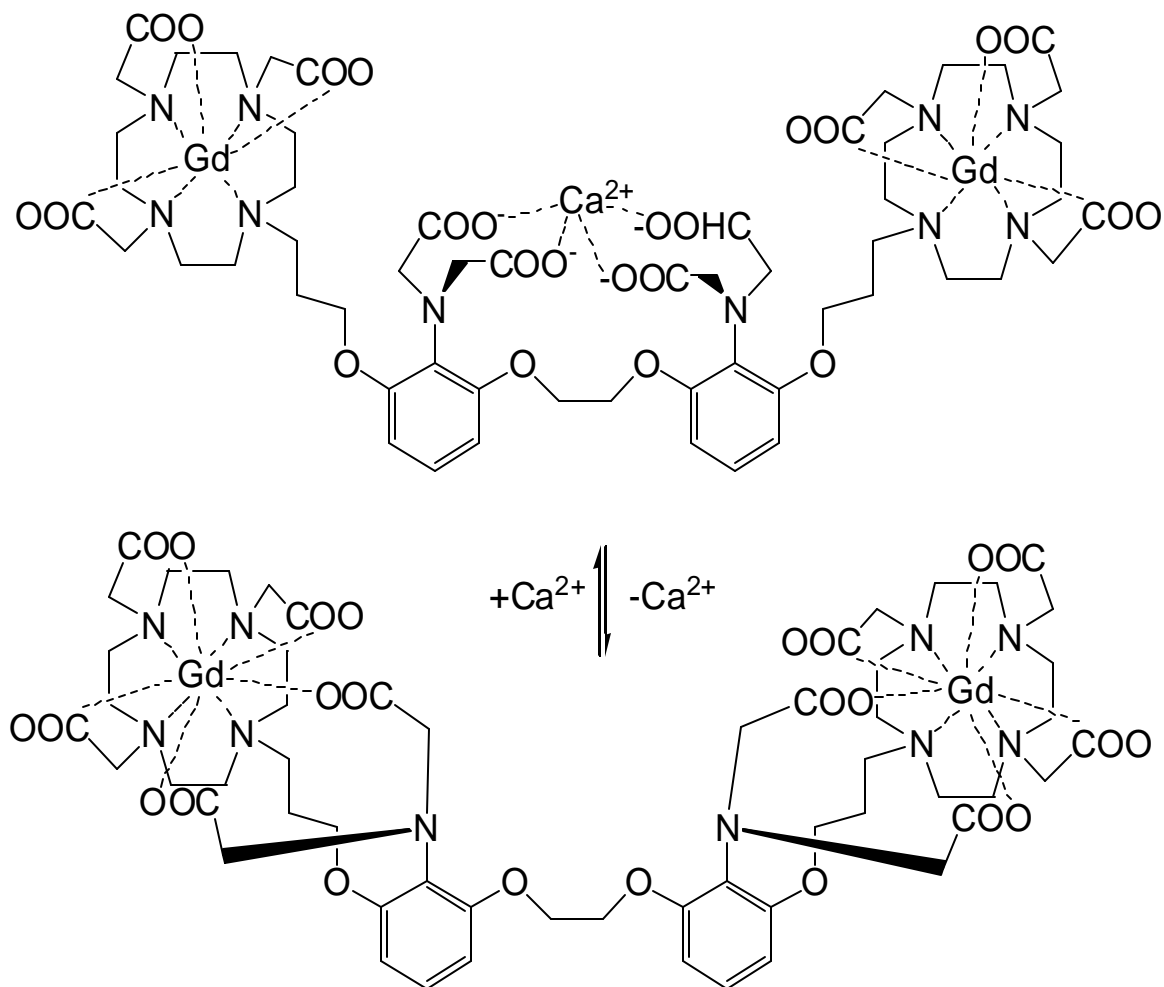


Figure 1.13: Contrast agent sensitive to the presence of calcium(II).¹⁵¹

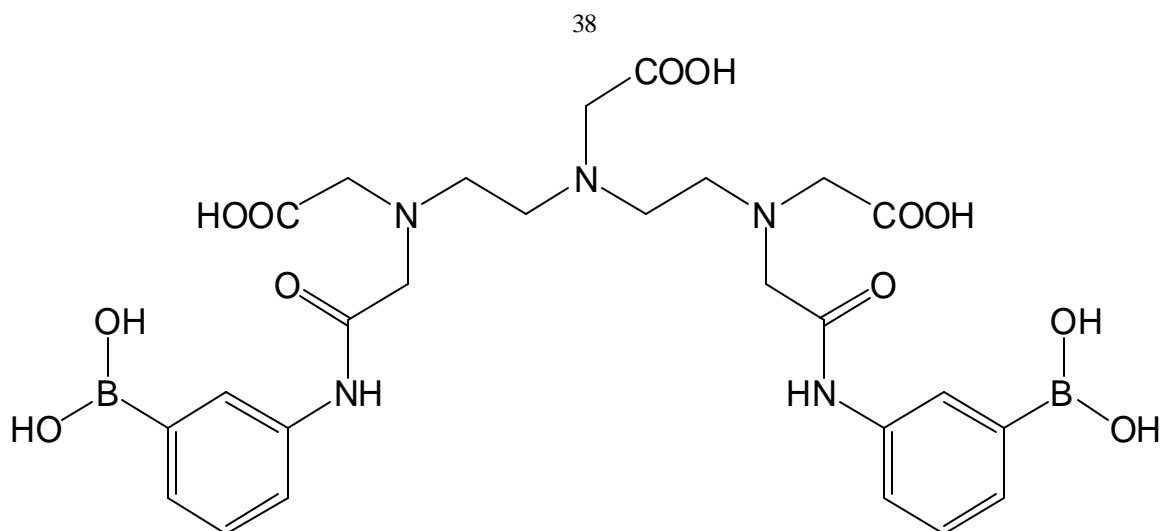


Figure 1.14: Contrast agent that differentiates between oxygenated and deoxygenated hemoglobin (ligand only).¹⁵³

partial pressures of dioxygen, the complex exists as a manganese(II) complex. After addition of dioxygen, the complex is oxidized to the manganese(III) complex. The relaxivity of manganese(II) is dependant on reorientation time while the relaxivity of manganese(III) is not. By increasing t_r , the relaxivity of the manganese(II) complex is increased fourfold while the relaxivity of the manganese(III) complex remains essentially unchanged. The agent has a good correlation between relaxivity and the partial pressure of dioxygen from zero to 40 torr of dioxygen.

Josephson and coworkers have developed a CLIO agent that can detect specific DNA sequences (**Figure 1.15**).¹⁵⁵ A DNA strand complementary to the target DNA strand is synthesized in two parts. CLIO particles are then modified with multiple copies of one of the complementary parts. Upon mixing of the modified CLIO particles with the target DNA strand, DNA hybridization followed by oligomerization of the CLIO particles occurs resulting in an increase in relaxivity.

Zinc is a key component of many enzymes, transcription factors, and synaptic vesicles. Hanaoka and coworkers have developed a series of contrast agents to detect zinc(II).^{156,157} Their design consists of gadolinium(III) DTPA modified with pyridine ligands and carboxylic acids (**Figure 1.16**). In the absence of zinc(II), water is bound to the gadolinium(III) ion. In the presence of zinc(II), the carboxylic acid and pyridine moieties coordinate to zinc(II) thus restricting the access of water to the gadolinium(III) ion. This decrease in q yields a decrease in relaxivity in the presence of zinc(II).

Overproduction of *L*-lactate occurs when the anaerobic glycolysis pathway becomes relevant in strokes, brain tumors, cysts, radiation therapy, metabolic disorders, and brain activation. Aime and coworkers have created a CEST agent that is responsive

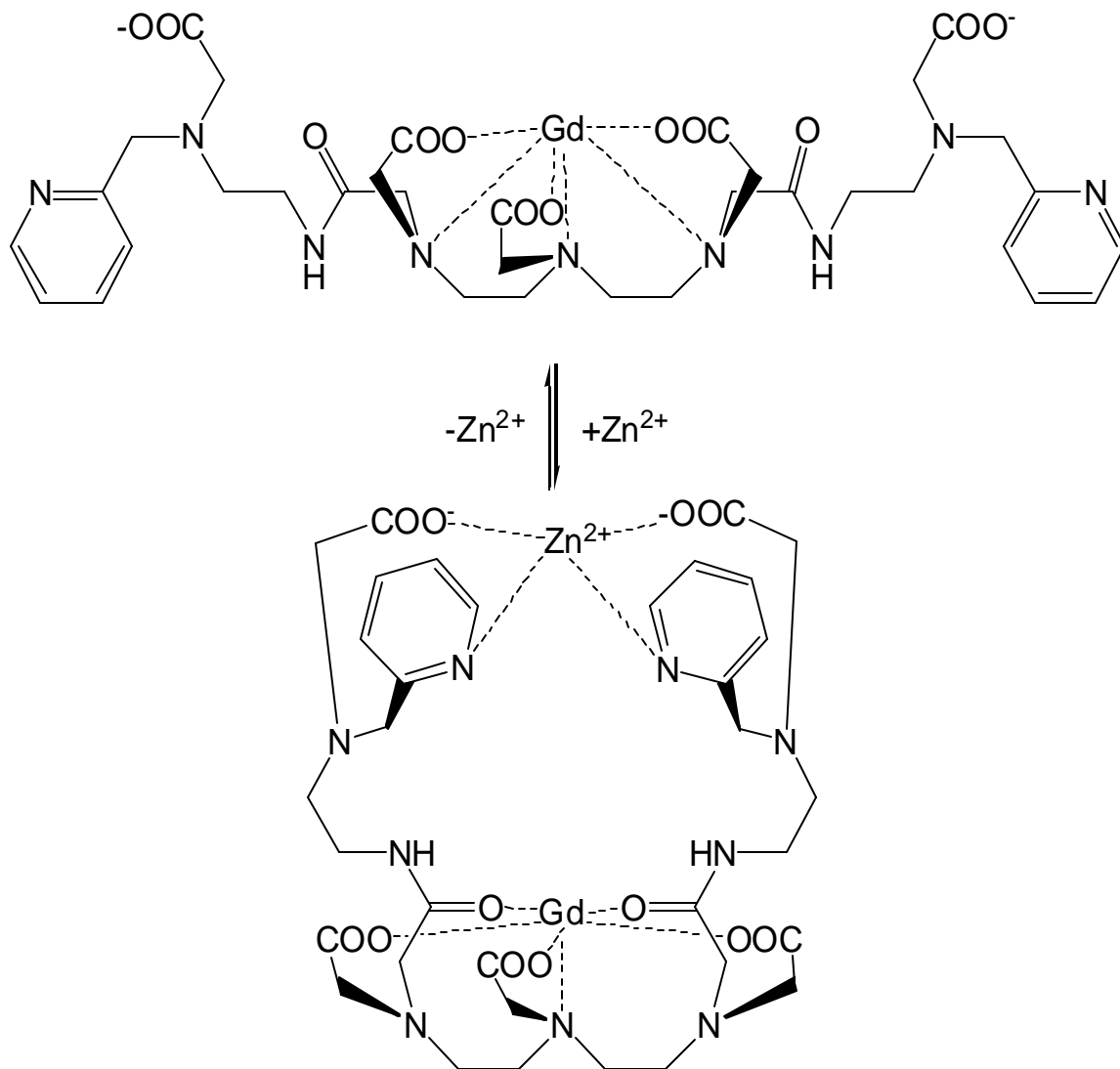


Figure 1.16: Contrast agent specific for zinc(II).¹⁵⁷

to lactate concentration (**Figure 1.17**).¹⁵⁸ The agent is an ytterbium(III) complex which changes Δn (the chemical shift separation in Hz between interchanging bound and bulk water proton pools) when the complex is bound to lactate. By irradiating the exchanging proton pool, saturation transfer to the water resonance occurs decreasing the water signal intensity, which determines the contrast in MRI.

Glogard and coworkers have prepared a MRI contrast agent that is responsive to the presence of radicals (**Figure 1.18**).¹⁵⁹ In this agent, gadolinium(III) chelates are conjugated to a liposome via a disulfide linker. The long reorientational motion of the liposome leads to an approximate doubling of the relaxivity of the liposome versus the free gadolinium(III) complexes. Upon exposure to radicals, the gadolinium(III) chelates are cleaved from the liposome, thus reducing the relaxivity of the agent.

pH-sensitive Agents

Increased glycolytic activity may cause a significant pH decrease in the extracellular region of certain tumors relative to surrounding healthy tissue. Because pH is an important physiological indicator, many research groups have designed pH-sensitive contrast agents. Mikawa and coworkers developed a MRI contrast agent that is responsive to pH (**Figure 1.19**).¹⁶⁰ The agent is based on a microenvironmental responsive polyion complex in the form of a mixture of two polymers. The complex exhibits a fifty percent increase in relaxivity upon decreasing pH from 7.0 to 5.0. The mechanism of how the complex works is unknown; however, it is detectable in the presence of tumors in mice but is not in the absence of tumors.¹⁶¹

Aime and coworkers have developed a pH-sensitive contrast agent with thirty gadolinium(III) chelates and 114 ornithine residues (**Figure 1.20**).¹⁶² The chelates are

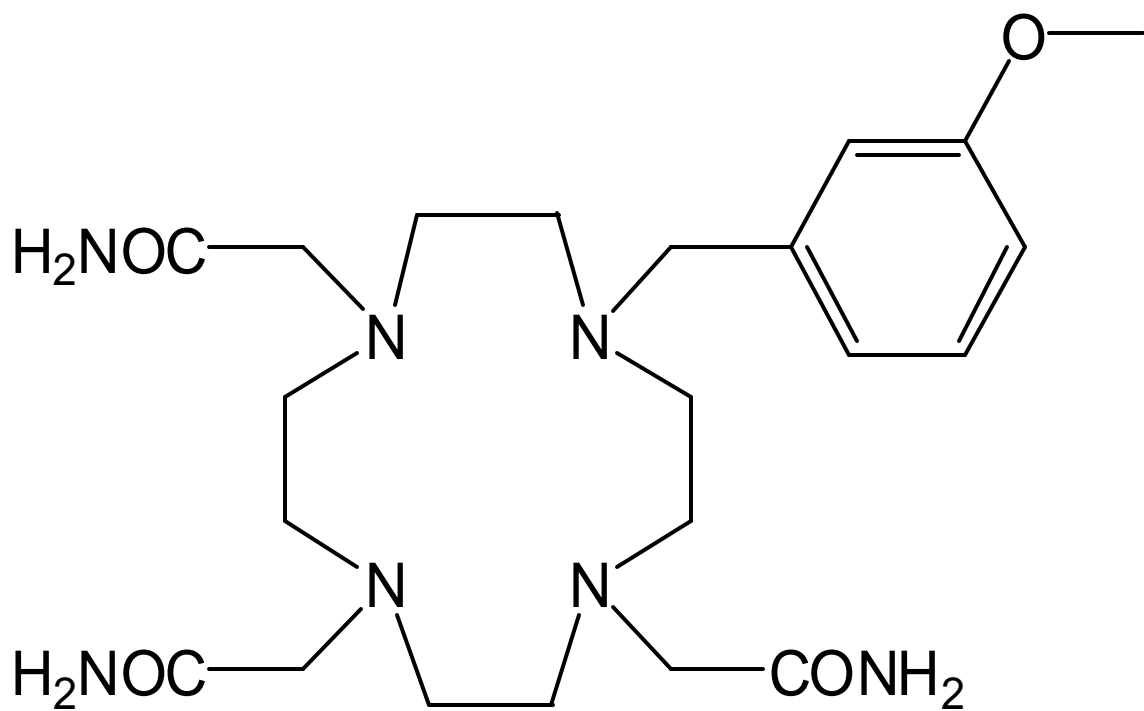


Figure 1.17: CEST contrast agent (ligand only) sensitive to *L*-lactate.¹⁵⁸

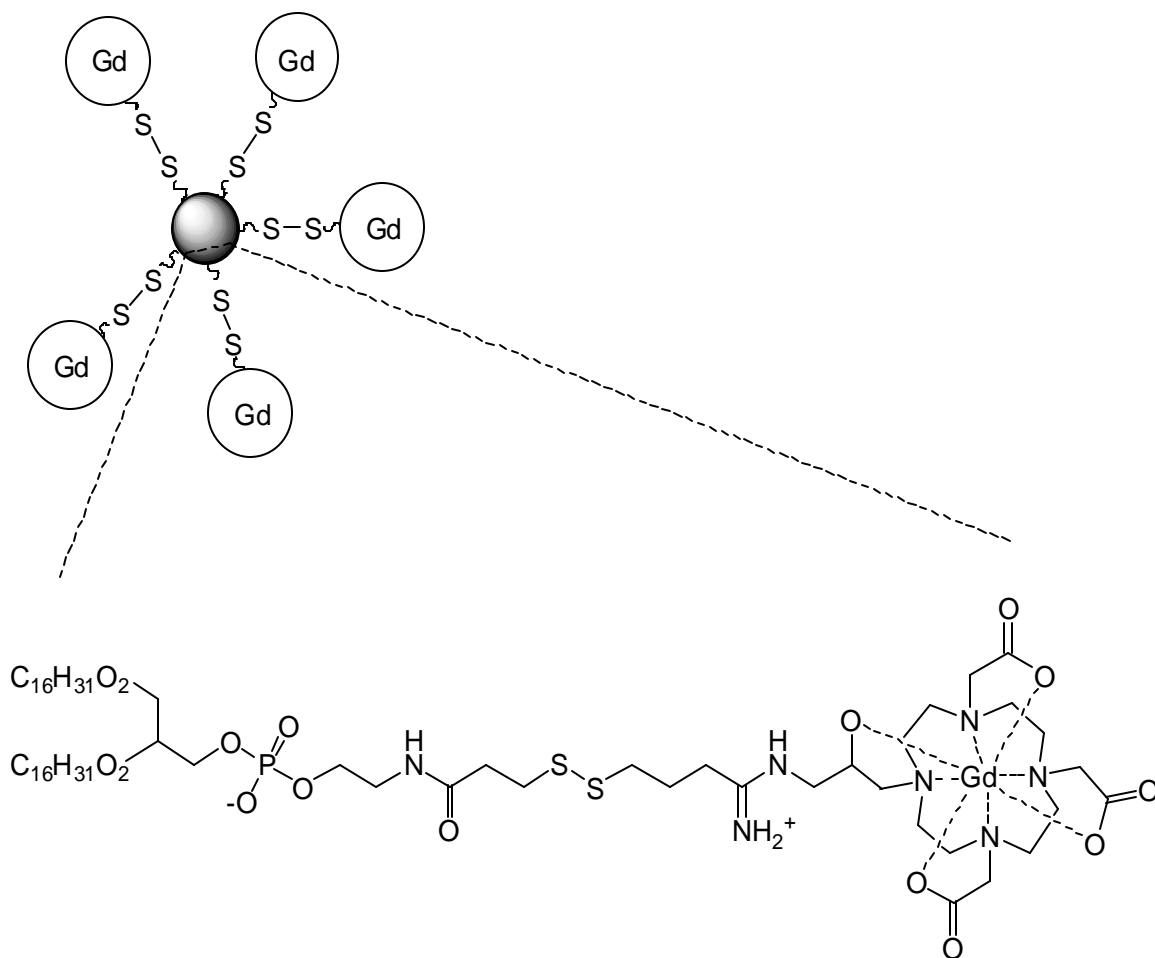


Figure 1.18: Schematic representation of a liposome based radical-responsive MRI contrast agent.¹⁵⁹

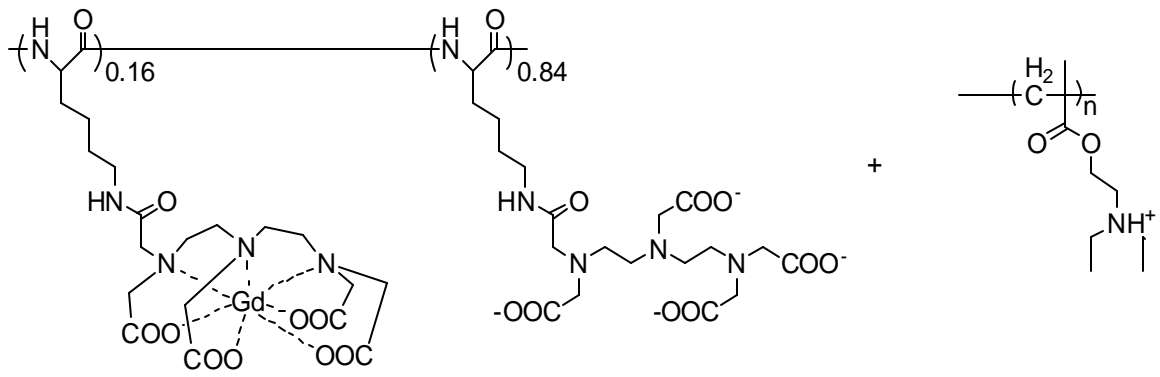


Figure 1.19: Contrast agent sensitive to pH based on a polyion complex composed of a mixture of two polymers.¹⁶⁰

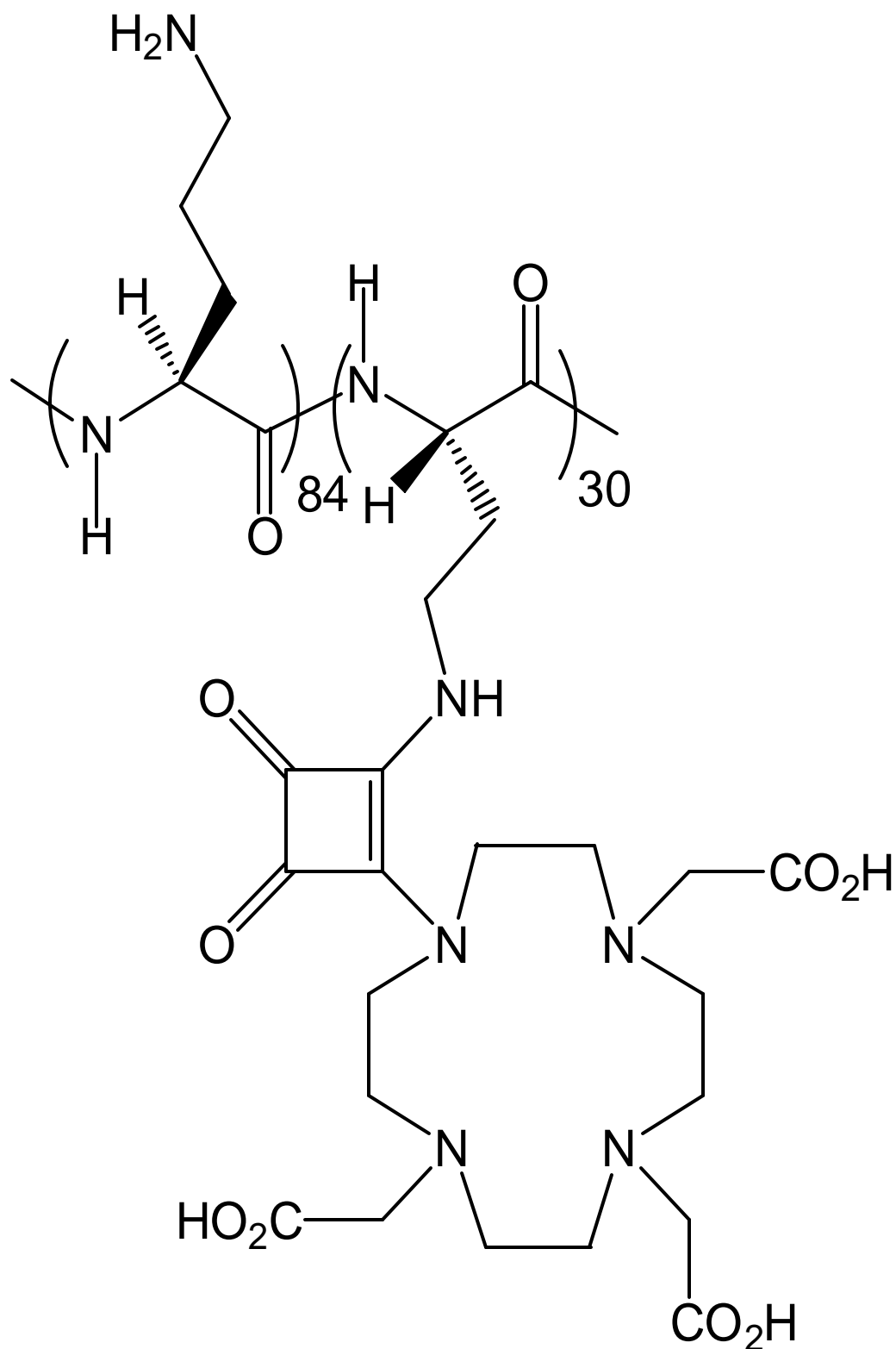


Figure 1.20: Contrast agent sensitive to pH based on a squaric ester containing polymer (ligand only).¹⁶²

conjugated to the amino acid chain via squaric esters, which readily react with amines. At low pH, the amines are protonated and do not interact with the squaric ester residues. When the pH rises, the amine side chains become deprotonated and interact with the squaric ester linkers. This interaction rigidifies the polymer creating an increase in t_r , which results in an increase in relaxivity. This agent is sensitive in the physiological range from pH 4.5 to 8.5.

Zhang and coworkers have developed a pH-sensitive contrast agent which is a tetraamide-based macrocyclic ligand with extended phosphonate noncoordinating side arms (**Figure 1.21**).¹⁶³ The agent demonstrates an increase in relaxivity upon increasing pH from 4 to 6. The relaxivity then decreases upon further increase of pH until 8.5. The change in relaxivity is ascribed to protonation of the phosphate side arms. Protonated side arms are believed to catalyze exchange of coordinated water molecules resulting in increased relaxivity reaching a maximum at pH 6. Below pH 6, the phosphate arms are over-protonated and interfere with water exchange resulting in the decrease in relaxivity. At pH above 6, the phosphate arms are not completely protonated resulting in slower water exchange and lower relaxivity.

Hovland and coworkers have developed a pH-sensitive contrast agent which is a DO3A derivative with a tertiary amine-containing side arm (**Figure 1.22**).¹⁶⁴ The side arm amine contains two long alkyl chains. When the amine is protonated (pH 3-6) the relaxivity is low. Upon deprotonation (pH 8-10), the agents form colloidal aggregates due to the higher lipophilicity of the deprotonated complex. The aggregation causes an increase in t_r and a subsequent increase in relaxivity of 142%.

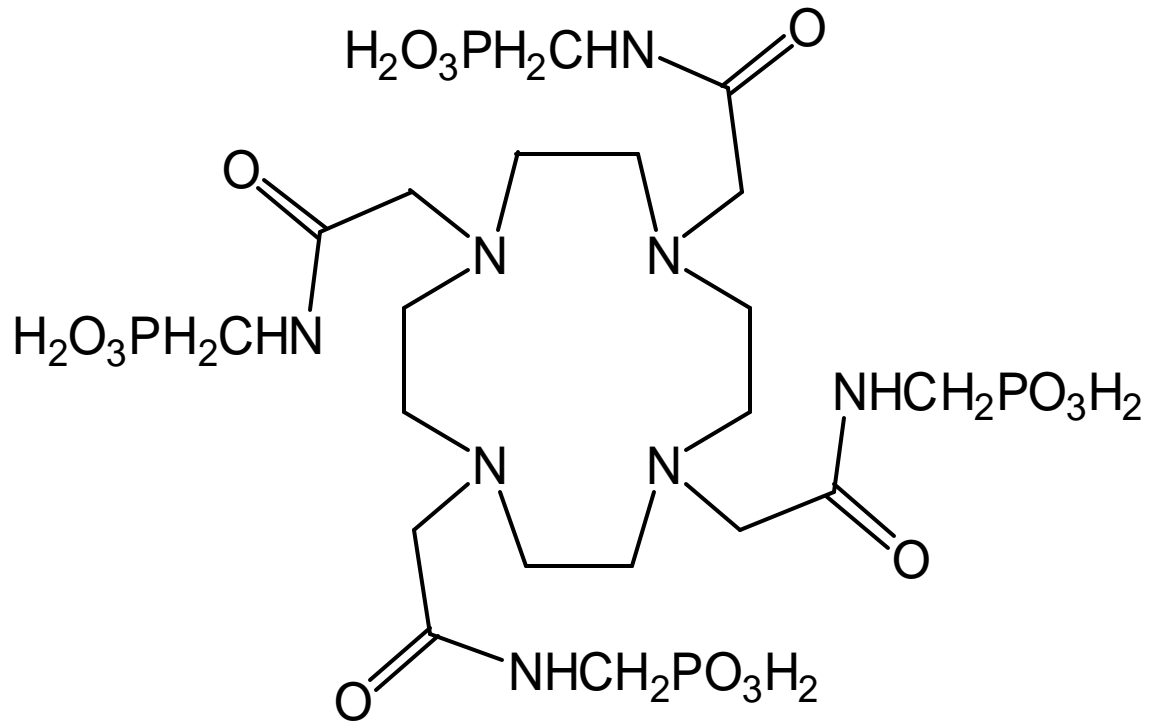


Figure 1.21: Contrast agent sensitive to pH based on a phosphate containing DOTA derivative (ligand only).¹⁶³

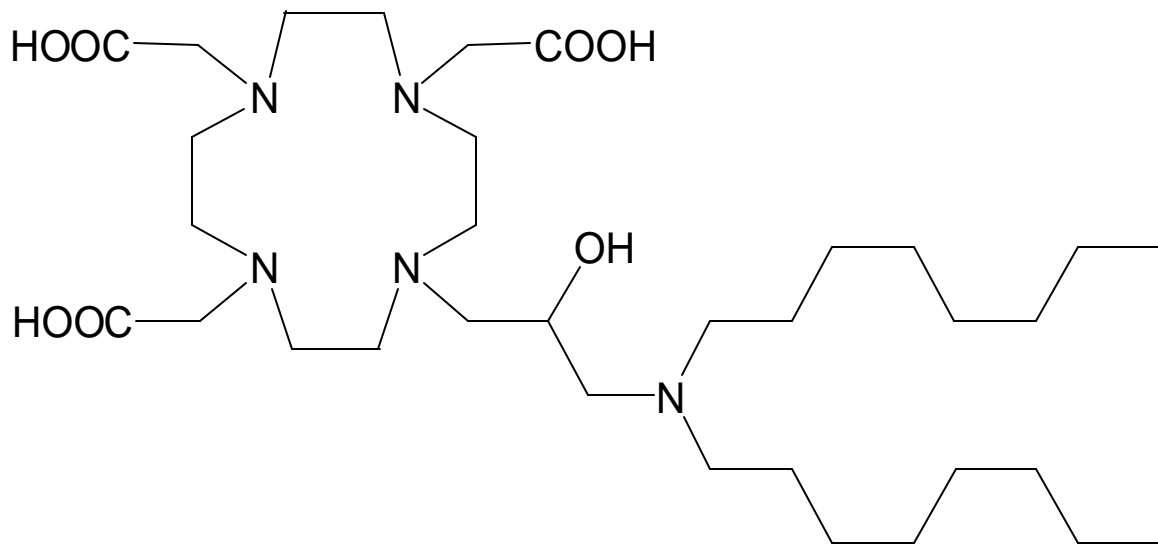


Figure 1.22: Contrast agent sensitive to pH based on amphilic molecules (ligand only).¹⁶⁴

Finally, Aime and coworkers have created a CEST agent which is responsive to changes in pH (**Figure 1.23**).¹⁶⁵ The agent is an ytterbium(III) complex of the tetraglycineamide derivative of DOTA. Saturation of the amide protons that are in close proximity to the paramagnetic center results in the best CEST agents to date. The observed effect is pH-dependent since k_{ex} for amide protons is pH-modulated. By irradiating the amide N-H resonances, saturation transfer to the water resonance occurs (increasing with pH from pH 5.5 to 8.1) leading to a decrease in the water signal intensity which determines the contrast in MRI.

Conclusions and Outlook

This chapter discussed the wide range of chemical and biological applications that exist for MRI contrast agents. Contrast agent enhanced MRI is an invaluable tool to the diagnosis of cancer and many other diseases, and recently in molecular imaging of experimental animals. With improved targeted delivery of these agents, the ability to diagnose diseases will become more sensitive, accurate, and ultimately simplified. Finally, activatable agents that respond to biological phenomena by altering the intensity of signal enhancement in a conditional fashion are steps toward unraveling the complex connectivity of developmental biological systems. Further, these agents may represent the prelude to complete, noninvasive, medical examinations that are safe, fast, and accurate.

Scope of Thesis

The design and synthesis of advanced MRI contrast agents is the focus of this thesis. Current, clinically used agents aid in the visualization of the extracellular space or blood pool in MRI. In order to further the usefulness of contrast agents, chemistry needs

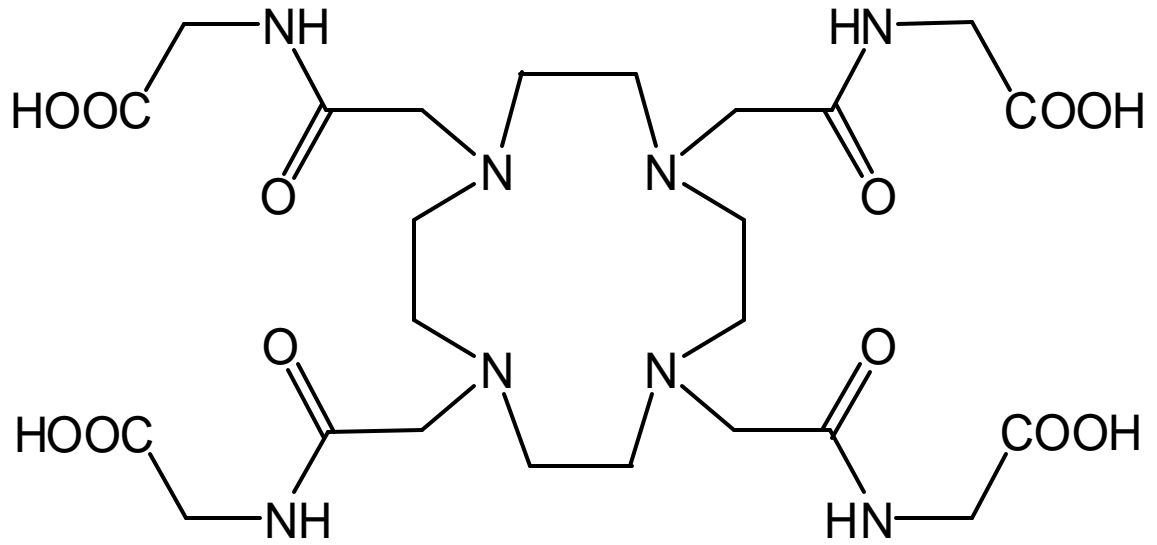


Figure 1.23: Contrast agent sensitive to pH based on CEST effects (ligand only).¹⁶⁵

to be used to develop agents that are responsive to biological phenomena and directed to specific regions. These two improvements are closely related in that many biologically significant molecules are located in specific parts of the body. An introduction into the field of MRI and contrast agents is presented in Chapter 1 along with a description of current diagnostic uses for contrast agents. Chapter 1 proceeds to outline previous literature attempts at site-specific delivery of contrast agents and the development of biologically responsive contrast agents.

In Chapters 2-4, efforts towards the design, synthesis, and testing of advanced contrast agents are presented. Many interesting biological targets for imaging reside inside the cell membrane. As the current generation of contrast agents is strictly extracellular, a method of intracellular delivery is needed in the field of MRI contrast agents. Cationic polyarginine oligomers were used to deliver gadolinium(III)-based contrast agents into the interior of cells (Chapter 2). The delivery was confirmed and studied using many orthogonal methods including inductively coupled plasma-mass spectrometry (ICP-MS), MRI, and the first published example of two-photon laser microscopy (TPLM) to image lanthanide based MRI contrast agents (Chapter 2). In Chapter 3, the synthesis of a series of contrast agents designed to cross the blood brain barrier (BBB) and label the A β -plaques associated with Alzheimer's disease is described. These agents were found to permeate cell membranes, and in Chapter 3, the intracellular properties of these agents are compared to the polyarginine agents from Chapter 2. In Chapter 4, attempts towards the creation of an advanced MRI contrast agent that is chemically altered by the activity of matrix metalloproteinases (MMPs) are revealed. Additionally, this chapter describes model complexes used to study the interaction of

peptides conjugated to macrocyclic chelates and their chelated lanthanide ions. Chapter 4 ends by describing an agent for the detection of MMP activity that builds on the lessons learned in the chapter.

References

- (1) A. E. Merbach and E. Toth(eds.), *The Chemistry of Contrast Agents in Medical Magnetic Resonance Imaging*; John Wiley & Sons, Ltd., New York, 2001.
- (2) S. Webb, *The Physics of Medical Imaging*; Institute of Physics Publishing, Bristol; Philadelphia, 1993.
- (3) D. M. J. Doble, M. Melchior, B. O'Sullivan, C. Siering, J. Xu, V. C. Pierre, and K. N. Raymond, *Inorg. Chem.* **2003**, *42*, 4930-4937.
- (4) J. Jin, *Electromagnetic Analysis and Design in Magnetic Resonance Imaging*; CRC Press, New York, 1999.
- (5) M. F. Tweedle and K. Kumar, *Top. Biol. Inorg. Chem.* **1999**, *2*, 1-43.
- (6) R. E. Jacobs, E. T. Ahrens, T. J. Meade, and S. E. Fraser, *Trends Cell Biol.* **1999**, *9*, 73-76.
- (7) D. E. Reichert, J. S. Lewis, and C. J. Anderson, *Coord. Chem. Rev.* **1999**, *184*, 3-66.
- (8) T. D. Mody and J. L. Sessler, *Perspect. Supramol. Chem.* **1999**, *4*, 245-294.
- (9) R. G. Pautler and A. P. Koretsky, *Neuroimage* **2002**, *16*, 441-448.
- (10) D. D. Schwert, J. A. Davies, and N. Richardson, *Top. Curr. Chem.* **2002**, *221*, 165-199.
- (11) V. Torchilin, J. Babich, and V. Weissig, *J. Liposome Res.* **2000**, *10*, 483-499.
- (12) V. P. Torchilin, *Adv. Drug Deliv. Rev.* **1997**, *24*, 301-313.
- (13) E. Unger, T. Fritz, G. Wu, D. Shen, B. Kulik, T. New, M. Crowell, and N. Wilke, *J. Liposome Res.* **1994**, *4*, 811-834.
- (14) R. B. Clarkson, *Top. Curr. Chem.* **2002**, *221*, 201-235.
- (15) A. Moore, E. Marecos, A. Bogdanov, Jr., and R. Weissleder, *Radiology* **2000**, *214*, 568-574.

- (16) J. Grimm, N. Karger, S. Lusse, S. Winoto-Morbach, B. Krisch, S. Muller-Hulsbeck, and M. Heller, *Invest. Radiol.* **2000**, *35*, 553-556.
- (17) J. Feng, X. Li, F. Pei, G. Sun, X. Zhang, and M. Liu, *Magn. Reson. Imaging* **2002**, *20*, 407-412.
- (18) K. J. Balkus, Jr. and J. Shi, *J. Phys. Chem.* **1996**, *100*, 16429-16434.
- (19) C. H. Reynolds, N. Annan, K. Beshah, J. H. Huber, S. H. Shaber, R. E. Lenkinski, and J. A. Wortman, *J. Am. Chem. Soc.* **2000**, *122*, 8940-8945.
- (20) S. Morel, E. Terreno, E. Ugazio, S. Aime, and M. R. Gasco, *Eur. J. of Pharmaceut. Biopharmaceut.* **1998**, *45*, 157-163.
- (21) J. Law, *Br. J. Radiol.* **1997**, *70*, 62-69.
- (22) K. G. Gilhuijs, M. L. Giger, and U. Bick, *Med. Phys.* **1998**, *25*, 1647-1654.
- (23) J. Brown, D. Buckley, A. Coulthard, A. K. Dixon, J. M. Dixon, D. F. Easton, R. A. Eeles, D. G. Evans, F. G. Gilbert, M. Graves, C. Hayes, J. P. Jenkins, A. P. Jones, S. F. Keevil, M. O. Leach, G. P. Liney, S. M. Moss, A. R. Padhani, G. J. Parker, L. J. Pointon, B. A. Ponder, T. W. Redpath, J. P. Sloane, L. W. Turnbull, L. G. Walker, and R. M. Warren, *Magn. Reson. Imaging* **2000**, *18*, 765-776.
- (24) C. Hayes, R. Padhani Anwar, and O. Leach Martin, *NMR Biomed.* **2002**, *15*, 154-163.
- (25) R. D. Mueller, J. Barkhausen, W. Sauerwein, and R. Langer, *J. Comput. Assist. Tomogr.* **1998**, *22*, 408-412.
- (26) W. A. Kaiser, *Radiologie* **1993**, *33*, 292-299.
- (27) C. A. Hulka, B. L. Smith, D. C. Sgroi, L. Tan, W. B. Edmister, J. P. Semple, T. Campbell, D. B. Kopans, T. J. Brady, and R. M. Weisskoff, *Radiology* **1995**, *197*, 33-38.
- (28) C. Frouge, J. M. Guinebretiere, G. Contesso, R. Di Paola, and M. Blery, *Invest. Radiol.* **1994**, *29*, 1043-1049.
- (29) M. A. Brown and R. C. Semelka, *MRI Basic Principles and Applications*; Wiley-Liss, Inc., New York, 1999.
- (30) J.-S. Yu, W. Kim Ki, M.-S. Park, and S.-W. Yoon, *J. Comput. Assist. Tomogr.* **2002**, *26*, 411-417.
- (31) I. J. Rowland, I. Rivens, L. Chen, C. H. Lebozer, D. J. Collins, G. R. ter Haar, and M. O. Leach, *Br. J. Radiol.* **1997**, *70*, 144-153.

- (32) W. E. Reddick, S. Wang, X. Xiong, J. O. Glass, S. Wu, S. C. Kaste, C. B. Pratt, W. H. Meyer, and B. D. Fletcher, *Cancer* **2001**, *91*, 2230-2237.
- (33) G. J. Hunter, L. M. Hamberg, N. Choi, R. K. Jain, T. McCloud, and A. J. Fischman, *Clin. Cancer Res.* **1998**, *4*, 949-955.
- (34) G. M. Kacł, E. Bruder, T. Pfammatter, F. Follath, F. Salomon, and J. F. Debatin, *J. Comput. Assist. Tomogr.* **1998**, *22*, 687-691.
- (35) K. Yamada, K. Miyahara, H. Sato, W. Nakayama, M. Sato, T. Hirose, H. Kato, H. Ikehira, Y. Tateno, H. Sugihara, and K. Furuhashi, *J. Vet. Med. Sci.* **1996**, *58*, 291-295.
- (36) P. Tervahartiala, L. Kivisaari, A. Lamminen, A. Maschek, H. Wohling, and C. G. Standertskjold-Nordenstam, *Eur. J. Radiol.* **1997**, *25*, 74-80.
- (37) R. Hammerstingl, S. Zangos, W. Schwarz, T. Rosen, W.-O. Bechstein, T. Balzer, and J. Vogl Thomas, *Acad. Radiol.* **2002**, *9 Suppl. 1*, S119-S120.
- (38) E. Furman-Haran, R. Margalit, D. Grobgeld, and H. Degani, *J. Magn. Reson. Imaging* **1998**, *8*, 634-641.
- (39) A. G. Maier, B. Kersting-Sommerhoff, J. W. Reeders, W. Judmaier, W. Schima, A. A. Annweiler, M. Meusel, and N. O. Wallengren, *J. Magn. Reson. Imaging* **2000**, *12*, 651-660.
- (40) H. Kobayashi, T. Saga, S. Kawamoto, N. Sato, A. Hiraga, T. Ishimori, J. Konishi, K. Togashi, and M. W. Brechbiel, *Cancer Res.* **2001**, *61*, 4966-4970.
- (41) S. D. Konda, M. Aref, S. Wang, M. Brechbiel, and E. C. Wiener, *Magn. Reson. Mater. Phys., Biol. Med.* **2001**, *12*, 104-113.
- (42) G. Adam, A. Muhler, E. Spuntrup, J. M. Neuerburg, M. Kilbinger, H. Bauer, L. Fucezi, W. Kupper, and R. W. Gunther, *Invest. Radiol.* **1996**, *31*, 267-274.
- (43) S. E. Matthews, C. W. Pouton, and M. D. Threadgill, *Adv. Drug Deliv. Rev.* **1996**, *18*, 219-267.
- (44) D. Sahani, R. Prasad Srinivasa, M. Maher, L. Warshaw Andrew, F. Hahn Peter, and S. Saini, *J. Comput. Assist. Tomogr.* **2002**, *26*, 126-128.
- (45) J. T. Halavaara and A. E. Lamminen, *J. Comput. Assist. Tomogr.* **1997**, *21*, 94-99.
- (46) Y. Ni, G. Marchal, X. Zhang, P. Van Hecke, J. Michiels, J. Yu, E. Rummeny, K. P. Lodemann, and A. L. Baert, *Invest. Radiol.* **1993**, *28*, 520-528.
- (47) G. N. Mann, H. F. Marx, L. L. Lai, and L. D. Wagman, *Ann. Surg. Oncol.* **2001**, *8*, 573-579.

- (48) M. Kobayashi, H. Tajiri, T. Hayashi, M. Kuroki, and I. Sakata, *Cancer Lett.* **1999**, *137*, 83-89.
- (49) Y. Takehara, H. Sakahara, H. Masunaga, S. Isogai, N. Kodaira, M. Sugiyama, H. Takeda, T. Saga, S. Nakajima, and I. Sakata, *Magn. Reson. Imaging* **2002**, *47*, 549-553.
- (50) V. Rousseau, D. Pouliquen, F. Darcel, P. Jallet, and J. J. Le Jeune, *Magn. Reson. Mater. Phys., Biol. Med.* **1998**, *6*, 13-21.
- (51) M. G. Harisinghani, S. Saini, G. J. Slater, M. D. Schnall, and M. D. Rifkin, *J. Magn. Reson. Imaging* **1997**, *7*, 161-163.
- (52) P. Wunderbaldinger, L. Josephson, C. Bremer, A. Moore, and R. Weissleder, *Magn. Reson. Med.* **2002**, *47*, 292-297.
- (53) C. Stets, S. Brandt, F. Wallis, J. Buchmann, F. J. Gilbert, and H. Heywang-Kobrunner Sylvania, *J. Magn. Reson. Imaging* **2002**, *16*, 60-68.
- (54) D. D. Stark, R. Weissleder, G. Elizondo, P. F. Hahn, S. Saini, L. E. Todd, J. Wittenberg, and J. T. Ferrucci, *Radiology* **1988**, *168*, 297-301.
- (55) P. F. Hahn, D. D. Stark, R. Weissleder, G. Elizondo, S. Saini, and J. T. Ferrucci, *Radiology* **1990**, *174*, 361-366.
- (56) P. H. Sugarbaker, *Radiology* **1990**, *174*, 621-626.
- (57) A. Tanimoto, *Microspheres, Microcapsules & Liposomes* **2001**, *3*, 525-558.
- (58) P. M. Taylor, J. M. Hawnaur, and C. E. Hutchinson, *Clin. Radiol.* **1995**, *50*, 215-219.
- (59) T. J. Vogl, R. Hammerstingl, W. Schwarz, M. G. Mack, P. K. Mueller, W. Pegios, H. Keck, A. Eibl-Eibesfeldt, J. Hoelzl, B. Woessmer, C. Bergman, and R. Felix, *Radiology* **1996**, *198*, 881-887.
- (60) A. F. Kopp, M. Laniado, F. Dammann, W. Stern, E. Gronewaller, T. Balzer, C. Schimpfky, and C. D. Claussen, *Radiology* **1997**, *204*, 749-756.
- (61) T. Suwa, S. Ozawa, M. Ueda, N. Ando, and M. Kitajima, *Int. J. Cancer* **1998**, *75*, 626-634.
- (62) C. H. Bush, C. R. Mladinich, and W. J. Montgomery, *J. Magn. Reson. Imaging* **1997**, *7*, 579-584.
- (63) S. Pauser, R. Reszka, S. Wagner, K. J. Wolf, H. J. Buhr, and G. Berger, *Anticancer Drug Des.* **1997**, *12*, 125-135.

- (64) J. D. Gleason, K. P. Nguyen, K. V. Kissinger, W. J. Manning, and R. L. Verrier, *J. Cardiovasc. Magn. Reson.* **2002**, *4*, 311-316.
- (65) E. Rossetti, G. Fragasso, R. Mellone, A. Vanzulli, A. Del Maschio, and S. L. Chierchia, *Cardiologia* **1999**, *44*, 653-659.
- (66) W. S. Kerwin, J. Cai, and C. Yuan, *Magn. Reson. Med.* **2002**, *47*, 1211-1217.
- (67) V. Weissig, J. Babich, and V. Torchilin, *Colloid. Surface. B* **2000**, *18*, 293-299.
- (68) S.-E. Stiriba, H. Frey, and R. Haag, *Angew. Chem. Int. Ed.* **2002**, *41*, 1329-1334.
- (69) L. J. Kroft, J. Doornbos, R. J. van der Geest, and A. de Roos, *J. Magn. Reson. Imaging* **1999**, *10*, 170-177.
- (70) G. M. Beache, S. F. Kulke, H. L. Kantor, P. Niemi, T. A. Campbell, D. A. Chesler, H. Gewirtz, B. R. Rosen, T. J. Brady, and R. M. Weisskoff, *Magn. Reson. Imaging* **1998**, *16*, 19-27.
- (71) K. E. Kellar, D. K. Fujii, W. H. H. Gunther, K. Briley-Saebo, M. Spiller, and S. H. Koenig, *Magn. Reson. Mater. Phys., Biol. Med.* **1999**, *8*, 207-213.
- (72) P. V. Prasad, J. Cannillo, D. R. Chavez, E. S. Pinchasin, R. P. Dolan, R. Walovitch, and R. R. Edelman, *Invest. Radiol.* **1999**, *34*, 566-571.
- (73) S. A. Schmitz, M. Taupitz, S. Wagner, K. J. Wolf, D. Beyersdorff, and B. Hamm, *J. Magn. Reson. Imaging* **2001**, *14*, 355-361.
- (74) Y. Rozenman, X. M. Zou, and H. L. Kantor, *Magn. Reson. Imaging* **1991**, *9*, 933-939.
- (75) M. Rausch, D. Baumann, U. Neubacher, and M. Rudin, *NMR Biomed.* **2002**, *15*, 278-283.
- (76) A. Giovagnoni, A. Fabbri, and F. Maccioni, *Abdom. Imaging* **2002**, *27*, 367-375.
- (77) N. Sabir, U. Sungurtekin, E. Erdem, and M. Nessar, *Int. J. Colorectal. Dis.* **2000**, *15*, 317-322.
- (78) V. Christmann, J. Rosenberg, J. Seega, and C.-M. Lehr, *Pharm. Res.* **1997**, *14*, 1066-1072.
- (79) F. Maccioni, A. Viscido, L. Broglia, M. Marrollo, R. Masciangelo, R. Caprilli, and P. Rossi, *Abdom. Imaging* **2000**, *25*, 219-228.
- (80) A. Rieber, K. Nussle, M. Reinshagen, H. J. Brambs, and A. Gabelmann, *Abdom. Imaging* **2002**, *27*, 394-399.

- (81) W. Schwizer, R. Fraser, J. Borovicka, G. Crelier, P. Boesiger, and M. Fried, *Dig. Dis. Sci.* **1994**, *39*, 101S-103S.
- (82) W. Schwizer, R. Fraser, H. Maecke, K. Siebold, R. Funck, and M. Fried, *Magn. Reson. Med.* **1994**, *31*, 388-393.
- (83) K. J. Balkus, Jr. and I. Bresinska, *J. Alloys Compd.* **1994**, *207-208*, 25-28.
- (84) S. W. Young, F. Qing, D. Rubin, K. J. Balkus, Jr., J. S. Engel, J. Lang, W. C. Dow, J. D. Mutch, and R. A. Miller, *J. Magn. Reson. Imaging* **1995**, *5*, 499-508.
- (85) D. L. Rubin, K. L. Falk, M. J. Sperling, M. Ross, S. Saini, B. Rothman, F. Shellock, E. Zerhouni, D. Stark, E. K. Outwater, U. Schmiedl, L. C. Kirby, J. Chezmar, T. Coates, M. Chang, J. M. Silverman, N. Rofsky, K. Burnett, J. Engel, and S. W. Young, *J. Magn. Reson. Imaging* **1997**, *7*, 865-872.
- (86) K. J. Balkus, Jr. and J. Shi, *Langmuir* **1996**, *12*, 6277-6281.
- (87) A. D'Arienzo, G. Scaglione, G. Vicinanza, F. Manguso, R. Bennato, G. Belfiore, M. Imbriaco, and G. Mazzacca, *Am. J. Gastroenterol.* **2000**, *95*, 720-724.
- (88) R. W. Briggs, Z. Wu, C. R. J. Mladinich, C. Stoupis, J. Gauger, T. Liebig, P. R. Ros, J. R. Ballinger, and P. Kubilis, *Magn. Reson. Imaging* **1997**, *15*, 559-566.
- (89) M. Matsumura, H. Nakagami, C.-J. Chen, S. Ito, and T. Konno, *Pharm. Acta Helv.* **1998**, *73*, 205-213.
- (90) M. Rudin, N. Beckmann, R. Porszasz, T. Reese, D. Bochelen, and A. Sauter, *NMR Biomed.* **1999**, *12*, 69-97.
- (91) A. Bashir, M. L. Gray, and D. Burstein, *Magn. Reson. Med.* **1996**, *36*, 665-673.
- (92) H. Lindegaard, J. Vallo, K. Horslev-Petersen, P. Junker, and M. Ostergaard, *Ann. Rheum. Dis.* **2001**, *60*, 770-776.
- (93) M. Klarlund, M. Ostergaard, E. Rostrup, H. Skjodt, and I. Lorenzen, *Scand. J. Rheumatol.* **2000**, *29*, 108-115.
- (94) H. M. Bonel, P. Schneider, M. D. Seemann, R. Huegeli, S. Srivastav, K. P. Lodemann, and M. Reiser, *Skeletal Radiol.* **2001**, *30*, 15-24.
- (95) G. M. Toney, H. A. Chavez, R. Ibarra, and J. R. Jinkins, *Invest. Radiol.* **2001**, *36*, 33-40.
- (96) W. Krause, N. Hackmann-Schlichter, F. K. Maier, and R. Muller, *Top. Curr. Chem.* **2000**, *210*, 261-308.
- (97) T. S. Huang, J. F. Zucherman, K. Y. Hsu, M. Shapiro, D. Lentz, and J. Gartland, *Spine* **2002**, *27*, 839-843.

- (98) A. Piironen, R. Kivisaari, P. Pitkaranta, V. P. Poutanen, P. Laippala, P. Laurila, and L. Kivisaari, *Eur. Radiol.* **1997**, *7*, 17-20.
- (99) J. Werner, J. Schmidt, A. L. Warshaw, M. M. Gebhard, C. Herfarth, and E. Klar, *Ann. Surg.* **1998**, *227*, 105-111.
- (100) A. A. Kasperlik-Zaluska, J. Walecki, W. Jeske, A. Migdalska, and A. Brezezinska, *J. Mol. Neurosci.* **1996**, *7*, 87-90.
- (101) L. Knespova and G. P. Krestin, *Eur. Radiol.* **1998**, *8*, 201-211.
- (102) H. Kobayashi, S. Kawamoto, S.-K. Jo, N. Sato, T. Saga, A. Hiraga, J. Konishi, S. Hu, K. Togashi, M. W. Brechbiel, and R. A. Star, *Kidney Int.* **2002**, *61*, 1980-1985.
- (103) V. P. Torchilin, *Adv. Drug Deliv. Rev.* **2002**, *54*, 235-252.
- (104) M. Kresse, S. Wagner, K. Philipp, K. Thode, R. H. Mueller, and W. Semmler, *Proceedings of the International Symposium on Controlled Release of Bioactive Materials* **1997**, *24th*, 93-94.
- (105) E. R. Wisner, K. L. Aho-Sharon, M. J. Bennett, S. G. Penn, C. B. Lebrilla, and M. H. Nantz, *J. Med. Chem.* **1997**, *40*, 3992-3996.
- (106) R. Weissleder, J. F. Heautot, B. K. Schaffer, N. Nossiff, M. I. Papisov, A. Bogdanov, Jr., and T. J. Brady, *Radiology* **1994**, *191*, 225-230.
- (107) P. Reimer, R. Weissleder, A. S. Lee, S. Buettner, J. Wittenberg, and T. J. Brady, *Radiology* **1991**, *178*, 769-774.
- (108) K. Thode, M. Luck, W. Schroder, T. Blunk, R. H. Muller, and M. Kresse, *J. Drug Target.* **1998**, *5*, 459-469.
- (109) D. Pouliquen and C. Chouly, *Microspheres, Microcapsules & Liposomes* **1999**, *2*, 343-382.
- (110) S. L. Fossheim, J.-M. Colet, S. Mansson, A. K. Fahlvik, R. N. Muller, and J. Klaveness, *Invest. Radiol.* **1998**, *33*, 810-821.
- (111) M. Federle, J. Chezmar, D. L. Rubin, J. Weinreb, P. Freeny, U. P. Schmiedl, J. J. Brown, J. A. Borrello, J. K. Lee, R. C. Semelka, R. Mattrey, A. H. Dachman, S. Saini, S. E. Harms, D. G. Mitchell, M. W. Anderson, H. H. Halford, 3rd, W. F. Bennett, S. W. Young, M. Rifkin, S. B. Gay, R. Ballerini, P. F. Sherwin, and R. O. Robison, *J. Magn. Reson. Imaging* **2000**, *12*, 689-701.
- (112) Y.-J. Fu and R.-X. Zhuo, *Chem. Res. Chinese U.* **1997**, *13*, 336-343.

- (113) M.-Y. Su, M. K. Samoszuk, J. Wang, and O. Nalcioglu, *NMR Biomed.* **2002**, *15*, 106-113.
- (114) M. Krause, K. K. Kwong, J. Xiong, E. S. Gragoudas, and L. H. Y. Young, *Ophthalmic Res.* **2002**, *34*, 241-250.
- (115) R. Weissleder, A. A. Bogdanov, Jr., and M. Papisov, *Handbook of Targeted Delivery of Imaging Agents* **1995**, 133-147.
- (116) Y. Okuhata, *Adv. Drug Deliv. Rev.* **1999**, *37*, 121-137.
- (117) G. A. Lemieux, K. J. Yarema, C. L. Jacobs, and C. R. Bertozzi, *J. Am. Chem. Soc.* **1999**, *121*, 4278-4279.
- (118) R. Bhorade, R. Weissleder, T. Nakakoshi, A. Moore, and C.-H. Tung, *Bioconjugate Chem.* **2000**, *11*, 301-305.
- (119) D. A. Sipkins, K. Gijbels, F. D. Tropper, M. Bednarski, K. C. P. Li, and L. Steinman, *J. Neuroimmunol.* **2000**, *104*, 1-9.
- (120) J. F. Kayyem, R. M. Kumar, S. E. Fraser, and T. J. Meade, *Chem. Biol.* **1995**, *2*, 615-620.
- (121) C. Curtet, F. Maton, T. Havet, M. Slinkin, A. Mishra, J.-F. Chatal, and R. N. Muller, *Invest. Radiol.* **1998**, *33*, 752-761.
- (122) E. C. Wiener, S. Konda, A. Shadron, M. Brechbiel, and O. Gansow, *Invest. Radiol.* **1997**, *32*, 748-754.
- (123) S. D. Konda, M. Aref, M. Brechbiel, and E. C. Wiener, *Invest. Radiol.* **2000**, *35*, 50-57.
- (124) D. A. Sipkins, D. A. Cheresch, M. R. Kazemi, L. M. Nevin, M. D. Bednarski, and K. C. P. Li, *Nat. Med.* **1998**, *4*, 623-626.
- (125) S. A. Anderson, R. K. Rader, W. F. Westlin, C. Null, D. Jackson, G. M. Lanza, S. A. Wickline, and J. J. Kotyk, *Magn. Reson. Med.* **2000**, *44*, 433-439.
- (126) A. Moore, P. Z. Sun, D. Cory, D. Hogemann, R. Weissleder, and M. A. Lipes, *Magn. Reson. Med.* **2002**, *47*, 751-758.
- (127) M. Zhao, M. F. Kircher, L. Josephson, and R. Weissleder, *Bioconjugate Chem.* **2002**, *13*, 840-844.
- (128) E. A. Schellenberger, A. Bogdanov, Jr., D. Hogemann, J. Tait, R. Weissleder, and L. Josephson, *Molecular Imaging* **2002**, *1*, 102-107.
- (129) A. Schellenberger Eyk, D. Hogemann, L. Josephson, and R. Weissleder, *Acad. Radiol.* **2002**, *9 Suppl 2*, S310-311.

- (130) M. Kresse, S. Wagner, D. Pfefferer, R. Lawaczeck, V. Elste, and W. Semmler, *Magn. Reson. Med.* **1998**, *40*, 236-242.
- (131) H. W. Kang, L. Josephson, A. Petrovsky, R. Weissleder, and A. Bogdanov, Jr., *Bioconjugate Chem.* **2002**, *13*, 122-127.
- (132) S. Ozawa, Y. Imai, T. Suwa, and M. Kitajima, *Recent Results Cancer Res.* **2000**, *155*, 73-87.
- (133) N. J. Abbott, D. C. Chugani, G. Zaharchuk, B. R. Rosen, and E. H. Lo, *Adv. Drug Deliv. Rev.* **1999**, *37*, 253-277.
- (134) W. M. Pardridge, *J. Cereb. Blood Flow Metab.* **1997**, *17*, 713-731.
- (135) M. A. Horsfield, M. A. Rocca, M. Cercignani, and M. Filippi, *Magn. Reson. Imaging* **2000**, *18*, 139-142.
- (136) D. Baleriaux, C. Colosimo, J. Rusalleda, M. Korves, G. Schneider, K. Bohndorf, G. Bongartz, M. A. van Buchem, M. Reiser, K. Sartor, M. W. Bourne, P. M. Parizel, G. R. Cherryman, I. Salerio, A. La Noce, G. Pirovano, M. A. Kirchin, and A. Spinazzi, *Neuroradiology* **2002**, *44*, 191-203.
- (137) O. Mykhaylyk, A. Cherchenko, A. Ilkin, N. Dudchenko, V. Ruditsa, M. Novoseletz, and Y. Zozulya, *J. Magn. Magn. Mater.* **2001**, *225*, 241-247.
- (138) S. Xu, E. K. Jordan, S. Brocke, J. W. M. Bulte, L. Quigley, N. Tresser, J. L. Ostuni, Y. Yang, H. F. McFarland, and J. A. Frankl, *J. Neurosci. Res.* **1998**, *52*, 549-558.
- (139) D. K. Kim, Y. Zhang, J. Kehr, T. Klason, B. Bjelke, and M. Muhammed, *J. Magn. Magn. Mater.* **2001**, *225*, 256-261.
- (140) D. K. Kim, W. Voit, W. Zapka, B. Bjelke, M. Muhammed, and K. V. Rao, *Mat. Res. Soc. Symp. Proc.* **2002**, *676*, Y8.32.31-Y38.32.36.
- (141) J. F. Poduslo, T. M. Wengenack, G. L. Curran, T. Wisniewski, E. M. Sigurdsson, S. I. Macura, B. J. Borowski, and C. R. Jack, *Neurobiol. Dis.* **2002**, *11*, 315-329.
- (142) A. Y. Louie, M. M. Huber, E. T. Ahrens, U. Rothbacher, R. Moats, R. E. Jacobs, S. E. Fraser, and T. J. Meade, *Nat. Biotechnol.* **2000**, *18*, 321-325.
- (143) R. A. Moats, S. E. Fraser, and T. J. Meade, *Angew. Chem., Int. Ed. Engl.* **1997**, *36*, 726-728.
- (144) P. L. Anelli, I. Bertini, M. Fragai, L. Lattuada, C. Luchinat, and G. Parigi, *Eur. J. Inorg. Chem.* **2000**, 625-630.

- (145) A. L. Nivorozhkin, A. F. Kolodziej, P. Caravan, M. T. Greenfield, R. B. Lauffer, and T. J. McMurry, *Angew. Chem. Int. Ed.* **2001**, *40*, 2903-2906.
- (146) A. Bogdanov, Jr., L. Matuszewski, C. Bremer, A. Petrovsky, and R. Weissleder, *Molecular Imaging* **2002**, *1*, 16-23.
- (147) J. M. Perez, T. O'Loughin, F. J. Simeone, R. Weissleder, and L. Josephson, *J. Am. Chem. Soc.* **2002**, *124*, 2856-2857.
- (148) M. Zhao, L. Josephson, Y. Tang, and R. Weissleder, *Angew. Chem. Int. Ed.* **2003**, *42*, 1375-1378.
- (149) S. Aime, M. Botta, M. Fasano, and E. Terreno, *Spectrochim. Acta* **1993**, *49A*, 1315-1322.
- (150) V. Comblin, D. Gilsoul, M. Hermann, V. Humblet, V. Jacques, M. Mesbahi, C. Sauvage, and J. F. Desreux, *Coord. Chem. Rev.* **1999**, *185-186*, 451-470.
- (151) W.-h. Li, S. E. Fraser, and T. J. Meade, *J. Am. Chem. Soc.* **1999**, *121*, 1413-1414.
- (152) W.-h. Li, G. Parigi, M. Fragai, C. Luchinat, and T. J. Meade, *Inorg. Chem.* **2002**, *41*, 4018-4024.
- (153) S. Aime, G. Digilio, M. Fasano, S. Paoletti, A. Arnelli, and P. Ascenzi, *Biophys. J.* **1999**, *76*, 2735-2743.
- (154) S. Aime, M. Botta, E. Gianolio, and E. Terreno, *Angew. Chem. Int. Ed.* **2000**, *39*, 747-750.
- (155) L. Josephson, J. M. Perez, and R. Weissleder, *Angew. Chem. Int. Ed.* **2001**, *40*, 3204-3206.
- (156) K. Hanaoka, K. Kikuchi, Y. Urano, and T. Nagano, *J. Chem. Soc., Perkin Trans. 2* **2001**, 1840-1843.
- (157) K. Hanaoka, K. Kikuchi, Y. Urano, M. Narazaki, T. Yokawa, S. Sakamoto, K. Yamaguchi, and T. Nagano, *Chem. Biol.* **2002**, *9*, 1027-1032.
- (158) S. Aime, D. Delli Castelli, F. Fedeli, and E. Terreno, *J. Am. Chem. Soc.* **2002**, *124*, 9364-9365.
- (159) C. Glogard, G. Stensrud, and S. Aime, *Magn. Res. Chem.* **2003**, *41*, 585-588.
- (160) M. Mikawa, N. Miwa, M. Brautigam, T. Akaike, and A. Maruyama, *Chem. Lett.* **1998**, 693-694.
- (161) M. Mikawa, N. Miwa, T. Akaike, and A. Maruyama, *Proceedings of the International Symposium on Controlled Release of Bioactive Materials* **1999**, *26th*, 1158-1159.

- (162) S. Aime, S. G. Crich, M. Botta, G. Giovenzana, G. Palmisano, and M. Sisti, *Chem. Commun.* **1999**, 1577-1578.
- (163) S. Zhang, K. Wu, and A. D. Sherry, *Angew. Chem. Int. Ed.* **1999**, 38, 3192-3194.
- (164) R. Hovland, C. Glogard, A. J. Aasen, and J. Klaveness, *J. Chem. Soc., Perkin Trans. 2* **2001**, 929-933.
- (165) S. Aime, A. Barge, D. D. Castelli, F. Fedeli, A. Mortillaro, F. U. Nielsen, and E. Terreno, *Magn. Reson. Med.* **2002**, 47, 639-648.

Chapter 2

Synthesis, Visualization, and Delivery Properties of Polyarginine-Labeled Magnetic Resonance Imaging Contrast Agents

The text of this chapter was taken in part from the following manuscripts:

Allen, M.J.; Meade, T.J. *J. Biol. Inorg. Chem.* **2003**, *8*, 746-750.

and

Allen, M.J.; MacRenaris, K.W.; Venkatasubramanian, P.N.; Meade, T.J. *Chem. Biol.* in press, with permission from Elsevier.

Introduction

The study of in vivo developmental events has undergone significant advances with the advent of biological molecular imaging techniques such as computer enhanced light microscopy imaging, positron emission tomography (PET), micro computed tomography (CT), and magnetic resonance imaging (MRI).¹⁻⁴ These techniques are revolutionizing the investigation of cellular and physiological processes. For example, light microscopy techniques are employed in the study of whole tissues and organisms using fluorescent indicator dyes. Recent advances in the development of tracers such as green fluorescent protein have provided exquisite details of cellular processes.^{5,6} However, light microscopy is limited by optical aberrations and light scattering to the outer 100 to 300 μm of a specimen.

One technique that has proven to be a powerful tool in clinical and biological settings is MRI, which offers a noninvasive means to map structure and function by sampling the amount, flow, and environment of water protons in vivo. The image is based upon the NMR signal from the protons of water, where the signal intensity in a given volume element is a function of the water concentration and relaxation times (T_1 and T_2). Intrinsic contrast can be augmented by the use of paramagnetic contrast agents in both clinical and experimental settings. Typically, the paramagnetic ion gadolinium(III) is used in MRI agents to decrease the local T_1 of water protons and therefore provide increased contrast.⁷

Contrast agents that will aid in the observation of ongoing developmental events in living animals have been prepared previously in the Meade laboratory. The descendants of early cells in an intact embryo can be labeled by microinjection of a

stable, nontoxic, membrane impermeable MR lineage tracer thus remaining within the originally labeled cell and its progeny.^{8,9} The acquired images can be used to generate a temporal series of high-resolution three-dimensional MR images. In this way it is possible to reconstruct the cell divisions and movements responsible by particular descendant(s).

A principle barrier to the development of MR contrast agents for investigating developmental biological questions is the ability to transport the agent across cellular membranes. Typical MR agents are restricted to the extracellular domains and there are few examples of membrane permeable MR contrast agents reported in the literature.¹⁰⁻¹⁶ Previously in the Meade laboratory, an agent that facilitated the co-transport of DNA and an MR contrast agent by receptor mediated endocytosis was prepared.¹⁷ While this agent is effectively delivered in sufficient quantity to be detected in cell cultures by MRI, it proved impractical for use in whole animals.

As part of research towards preparing contrast agents that cross cell membranes a number of small molecules that facilitate transport of charged and uncharged species were investigated. This work focused on the synthesis of membrane permeable molecules covalently attached to the lanthanide binding chelate 1,4,7,10-tetraazacyclododecane -N,N',N'',N'''-tetraacetic acid (DOTA). The selection of polyarginine (8-16 monomer units) was due to published work that these compounds are able to cross cell membranes.^{18,19}

The mechanism of polyarginine delivery is not completely understood, however it cannot be explained by adsorptive-mediated or receptor-mediated endocytosis.¹⁹ The delivery mechanism is believed to involve electrostatic interactions between the

guanidinium groups of the arginine oligomers and anions on the cell surface such as phosphate, carboxylate, sulphonate, and sulfate.²⁰⁻²³ Once polyarginine is hydrogen bonded to the cell surface, it is internalized through an unknown mechanism that is independent of receptors, transporters, and endocytosis.²⁰ Inside the cell, the oligomer is released from the cell membrane or sent back to the extracellular environment (**Figure 2.1**). Longer oligomers (>16 units) remain membrane bound and are not internalized, likely due to the strong multivalent binding of the cell surface, while shorter peptides (<6 units) are not internalized, because of insufficient interaction between the small number of guanidinium groups with the cell surface.²¹

In this chapter the synthesis and in vitro testing of gadolinium(III) contrast agents conjugated to polyarginine that are able to permeate cell membranes are described. In addition, two-photon laser spectroscopy (TPLM) is used as a method of observing the europium(III) derivative of the agent in cell culture. This is the first published report of visualizing a MRI contrast agent with TPLM. Finally, thorough cell culture testing of the delivery properties of the series of lanthanide(III) based MRI contrast agents is reported along with visualization using MRI.

Results

Synthesis and Physical Characterization

Compounds **1-9** were synthesized as shown in **Scheme 2.1**. Standard peptide synthesis techniques were used to prepare eight, twelve, and sixteen amino acid polyarginine oligomers that were subsequently conjugated to 1,4,7,10-tetraazacyclododecane-1,4,7-tris(acetic acid-*tert*-butyl ester)-10-acetic acid [DOTA(*tris-t*-Bu ester)].²⁴ The conditions used to cleave the peptides from the resin simultaneously

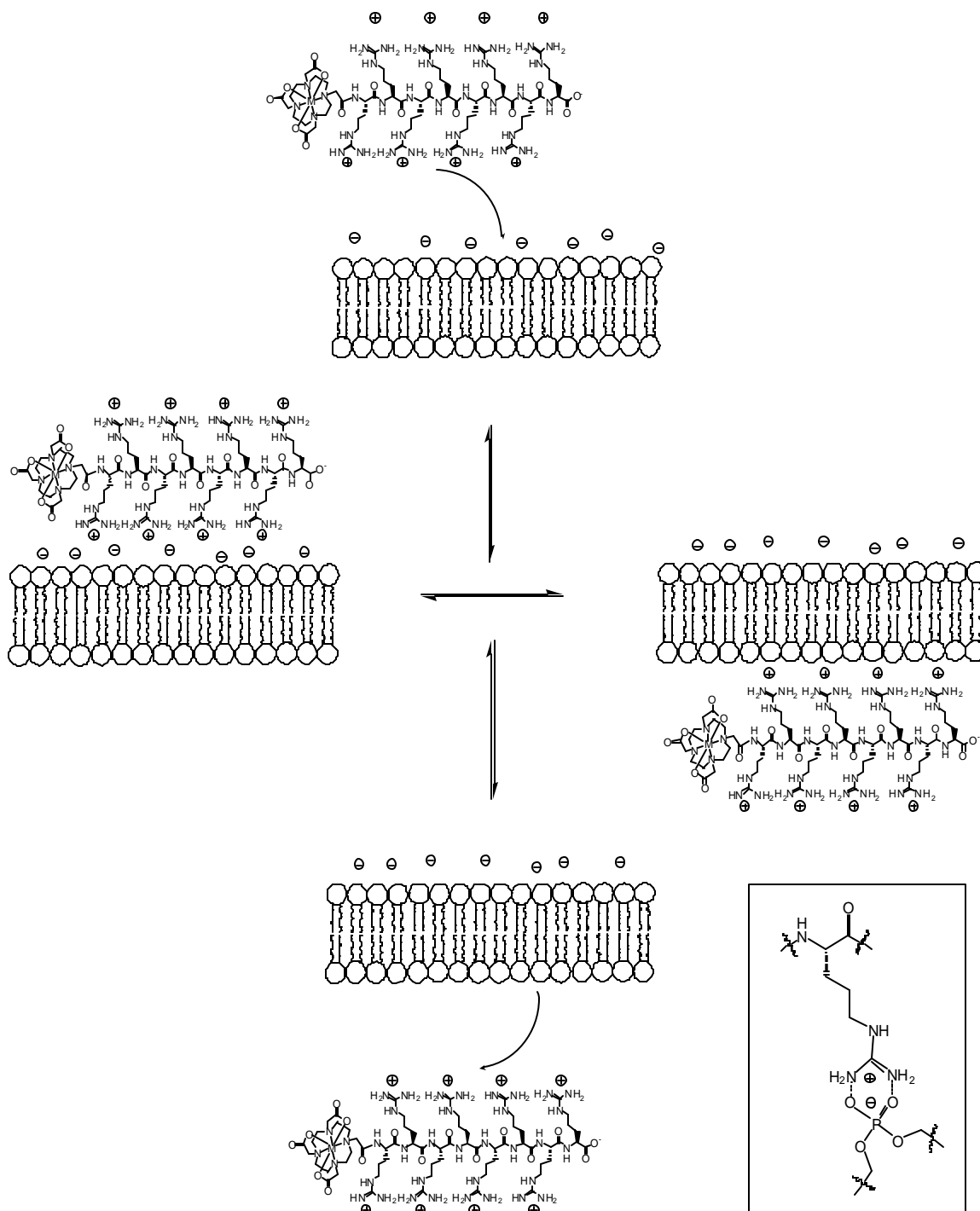
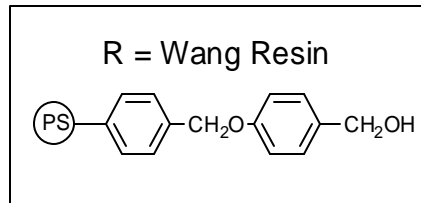
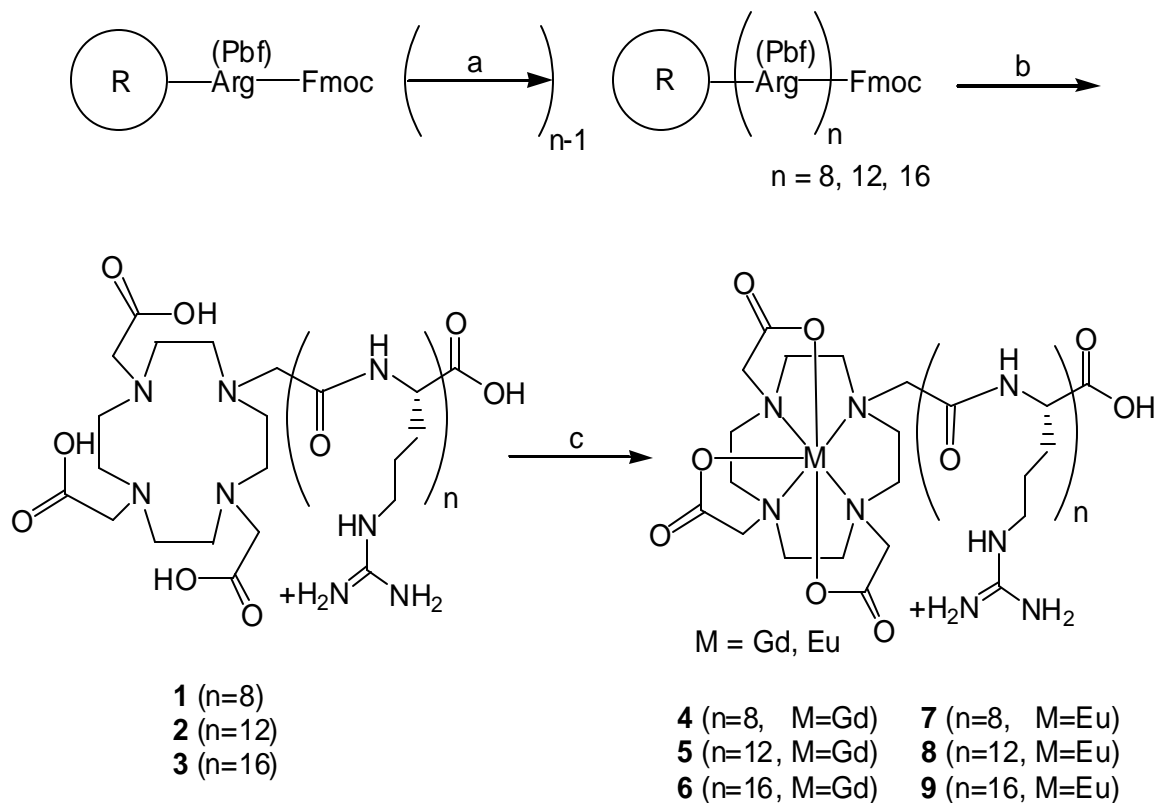


Figure 2.1: Schematic of hypothesized mechanism of trans-membrane polyarginine delivery. Inset: Chemical structure of the putative bidentate hydrogen-bonding interacting proposed between the guanidinium headgroup of arginine and the phosphates present in lipid bilayers.²¹



Scheme 2.1: Synthesis of polyarginine containing lanthanide chelates: (a) (1) Piperidine, DMF (2) Fmoc-R(Pbf)-OH, HATU, DMF, DIPEA; (b) (1) Piperidine, DMF (2) DOTA(tris-*t*-bu ester), HATU, DMF, DIPEA (3) 95% TFA, 2.5% H₂O, 2.5% TIS; (b) Eu(OH)₃ or Gd(OH)₃ in water at 80 °C for 12 hours.

deprotected the *t*-butyl esters on the ligand. The desired lanthanide ion was added using the appropriate lanthanide hydroxide. Control compounds of gadolinium(III) 1,4,7,10-tetraazacyclododecane-1,4,7-trisacetic acid (DO3A) (**10**) and europium(III) DO3A (**11**) were prepared by chelating the appropriate lanthanide hydroxide to DO3A after converting the *t*-butyl esters of DO3A(tris-*t*-Bu ester) into carboxylic acids using trifluoroacetic acid (TFA). Ligands were characterized using ¹H NMR spectroscopy and mass spectrometry. Final products were purified on a Sephadex G-25 column or by HPLC using an Aquasil C-18 column (ThermoHypersil-Keystone, Bellefonte, PA) and characterized by mass spectrometry and elemental analysis.

Relaxivity measurements were acquired by taking the slope of a plot of T_1^{-1} versus concentration, where relaxivity is a measure of the ability of a contrast agent to shorten T_1 (**Table 2.1**). Measurements were taken in 10 mM 3-(*N*-morpholino)propane sulfonic acid (MOPS), 100 mM sodium chloride, 20 mM sodium bicarbonate, and 4 mM sodium phosphate monobasic at pH 7.41, 59.97 MHz, and 37 °C. There is a high probability that the counter-anions were trifluoroacetic acid (TFA).^{25,26} However, since the exact nature of the counter-anion to arginine was not known, gadolinium concentrations for relaxivity measurements were determined by inductively coupled plasma-mass spectrometry (ICP-MS) of the measured solutions. Determination of the gadolinium concentration by ICP-MS allowed for the calculation of the molar concentration without knowing the exact identity of the counter-anions.

Octanol-water partition coefficients were obtained by dissolving 7-12 mg of **4**, **5**, or **6** into mixtures of 500 μ L water and 500 μ L 1-octanol. The resulting mixture was shaken vigorously for two hours on a Lab-Line lab rotator (model number 1304). The

Compound	Relaxivity ($\text{mM}^{-1}\text{s}^{-1}$)	Octanol-Water Partition Coefficient
4	6.8	0.0233 ± 0.0003
5	4.8	0.117 ± 0.039
6	4.4	0.104 ± 0.068

Table 2.1: Relaxivity values and octanol-water partition coefficients measured for **4**, **5**, and **6**. Relaxivity measured at 59.97 MHz, and 37 °C in 10 mM MOPS, 100 mM NaCl, 20 mM NaHCO₃, and 4 mM NaH₂PO₄ at pH 7.41. Values for partition coefficients are plus or minus one standard deviation.

solvent layers were allowed to separate, and 400 μL of each layer were removed. The solvent was removed under reduced pressure and the mass of material from each layer was measured. The reported values are for the mass of compound in the 1-octanol layer divided by the mass of compound in the water layer. All octanol-water measurements were repeated in triplicate and the average value is reported. Relaxivity values and octanol-water partition coefficients are listed in **Table 2.1**.

Cell Studies

Proliferation and Viability Assays

All cell experiments described in this paper were repeated in at least triplicate. To determine the toxicity of **7**, **8**, and **9** a 3-(4,5-dimethylthiazolyl-2)-2,5-diphenyltetrazolium bromide (MTT) assay was performed. Mouse fibroblast (NIH/3T3) cells were plated at 150,000 cells/mL in a Costar 96 well plate (polystyrene, flat bottom, tissue culture treated, black with clear bottom) and incubated overnight. Solutions of **7**, **8**, and **9** in Dulbecco's Phosphate Buffered Saline (DPBS) were added to the wells to give concentrations in the wells ranging from 1 mM to 44 mM. The plate was incubated for one hour at which point 10 μL of MTT was added to each well and incubated for four hours at 37 $^{\circ}\text{C}$ in a 5% carbon dioxide incubator. The detergent reagent supplied with the MTT assay kit (100 μL) was added to each well and incubated in the dark at ambient temperature overnight. The absorbance at 570 nm was measured with background subtraction and used to determine toxicity. None of the compounds affected cell proliferation below 10 mM. Additionally, trypan blue assays were performed in all subsequent experiments. In the concentration ranges tested, cells treated with **4-9** were greater than 95% viable.

Two-Photon Laser Microscopy

For TPLM experiments, NIH/3T3 cells were grown in a sixteen-well Nunc™ Lab-Tek™ ChamberSlide™ system (Fisher Scientific) with Dulbecco's modified Eagle's (DME) medium modified to contain 4 mM L-glutamine, 4.5 g/L glucose, and 1.5 g/L sodium bicarbonate and supplemented with ten percent bovine calf serum (BCS) in a five percent CO₂ incubator. The cells were incubated with **9** (0.3 mM in modified DME medium) for one hour and subsequently rinsed three times for approximately ten seconds with fresh modified DME maintained at 37 °C with a water bath to insure removal of extracellular and unbound contrast agent. The detachable wells were then removed and the glass slide was scored with a diamond tipped glass cutter and snapped in half to create a small enough surface to mount in a 60 mm diameter Petri dish using aquarium cement. The cells were then covered with CO₂-independent medium modified to contain 4 mM L-glutamine. A Plexiglas cover for the Petri dish with a hole large enough for the microscope objective to fit through was used to cover the Petri dish in order to minimize evaporation of the medium. Control experiments of untreated cells and cells treated with **11** were performed in the same manner.

The results of the TPLM experiments shown in **Figure 2.2** reveal that **9** is taken up by the cells. The small background signal seen in the control cells is due to autofluorescence caused by TPLM excitation at 750 nm. The cells treated with **11** show only autofluorescence intrinsic to the cells. In comparison to traditional fluorescence dyes, complex **9** has a weak signal due to the relatively weak emission of europium(III) complexes.

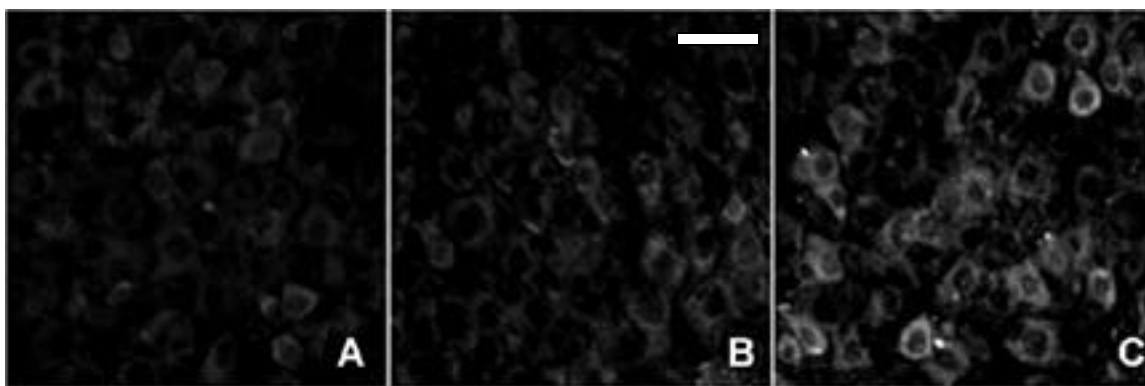


Figure 2.2: Two-photon laser microscopy image ($\lambda_{\text{EX}} = 750 \text{ nm}$) of NIH/3T3 cells, A: untreated control where signal is due to autofluorescence of the cells, B: cells incubated with **11** for one hour and rinsed prior to imaging, and C: cells incubated with **9** for one hour and rinsed prior to imaging. The scale bar represents $50 \mu\text{m}$.

T₁ Studies

Experiments similar to the TPLM study were repeated using **6** and a Bruker mq60 NMR Analyzer for determining uptake of the agent by the cells as a function of change in T_1 . NIH/3T3 cells were grown in CorningTM brand tissue culture flasks (25 cm² or 75 cm² with vent cap) (Fisher Scientific) using the same modified DME medium as in the TPLM experiments. Cells were incubated with 0.33 mM **6** in modified DME medium for one hour at 37 °C in a five percent CO₂ incubator at which time they were rinsed three times with either fresh modified DME medium or DPBS maintained at 37 °C. Each rinse was 2-3 milliliters, in volume, lasted approximately ten seconds, and was to insure removal of extracellular and unbound contrast agent. The cells were then exposed to 250 μL of 0.25% trypsin and harvested at which point they were counted using a hemocytometer and checked for viability using a trypan blue assay.²⁷ For the medium rinsed cells the average number of cells per sample was 200,000; there was an average of 1,000,000 cells for the cells washed with DPBS. Cells were >98% viable after exposure to **6**. The T_1 of the trypsin/cell suspensions were measured. These experiments were repeated in triplicate. Untreated cells and cells treated with **10** were examined in an analogous fashion. The T_1 of cells from these experiments are listed in **Table 2.2**.

To determine the effect of varying polyarginine oligomer length on T_1 enhancement upon uptake by NIH/3T3 cells, experiments were performed using a Bruker mq 60 NMR Analyzer. NIH/3T3 cells were grown in CorningTM brand tissue culture flasks (75 cm² with vent cap) using DMEM modified to contain 4 mM L-glutamine, 4.5 g/L glucose, 1.5 g/L sodium bicarbonate and supplemented with 10% BCS. Cells were incubated with 0.3 mM **4**, **5**, or **6** in modified DMEM containing 10% BCS for one hour

	6/medium	10/medium	untreated/medium	6/buffer	untreated/buffer
Trial 1	3.69	3.73	3.83	3.09	3.96
Trial 2	3.66	3.78	3.76	3.35	3.95
Trial 3	3.63	3.77	3.77	3.50	3.87
Average	3.66	3.76	3.79	3.31	3.93

Table 2.2: Results of T_1 study of NIH/3T3 cells incubated with 0.3 mM **6**, **10**, and untreated cells. After incubation cells were rinsed with either fresh modified DME medium or DPBS. T_1 values were measured at 60 MHz and 37 °C. Units for T_1 are s.

at 37 °C in a 5% carbon dioxide incubator at which time they were rinsed three times with DPBS (2-3 mL) maintained at ambient temperature to insure removal of extracellular and unbound contrast agent. The cells were exposed to 250 μ L of 0.25% trypsin and harvested at which point they were counted using a hemacytometer and checked for viability using a trypan blue assay ²⁷. There was an average of 1,000,000 cells per flask, and all cells were >98% viable after exposure to **4**, **5**, or **6** by trypan blue assay. The T_1 of the trypsin/cell suspensions were measured. Untreated cells were examined in an analogous fashion. The average T_1 of the cell suspensions were 3.06 \pm 0.13 s for **4**, 3.13 \pm 0.41 s for **5**, 3.22 \pm 0.21 s for **6**, and 3.96 \pm 0.01 s for untreated cells. The results of these experiments are shown in **Figure 2.3**.

Concentration Effects

To examine the effect of contrast agent concentration on cellular uptake, ICP-MS was utilized. NIH/3T3 cells were grown in Costar 96 well plate (polystyrene, flat bottom, tissue culture treated, black with clear bottom) with modified DMEM containing 10% BCS in a 5% carbon dioxide incubator. Cells were incubated with **4**, **5**, or **6** for one hour at 37 °C with concentrations of 0.01, 0.1, 0.5, 3, and 10 mM in modified DMEM containing 10% BCS in a 5% carbon dioxide incubator. At the end of the incubation period, the medium was removed and the cells were rinsed in triplicate with DPBS at ambient temperature. The cells were exposed to 100 μ L of 0.25% trypsin and harvested at which point they were counted using a hemacytometer. There was an average of 140,000 cells per well. The trypsin/cell suspensions were incubated with concentrated nitric acid at 80 °C for four hours. The dissolved cells were diluted to 5 mL. The final cell solutions were in 3% nitric acid with 5 ppb of indium as an internal standard. The

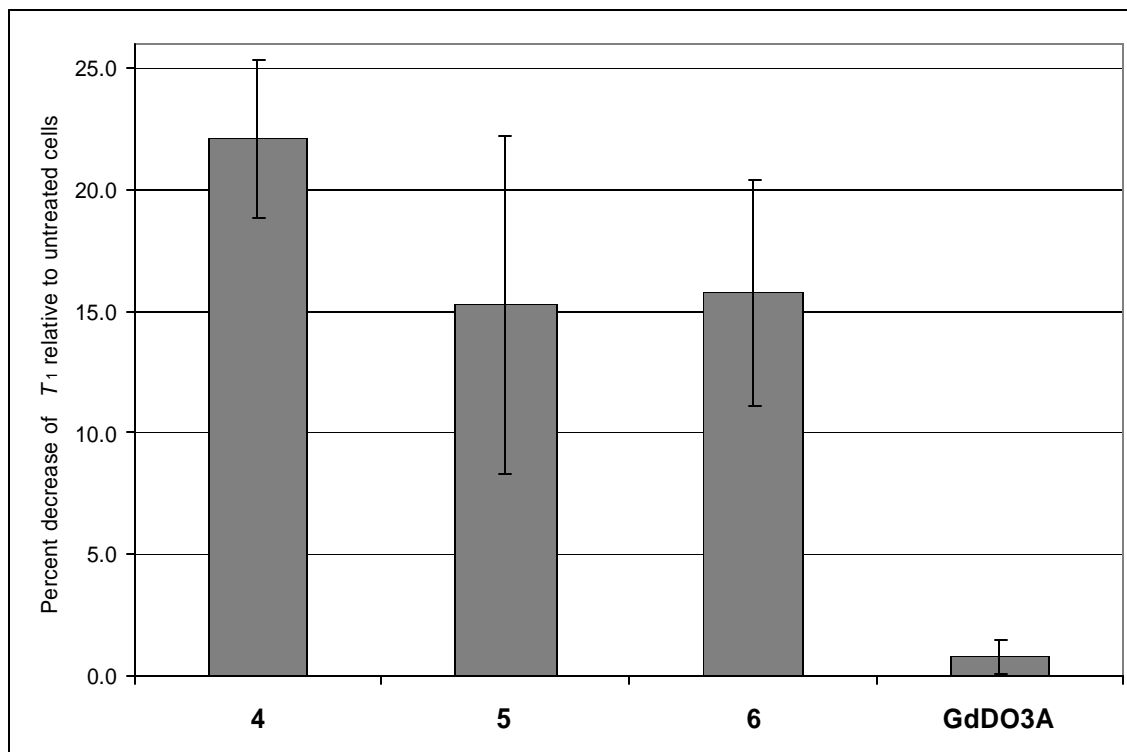


Figure 2.3: Results of T_1 study of NIH/3T3 cells incubated with 0.3 mM **4**, **5**, **6**, and gadolinium(III) DO3A (1,4,7-tris-carboxymethyl-1,4,7,10-tetraazacyclododecane). After incubation cells were rinsed with DPBS. T_1 values were measured at 60 MHz and 37 °C. The graph depicts the percent change in T_1 from untreated NIH/3T3 cells. Error bars represent one standard deviation.

samples were analyzed by ICP-MS. The amount of gadolinium per cell was calculated and is shown in **Figure 2.4**.

Incubation Time

In determining the effect of incubation time on uptake of the polyarginine contrast agents, ICP-MS was utilized. NIH/3T3 cells were grown in CorningTM brand tissue culture flasks (25 cm² with vent cap) with modified DMEM containing 10% BCS in a 5% carbon dioxide incubator. Cells were incubated with **7**, **8**, or **9** (0.3 mM in modified DMEM containing 10% BCS) for periods of one-half, one, two, four, ten, or twenty-four hours at 37 °C in a 5% carbon dioxide incubator. At the end of the incubation period, the medium was removed and the cells were rinsed in triplicate with DPBS at ambient temperature. The cells were exposed to 250 µL of 0.25% trypsin and harvested at which point they were counted using a hemacytometer and checked for viability using a trypan blue assay ²⁷. The average number of cells per flask ranged from 4,500 to 15,000 and increased with increasing incubation time. All cells were >98% viable after exposure to **7**, **8**, or **9** by trypan blue assay. The trypsin/cell suspensions were incubated with 500 µL of concentrated nitric acid at 80 °C for four hours. The dissolved cells were diluted to 10 mL. The final cell solutions were in 3% nitric acid with 5 ppb of indium as an internal standard. The samples were analyzed by ICP-MS. The amount of gadolinium per cell was calculated, and no significant difference of uptake of gadolinium per cell was observed between any of the incubation times.

Washout Studies

In studying the rate at which the polyarginine contrast agents leached from the cells, ICP-MS was used. NIH/3T3 cells, that exhibit contact inhibited growth, were

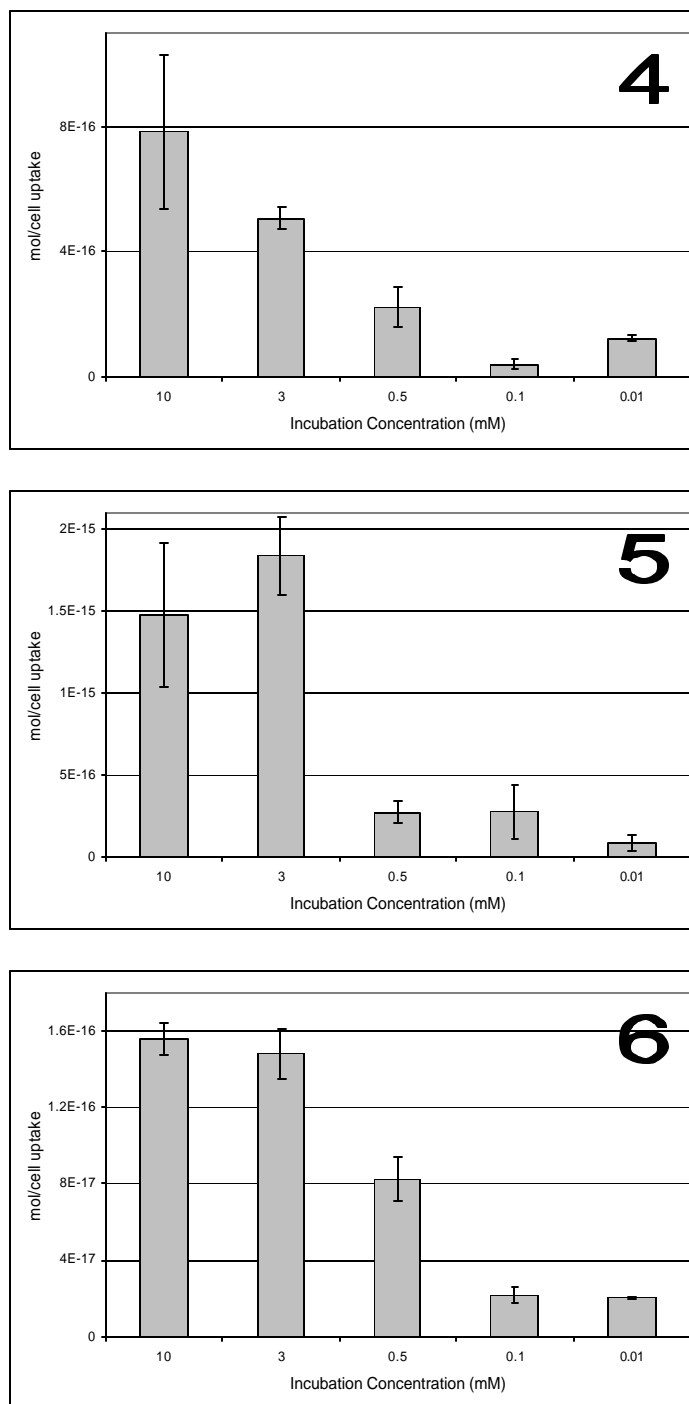


Figure 2.4: Demonstration of the dependence of uptake of 4-6 on incubation concentration. After incubation, NIH/3T3 cells were rinsed with DPBS, treated with trypsin, dissolved in nitric acid, and analyzed with ICP-MS. The graphs show uptake per cell plotted against incubation concentration. Error bars represent one standard deviation.

grown in 25 cm² CorningTM brand tissue culture flasks with modified DMEM containing 10% BCS in a 5% carbon dioxide incubator. A monolayer of cells were incubated with **4**, **5**, or **6** (0.3 mM in modified DMEM containing 10% BCS) for one hour at 37 °C in a 5% carbon dioxide incubator. At the end of the incubation period, the medium was removed and the cells were rinsed in triplicate with DPBS at ambient temperature. Fresh medium (5 mL) was applied to the cells and they were returned to the incubator. After periods of 24, 48, 72, and 96 hours, the medium was removed and replaced with fresh medium after triplicate rinsing with DPBS. The removed medium was analyzed for gadolinium concentration using ICP-MS. After removal of the medium at 96 hours, the cells were exposed to trypsin and prepared for ICP-MS as described previously. This process was repeated with sampling times of 1, 3, 6, and 10 hours. The results of these experiments are shown in **Figure 2.5**. The amount of gadolinium remaining in the cells after 96 hours was 3×10^{-19} - 5×10^{-19} mol/cell for all three compounds.

Cell Type Specificity

To determine if the uptake of the polyarginine contrast agents was specific to NIH/3T3 cells, the uptake of **7**, **8**, and **9** was examined using NIH/3T3, canine kidney epithelial (MDCK), and mouse macrophage (RAW 264.7) cells. Cells were grown in Costar 12 well plates (polystyrene, tissue culture treated) in a 5% carbon dioxide incubator at 37 °C with modified DMEM containing 10% BCS for the NIH/3T3 cells; EMEM modified to contain 1.0 mM sodium pyruvate, 0.1 mM nonessential amino acids, 1.5 g/L sodium bicarbonate and supplemented with 10% FBS for the MDCK cells; and modified DMEM containing 10% FBS for the RAW 264.7 cells. Cells were incubated with **7**, **8**, or **9** in the appropriate medium for one hour at 37 °C in a 5% carbon dioxide

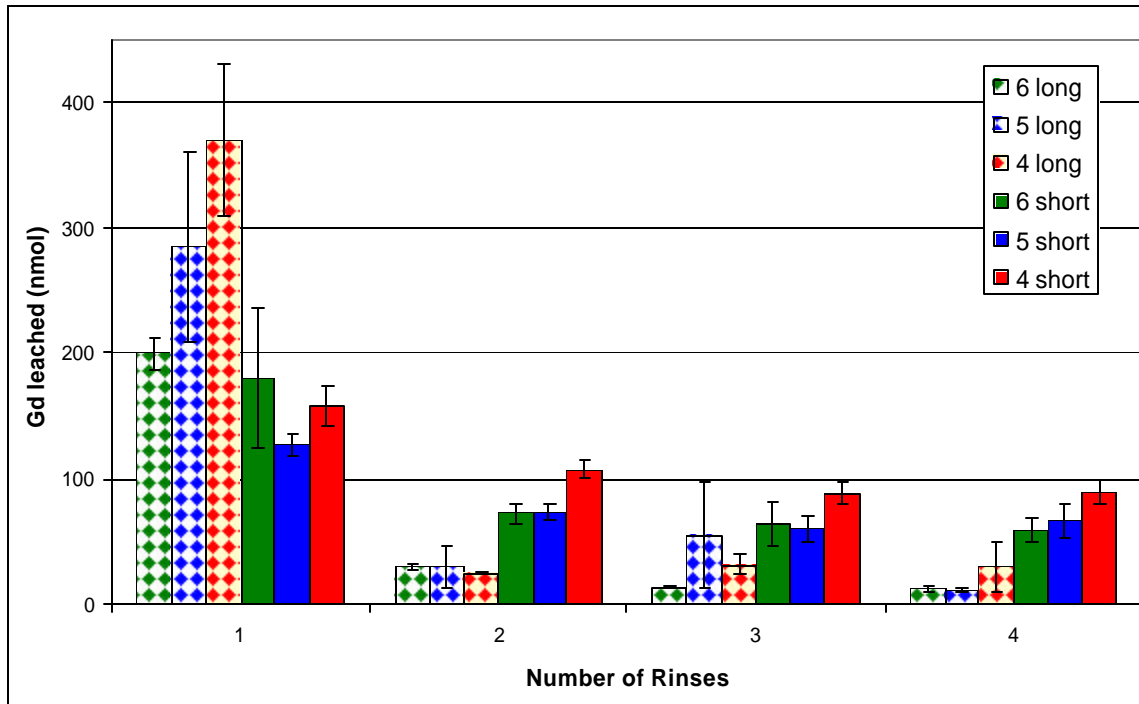


Figure 2.5: Washout rate of **4-6** from NIH/3T3 cells as a function of the number of rinses. Cells were incubated for one hour and then medium was changed. After each rinse period the medium was removed and analyzed using ICP-MS. Long incubation times were 24, 48, 72, and 96 hours. Short incubation times were 1, 3, 6, and 10 hours. Error bars represent one standard deviation.

incubator. At the end of the incubation period, the medium was removed and the cells were rinsed in triplicate with DPBS at ambient temperature. NIH/3T3 and MDCK cells were exposed to 0.25% trypsin and RAW 264.7 cells were removed using a cell scraper. The cell suspensions were prepared for ICP-MS as described previously. The samples were analyzed by ICP-MS, and the amount of gadolinium per cell was calculated and is shown in **Figure 2.6**.

MR Imaging

To determine the viability of these agents for MRI, NIH/3T3 cells were grown in CorningTM brand tissue culture flasks (75 cm² with vent cap) using modified DMEM containing 10% BCS. Cells were incubated with 3 mM **4** in modified DMEM containing 10% BCS for one hour at 37 °C in a 5% carbon dioxide incubator at which time they were rinsed three times with DPBS (2-3 mL) maintained at ambient temperature. The cells were exposed to 1 mL of 0.25% trypsin and harvested at which point they were counted using a hemacytometer. An average of 5,000,000 cells were loaded into NMR tube coaxial inserts (catalog number WGS-5BL, Wilmad, NJ) as trypsin suspensions. Spin-lattice relaxation time (T_1) of unlabeled cells was 2.53 ± 0.21 s. Labeling with **4** resulted in the reduction of T_1 to 1.64 ± 0.03 s. Based on this difference in T_1 values, contrast between treated and untreated cells was generated in T_1 -weighted spin-echo images using a short recycle time (TR) of 500 ms. The result of the imaging experiment is shown in **Figure 2.7**. It can be seen from the image that the signal intensity of the untreated cells is similar to that of deionized water which has a long T_1 . Both untreated cells and deionized water appear dark; in contrast, the intensity of treated cells is higher

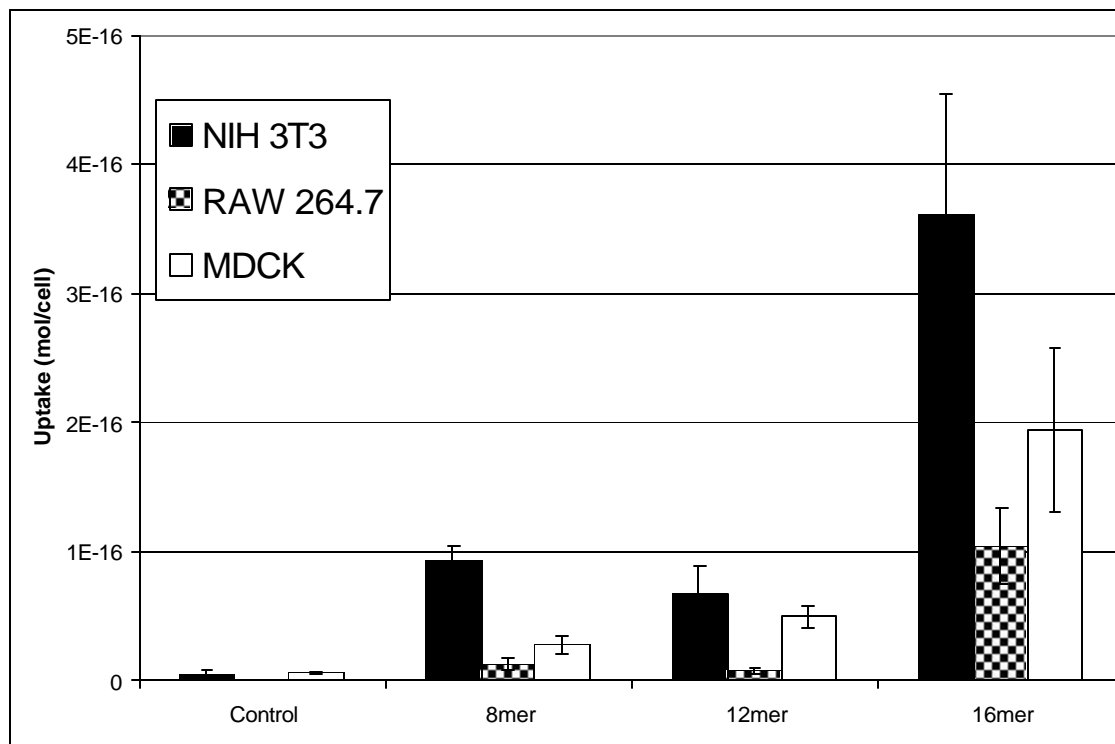


Figure 2.6: Cell type specificity for **7-9**. Cells were incubated with compound for one hour and rinsed with DPBS, treated with trypsin, dissolved in nitric acid, and analyzed with ICP-MS. The graph shows uptake per cell for each cell type plotted against complex. Incubation concentration of **7-9** was constant within each group of cells, but was not constant from compound to compound. Error bars represent one standard deviation.

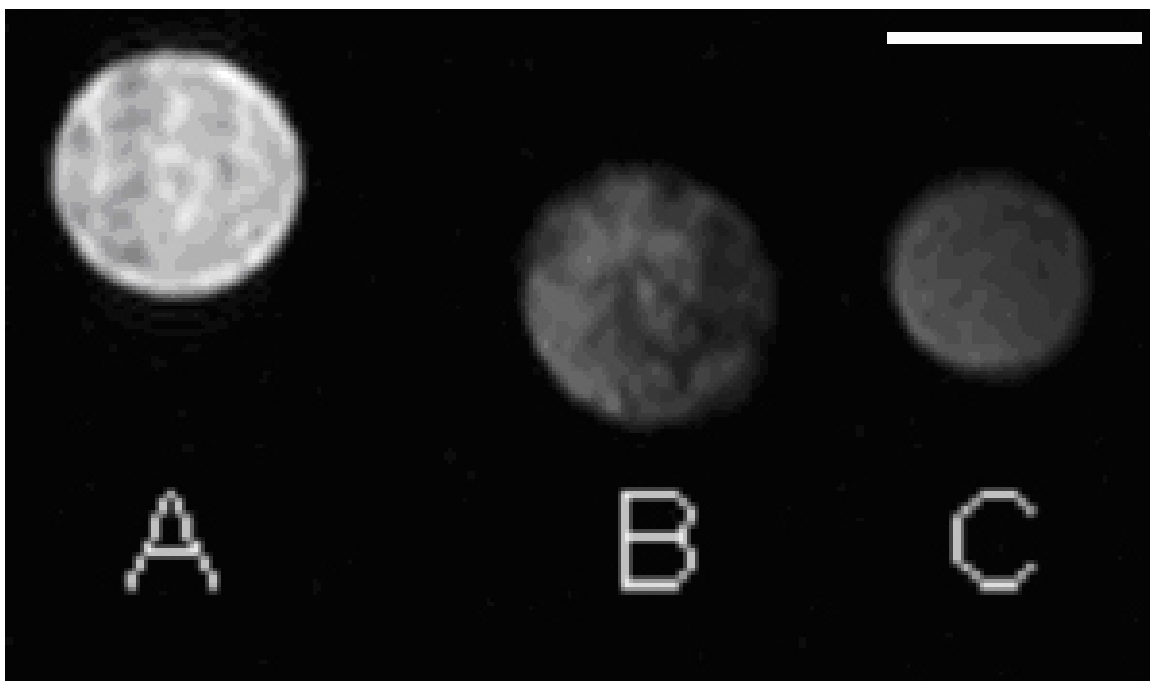


Figure 2.7: T_1 -weighted spin-echo MR images of NIH/3T3 cells at 9.4 T. Images were obtained using a spin-echo pulse sequence with TR 500 ms, echo delay time (TE) 16 ms: (A) NIH/3T3 cells incubated with **4**, (B) Untreated NIH/3T3 cells, (C) Deionized water in a capillary tube as a spatial marker. The scale bar represents 1.2 mm.

by a factor of three and they appear bright. Treatment of NIH/3T3 cells with **4** decreases the T_1 of the cells and renders them bright in a T1-weighted MR image.

Discussion

Physical Characterization

The relaxivities and octanol-water partition coefficients of **4-6** are listed in **Table 2.1**.

The values for relaxivity range from $4.4 \text{ mM}^{-1}\text{s}^{-1}$ to $6.8 \text{ mM}^{-1}\text{s}^{-1}$ with the longer polyarginine oligomers having smaller relaxivities. These values are slightly higher but on the same order of magnitude as Gadolinium(III) 1,4,7,10-tetraazacyclododecane-1-hydroxypropyl-3,7,10-trisacetic acid, ProHanceTM, which has a relaxivity of $3.1 \text{ mM}^{-1}\text{s}^{-1}$ when measured at the same field strength, temperature, and in the same buffer. This result demonstrates that complexes **4-6** can be used as effective MRI contrast agents.

The octanol-water partition coefficients are all less than one, with the value for **4** less than the values of **5** and **6**. The partition coefficient is a measure of hydrophilicity, and the values measured show that the smaller (n=8) polyarginine complex is more hydrophilic than the larger (n=12, 16) oligomers. This is a fascinating result, because the hydrophilicity would be expected to increase with the addition of the hydrophilic amino acid arginine. Interestingly, no direct correlation between the octanol-water partition coefficients of these complexes and membrane permeability was found. This supports previous reports that octanol-water partition coefficients alone are not a reliable indicator of membrane permeability, and other factors must be taken into account when predicting membrane permeability.²⁸⁻³⁰

Cell Studies

Proliferation and Viability Assays

To determine the toxicity of **4-9**, MTT and Trypan blue assays were performed. An MTT proliferation assay was performed with **7-9** and demonstrated that all compounds did not affect cell proliferation or viability of NIH/3T3 cells up to 10 mM. Above 10 mM, cells began to show signs of death both in morphology and through a decrease in absorbance in the MTT assay. Trypan blue viability studies were performed on all experiments discussed in this paper. All cells regardless of type incubated with **4-9** at concentrations up to 10 mM for all incubation times studied were at least 98% viable. These proliferation and viability assays justify the future use of polyarginine as a means of intracellular delivery of activatable contrast agents in vivo.

Two-Photon Laser Microscopy

Two-photon laser microscopy (TPLM) is similar to confocal microscopy. In both methods a laser beam is raster-scanned over a specimen, and the resulting fluorescence is detected using a photomultiplier tube. The detected fluorescence is used to produce an image on a computer.³¹ In TPLM, two infrared laser beams are focused, and two infrared photons must collide with a fluorophore to excite the fluorophore to a state identical to that achieved with one photon of approximately half the wavelength as in confocal microscopy (**Figure 2.8**). The nature of TPLM allows for the excitation of ultraviolet-excitable labels without an ultraviolet laser. This property of TPLM is critical to its use in observing lanthanide(III) based MRI contrast agents.

Europium(III) and gadolinium(III) possess large energy gaps between emissive and ground states, and therefore exhibit long-lived luminescence in aqueous solution

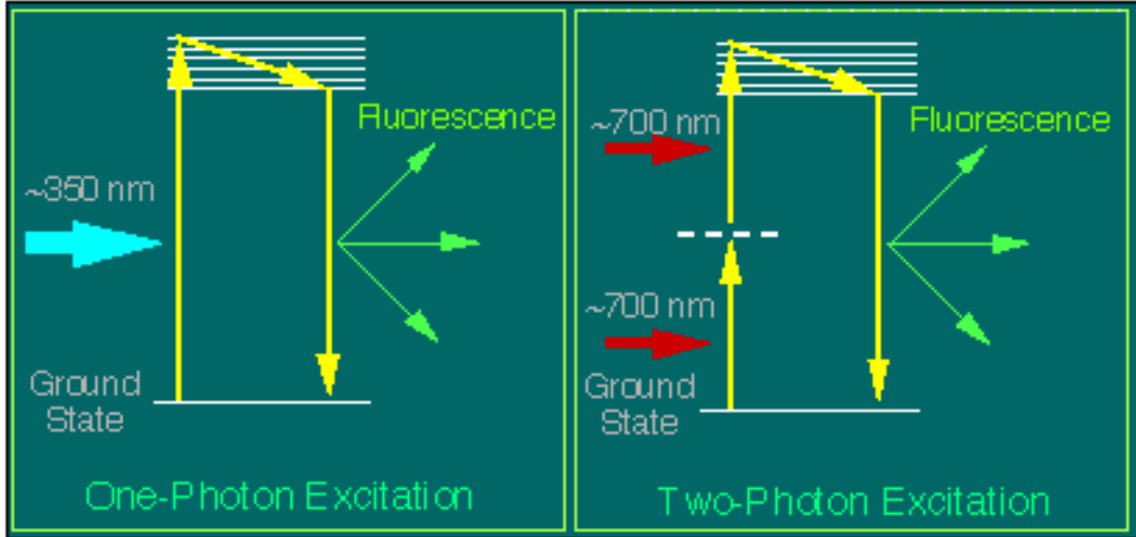


Figure 2.8: Schematic demonstrating the difference between the absorption of one and two photons of light leading to fluorescence in single-photon or two-photon laser microscopy, respectively.³²

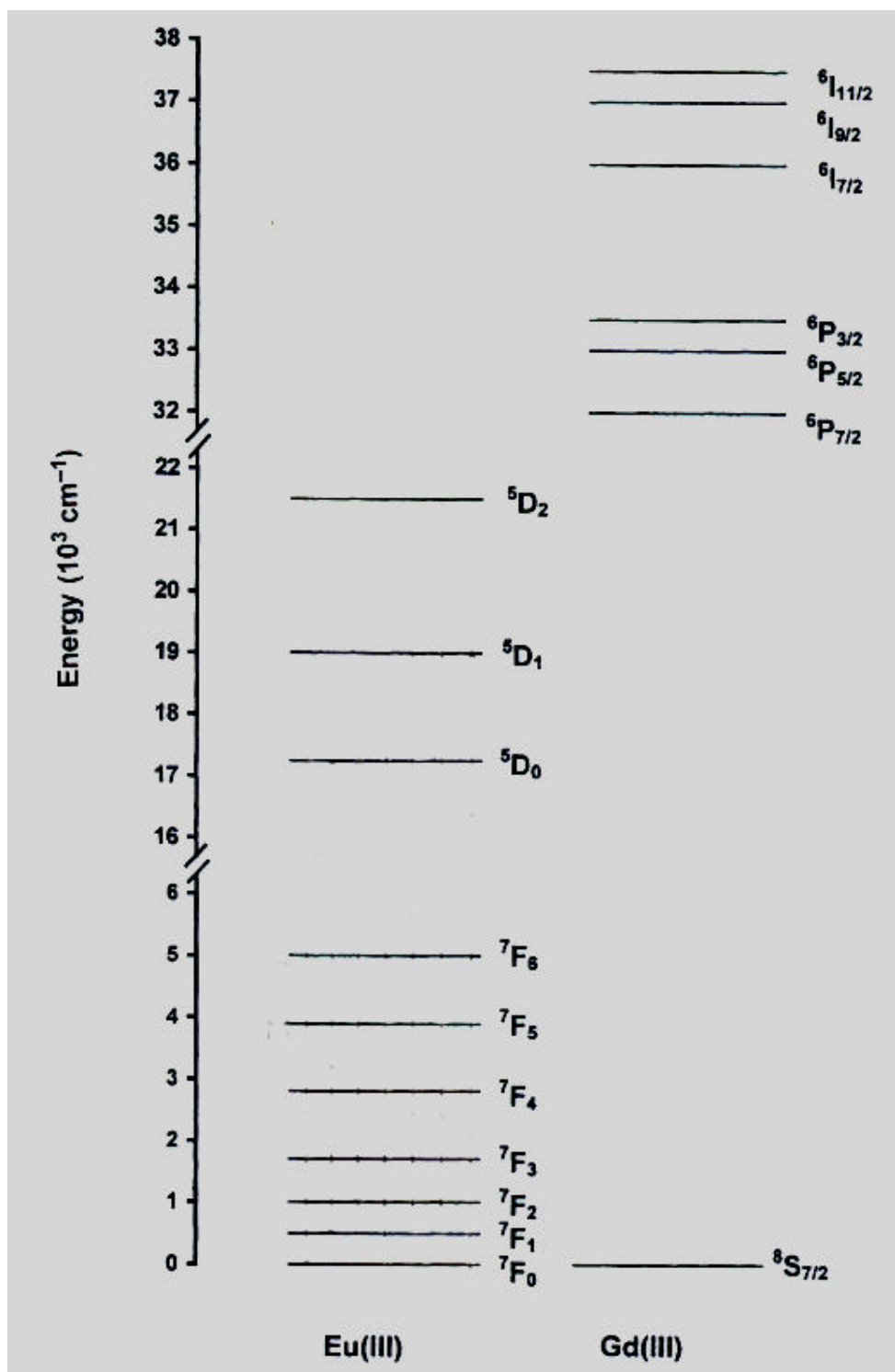


Figure 2.9: Molecular orbital diagram for europium(III) and gadolinium(III) demonstrating the large energy difference needed to excite gadolinium(III) (273 nm) versus europium(III) (375 nm). Figure modified from reference 7.

(>0.1ms). However, gadolinium(III) has a larger energy gap and requires excitation at 273 nm, whereas europium(III) can be excited at 375 nm (**Figure 2.9**).⁷ The excitation wavelength of 375 nm is in a suitable range for TPLM excitation at 750 nm (2 x 375 nm = 750 nm) which makes **9** a suitable TPLM dye. Hence TPLM experiments were carried out using **9** instead of **6**. The results of the TPLM experiments demonstrate that polyarginine is able to deliver lanthanide chelates into NIH/3T3 cells and that TPLM is a viable method for observing the behavior of lanthanide(III) based contrast agents in cells (**Figure 2.2**). The ability to use TPLM offers a method that is both quicker and of higher resolution than MRI for observing MR contrast agents.

T₁ Studies

The T_1 of cells from these experiments are listed in **Table 2.2**. Cells treated with **6** and rinsed with medium had significantly shorter T_1 values than both controls and the two controls were not significantly different from each other (>95% confidence for 5 degrees of freedom in a student T test).³³ This experiment confirms TPLM results that the polyarginine agent was taken up by the cells in levels detectable magnetically as well as optically while the control compound **10** was not. While there was a 3.4% difference between cells treated with **6** and rinsed with medium and control, there was a 16% difference between cells treated with **6** and rinsed with buffer and control. This variance is most likely due to metal ions in residual buffer shortening the T_1 of control cells.

Importantly, these experiments demonstrate that the polyarginine-modified MR contrast agent **6** is either bound to, or internalized by cells. Additionally, it shows that while triplicate washing with fresh cell culture medium is an effective means to remove

free contrast agent to significantly low levels, washing with a buffer solution provides a better means to measure the uptake of contrast agent versus controls.

To examine the relative effect on T_1 of **4-6**, NIH/3T3 cells were analyzed by T_1 analysis (**Figure 2.3**). Cells treated with **4-6** and rinsed with medium had significantly shorter T_1 values than untreated control cells and cells treated with the extracellular contrast agent gadolinium(III) 1,4,7,10-tetraazacyclododecane-1,4,7-trisacetic acid, **10**; however, no significant difference was detected between cells treated with **4-6** (>95% confidence for 5 degrees of freedom in a student T test).³³ The two T_1 measuring experiments demonstrate that compounds **4-6** enter cells and that once internalized by cells, all three compounds equally enhance contrast in MRI.

Concentration Effects

ICP-MS is a type of mass spectrometry that utilizes a plasma nebulizer as an atomizer and ionizer (**Figure 2.10**).³⁴ The technique has a high degree of selectivity, good precision and accuracy and low detection limits (ppb). Additionally this method can be highly automated to allow for the concentration determination of a large number of samples (hundreds) in a relatively short-time period (hours). This high throughput, sensitive method lends itself perfectly to studying the cell culture properties of **4-9**.

Since **4-9** were found to be non-toxic up to 10 mM, a range of concentrations from 0.01 mM to 10 mM was tested to determine the amount of material taken up by NIH/3T3 cells as a function of concentration. The trends for compounds **4-6** were very similar (**Figure 2.4**). Uptake at low concentrations (0.01-0.1 mM) was minimal and did not appear to change. From 0.1 mM to 3 mM a dramatic increase in uptake occurred corresponding to increasing incubation concentration. This trend ceased at 3 mM at

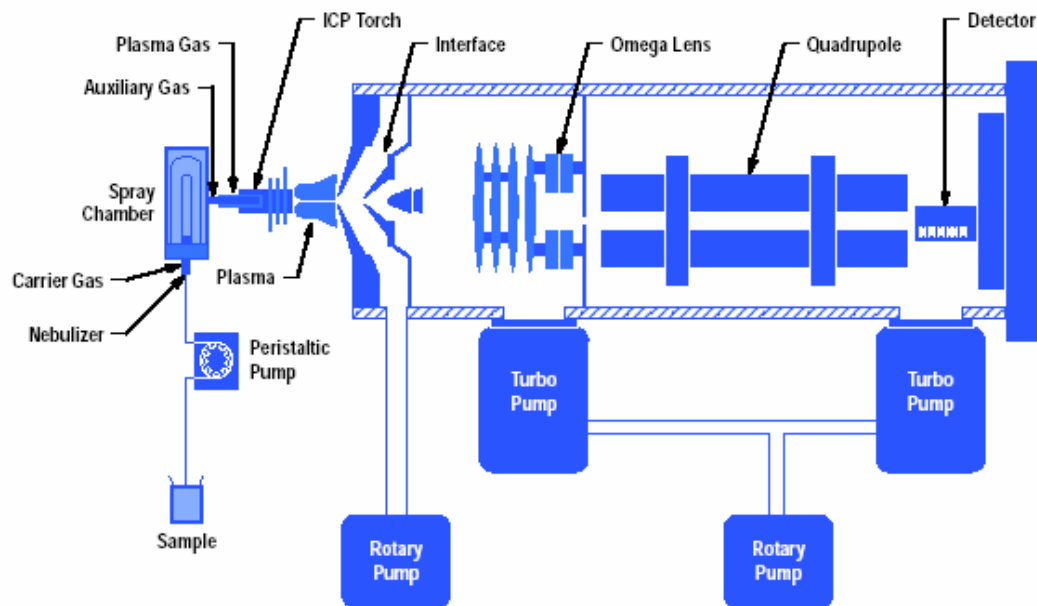


Figure 2.10: Schematic of ICP-MS: Liquid samples are sent through a nebulizer, atomized by the argon plasma, and detected using a mass spectrometry setup.³⁵

which point no increase in uptake was observed with increasing concentration. This study demonstrates that uptake of **4-6** is concentration dependant between 0.1 and 3 mM and appears to plateau outside of this range.

Incubation Time and Washout Studies

Interestingly, the amount of contrast agent taken up per cell was not dependent on the length of incubation when monitored from 0.5 to 24 hours; however, the washout rate of **4-6** was dependent on time and the number of rinses. This dual dependence is shown in **Figure 2.5** in which the total amount of gadolinium released from an entire plate of cells is plotted against the number of rinses and the duration of the rinses. For both long-time medium changes (24, 48, 72, 96 hours) and short-time medium changes (1, 3, 6, 10 hours) more compound leached from the cells on the first rinse (24 hours or 1 hour) than on subsequent rinses. Washout from the cells for subsequent rinses remained constant. The difference in the amount released between the first and subsequent rinses was larger for the long-times than the short-times. Additionally, >99% of the gadolinium was released from the cells by the end of the fourth rinse (calculated using the residual gadolinium content at the end of the experiment and the amount of gadolinium taken up by the cells from **Figure 2.4**). The results demonstrate that there is both time dependence and dependence on the number of rinses for the washout of **4-6**. These experiments support the proposed delivery mechanism in which electrostatics play a key role.²⁰ The cell surface should reach an electrostatic equilibrium with the polyarginine complex quickly because of the massive excess of compound. The dependence on the number of rinses of the washout also supports this theory because in every rinse, an equilibrium would be reached leaving less compound to be leached out in subsequent rinses.

Cell Type Specificity

Three cell types (NIH/3T3, RAW 264.7, and MDCK) were incubated with **7-9** to determine if uptake of the agents was cell type specific (**Figure 2.6**). The experiment demonstrated that **7-9** were taken up by all three cell types, and that there was a difference in the amount of agent taken up per cell. The highest loading of agent was seen in NIH/3T3 cells, and the lowest loading was seen in RAW 264.7 cells. The smaller amount take up per cell for the RAW 264.7 cells likely is due, at least in part, to the smaller size of these cells relative to the other two cell types. The uptake trend between cell lines was the same for all of the three compounds tested.

MR Imaging

MRI studies were performed to examine the ability of **4** to enhance contrast in an MRI image of NIH/3T3 cells (**Figure 2.7**). This experiment demonstrated that cells treated with polyarginine based contrast agents show increased contrast in an MR image. Importantly, the concentration used in this experiment was well below the level toxic to cells. The results of this experiment together with the results of other experiments suggest that polyarginine containing contrast agents are cell type specific because they label some cell types more heavily than others. Additionally, the time necessary to label cells enough to be visualized by MRI is short (=0.5 hours). This is a critical experiment that demonstrates the ability of these agents to be used in the study of biological phenomena using MRI.

Conclusion

This chapter demonstrated that conjugates of MR contrast agents and transport molecules that are capable of permeating cell membranes have been prepared. Cellular

uptake was confirmed using TPLM to visualize the presence of the contrast agent in cell culture. Further, the uptake of the agent by cells was orthogonally confirmed by bulk T_1 analysis. The behavior of these modified MR agents in cell culture was examined in depth. The effect of the length of oligomer on T_1 enhancement and cellular uptake as well as the effect of incubation time, concentration, and cell type on uptake were examined. Toxicity and washout studies were performed as well as in vitro MR imaging. The properties of the lanthanide complexes described in this paper are well suited for use in the study of biological systems with MRI. The preparation of a reliable intracellular delivery system offers the hope for an extremely powerful tool for the study of in vivo biological activity.

Experimental Procedures

All reagents and solvents were the highest commercially available grades and used without further purification. 1,4,7,10-tetraazacyclododecane-1,4,7-tris(acetic acid-*tert*-butyl ester)-10-acetic acid [DOTA(*tris-t*-Bu ester)] and 1,4,7-tris-*tert*-butoxycarbonylmethyl-1,4,7,10-tetraazacyclododecane [DO3A(*tris-t*-Bu ester)] was purchased from Macrocyclics (Dallas, TX). Resins and amino acids were purchased from Novabiochem (San Diego, CA). NIH/3T3 cells; MDCK cells; RAW 264.7 cells; MTT assay kit; Dulbecco's Modified Eagle's Medium (DMEM) with 4 mM L-glutamine modified to contain 4.5 g/L glucose and 1.5 g/L sodium bicarbonate; and Eagle's Minimal Essential medium (EMEM) with Earle's BSS and 2 mM L-glutamine modified to contain 1.0 mM sodium pyruvate, 0.1 mM nonessential amino acids, and 1.5 g/L sodium bicarbonate were purchased from American Type Culture Collection (ATCC) (Manassas, VA). Dulbecco's Phosphate Buffered Saline (DPBS) w/o calcium and

magnesium, fetal bovine serum (FBS), bovine calf serum (BCS), 0.25% trypsin, trypan blue, vent-cap flasks, multiwell plates, and cell scrapers were purchased from Fisher Scientific. Dulbecco's Modified Eagle's (DME) High Glucose cell culture medium, L-Glutamine, and Trypsin were purchased from Irvine Scientific (Santa Ana, CA). Bovine Calf Serum (BCS) and CO₂-independent medium were purchased from Gibco BRL Life Technologies (Carlsbad, CA). All other starting materials were purchased from Aldrich (Milwaukee, WI).

¹H NMR spectra were obtained on a Varian mercury spectrometer at 300 MHz for verification of synthesis. Spectra were obtained in D₂O using a value of 4.80 ppm as an internal reference. Mass spectrometry samples were analyzed using electrospray ionization (ESI), quadrupole mass spectrometry or matrix-assisted laser desorption ionization time of flight (MALDI-TOF) mass spectrometry in the PPMAL – Protein/Peptide MicroAnalytical Laboratory, California Institute of Technology, Beckman Institute. Results reported for *m/z* are for [M + H⁺]⁺ or [M – H⁺]⁻. Elemental analyses were performed at Desert Analytics Laboratory, Tucson, AZ. The longitudinal water proton relaxation rate at 59.97 MHz was measured by using a Bruker mq60 NMR Analyzer (Bruker Canada, Milton, Ont. Canada) operating at 1.5 T, by means of the standard inversion-recovery technique (20 data points, 8 scans each). A typical 90°-pulse length was 6.16 μs and the reproducibility of the *T*₁ data was ± 0.3%. Temperature was maintained by the instrument at 37 °C. Cells were counted using a Bright-Line hemacytometer. MTT assays were performed using a Bio-Tek Synergy HT plate reader. Inductively Coupled Plasma Mass Spectrometry (ICP-MS) was performed either at Desert Analytics Laboratory (Tucson, AZ), or at Northwestern University's Analytical

Services Laboratory (ASL) on a PQ ExCell Inductively Coupled Plasma Mass Spectrometer. Two-photon laser microscopy imaging was performed with a Molecular Dynamics Sarastro 2000 confocal laser-scanning microscope and a Coherent Mira 900 Titanium: Sapphire Mode-locked laser. The microscope stage and surrounding area were kept at 34 °C under atmospheric CO₂ for the duration of imaging. MR studies were performed on a General Electric/Bruker, Omega 400 WB imaging spectrometer fitted with Accustar shielded gradients at ambient temperature (20 °C). Spin-lattice relaxation time was measured using an inversion recovery pulse sequence. Images were acquired using a spin-echo imaging pulse sequence. MR measurements were carried out on freshly harvested cells. Cells were allowed to settle in NMR sample tubes under gravitational force prior to their placement in the magnet.

DOTA-(arginine)₈ (**1**): Polystyrene-based Wang resin containing an Fmoc protected arginine residue (1.7 g, 0.50 mmol/g) was swelled in dichloromethane for 30 min and washed four times with peptide synthesis grade dimethylformamide (DMF). The resin was treated twice with a solution of 20% piperidine (20 mL) in DMF for ten minutes. The resin was washed four times with DMF. In a separate vial, Fmoc protected arginine (3.0 g, 4.6 mmol), *O*-(7-azabenzotriazol-1-yl)-1,1,3,3-tetramethyluronium hexafluorophosphate (HATU) (1.7 g, 4.4 mmol), and DMF (5 mL) were combined and diisopropylethylamine (DIPEA) (1.6 mL, 9.2 mmol) was added. The resulting solution was added to the resin and allowed to react under argon for three hours. The resin was drained and rinsed four times with DMF. This procedure was repeated six times to yield a Fmoc protected 8mer of polyarginine bound to Wang resin. The resin was treated with piperidine and washed with DMF as described above. In a separate vial, 1,4,7,10-

tetraazacyclododecane-1,4,7-tris(acetic acid-*t*-butyl ester)-10-acetic acid [DOTA(tris-*t*-Bu ester)] (1.1 g, 2.0 mmol), HATU (0.72 g, 1.9 mmol), and DMF (5 mL) were combined and DIPEA (1.7 mL, 10 mmol) was added. The resulting solution was added to the resin and allowed to react under argon for twelve hours. The solvent was removed and the resin was washed four times with DMF, four times with dichloromethane, four times with methanol, and dried under vacuum. A 30 mL solution of 95% trifluoroacetic acid (TFA), 2.5% triisopropylsilane, and 2.5% water was added to the resin and mixed for one hour then drained. The resin was rinsed with 15 mL TFA. The filtrate and rinse were combined and reduced in volume to ten milliliters. Forty milliliters of -20 °C methyl *tert*-butyl ether (MTBE) was added to precipitate a white solid. The solid was washed three times with cold MTBE, taken up in water and freeze dried to a white powder. The white powder was exposed to the TFA solution for seven hours, washed with cold MTBE as above, and freeze dried to yield a white solid. Yield = 1.31 g. ¹H NMR (D₂O): δ = 1.63 (m, 16H), 1.80 (m, 16H), 2.6-3.8 (m, 24H), 3.18 (m, 16H), 4.30 (m, 8H); MS Calcd for C₆₄H₁₂₄N₃₆O₁₆ [M + H⁺]⁺: 1654.0, found 1653.8.

DOTA-(arginine)₁₂ (**2**): Polystyrene-based Wang resin containing an Fmoc protected arginine residue (1.7 g, 0.50 mmol/g) was swelled in dichloromethane for 30 min and washed four times with peptide synthesis grade DMF. The resin was treated twice with a solution of 20% piperidine (20 mL) in DMF for ten minutes. The resin was washed four times with DMF. In a separate vial, Fmoc protected arginine (3.0 g, 4.6 mmol), HATU (1.7 g, 4.4 mmol), and DMF (5 mL) were combined and DIPEA (1.6 mL, 9.2 mmol) was added. The resulting solution was added to the resin and allowed to react under argon for three hours. The resin was drained and rinsed four times with DMF.

This procedure was repeated ten times to yield an Fmoc protected 12mer of polyarginine bound to Wang resin. The resin was treated with piperidine and washed with DMF as described above. In a separate vial, DOTA(tris-*t*-Bu ester) (1.1 g, 2.0 mmol), HATU (0.72 g, 1.9 mmol), and DMF (5 mL) were combined and DIPEA (1.7 mL, 10 mmol) was added. The resulting solution was added to the resin and allowed to react under argon for twelve hours. The solvent was removed and the resin was washed four times with DMF, four times with dichloromethane, four times with methanol, and dried under vacuum. A 30 mL solution of 95% TFA, 2.5% triisopropylsilane, and 2.5% water was added to the resin and mixed for one hour then drained. The resin was rinsed with 15 mL TFA. The filtrate and rinse were combined and reduced in volume to ten milliliters. Forty milliliters of -20 °C MTBE was added to precipitate a white solid. The solid was washed three times with cold MTBE, taken up in water and freeze dried to a white powder. The white powder was exposed to the TFA solution for seven hours, washed with cold MTBE as above, and freeze dried to yield a white solid. Yield = 1.67 g. ¹H NMR (D₂O): δ = 1.62 (m, 24H), 1.79 (m, 24H), 2.6-3.8 (m, 24H), 3.17 (m, 24H), 4.27 (m, 12H); MS Calcd for C₈₈H₁₇₂N₅₂O₂₀ [M + H⁺]⁺: 2279.7, found 2280.0.

DOTA-(arginine)₁₆ (**3**): Polystyrene-based Wang resin containing an Fmoc protected arginine residue (1.7 g, 0.50 mmol/g) was swelled in dichloromethane for 30 min and washed four times with peptide synthesis grade DMF. The resin was treated twice with a solution of 20% piperidine (20 mL) in DMF for ten minutes. The resin was washed four times with DMF. In a separate vial, Fmoc protected arginine (3.0 g, 4.6 mmol), HATU (1.7 g, 4.4 mmol), and DMF (5 mL) were combined and DIPEA (1.6 mL, 9.2 mmol) was added. The resulting solution was added to the resin and allowed to react

under argon for three hours. The resin was drained and rinsed four times with DMF. This procedure was repeated fourteen times to yield an Fmoc protected 16mer of polyarginine bound to Wang resin. The resin was treated with piperidine and washed with DMF as described above. In a separate vial, DOTA(tris-*t*-Bu ester) (1.1 g, 2.0 mmol), HATU (0.72 g, 1.9 mmol), and DMF (5 mL) were combined and DIPEA (1.7 mL, 10 mmol) was added. The resulting solution was added to the resin and allowed to react under argon for 12 hours. The solvent was removed and the resin was washed four times with DMF, four times with dichloromethane, four times with methanol, and then dried under vacuum. A 30 mL solution of 95% TFA, 2.5% triisopropylsilane, and 2.5% water was then added to the resin and mixed for one hour then drained. The resin was rinsed with 15 mL TFA. The filtrate and rinse were combined and reduced in volume to ten milliliters. Forty milliliters of -20 °C MTBE was added to precipitate a white solid. The solid was washed three times with cold MTE, taken up in water and freeze dried to a white powder. The white powder was exposed to the TFA solution for seven hours, washed with cold MTBE as above, and freeze dried to yield a white solid. Yield = 2.19 g. ¹H NMR (D₂O): δ = 1.55 (m, 32H), 1.72 (m, 32H), 2.6-3.8 (m, 24H), 3.10 (m, 32H), 4.21 (m, 16H); MS Calcd for C₁₁₂H₂₂₀N₆₈O₂₄ [M + H]⁺: 2902.8, found 2903.0.

General Lanthanide(III) Complex Synthesis

To a solution of the free ligand in water (16-32 mM) was added gadolinium(III) hydroxide monohydrate or **12** (1.3 equiv.). The reaction mixture was heated to 80 °C and stirred for twelve hours. The reaction mixture was then cooled to ambient temperature and the pH was adjusted to 11 with aqueous ammonium hydroxide. The mixture was

filtered through a 0.2 μm syringe filter, purified using Sephadex-G25 size exclusion chromatography, and freeze dried to yield a white solid.

DOTA-(arginine)₈ gadolinium(III) (4): Yield: 0.618 g (86.7%). MS Calcd for $\text{C}_{64}\text{H}_{120}\text{GdN}_{36}\text{O}_{16}$ $[\text{M} + \text{H}]^+$: Gd isotope pattern centered at 1808.1, found Gd isotope pattern centered at 1808.1.

DOTA-(arginine)₁₂ gadolinium(III) (5): Yield: 0.651 g (68.3%). MS Calcd for $\text{C}_{88}\text{H}_{168}\text{GdN}_{52}\text{O}_{20}$ $[\text{M} + \text{H}]^+$: Gd isotope pattern centered at 2432.9, found Gd isotope pattern centered at 2432.9.

DOTA-(arginine)₁₆ gadolinium(III) (6): Yield: 0.881 g (60.6%). MS Calcd for $\text{C}_{112}\text{H}_{217}\text{GdN}_{68}\text{O}_{24}$ $[\text{M} + \text{H}]^+$: Gd isotope pattern centered at 3058.7, found Gd isotope pattern centered at 3059.0.

DOTA-(arginine)₈ europium(III) (7): Yield: 0.466 g (80.7%). MS Calcd for $\text{C}_{64}\text{H}_{120}\text{EuN}_{36}\text{O}_{16}$ $[\text{M} + \text{H}]^+$: Gd isotope pattern centered at 1802.8, found Gd isotope pattern centered at 1802.2.

DOTA-(arginine)₁₂ europium(III) (8): Yield: 0.527 g (70.0%). MS Calcd for $\text{C}_{88}\text{H}_{168}\text{EuN}_{52}\text{O}_{20}$ $[\text{M} + \text{H}]^+$: Gd isotope pattern centered at 2427.3, found Gd isotope pattern centered at 2427.0.

DOTA-(arginine)₁₆ europium(III) (9): Yield: 0.573 g (76.0%). MS Calcd for $\text{C}_{112}\text{H}_{217}\text{EuN}_{68}\text{O}_{24}$ $[\text{M} + \text{H}]^+$: Eu isotope pattern centered at 3054.7, found Eu isotope pattern centered at 3054.6.

Gadolinium(III) 1,4,7,10-tetraazacyclododecane-1,4,7-triacetic acid (10): 1,4,7-tris-*tert*-butoxycarbonylmethyl-1,4,7,10-tetraazacyclododecane (0.313 g, 0.609 mmol) was dissolved in trifluoroacetic acid (25 mL) and stirred for two hours. The

trifluoroacetic acid was removed and the residue washed with cold MTBE. The resulting residue was taken up in water (10 mL) and gadolinium(III) hydroxide (0.165 g, 0.731 mmol) was added. The reaction mixture was stirred at 80 °C for twelve hours and cooled to ambient temperature. The pH of the reaction mixture was adjusted to 11 with ammonium hydroxide. The reaction mixture was filtered through a 0.2 µm syringe filter and HPLC purification (Aquasil C-18 column (Keystone, PA)) yielded 0.572 g (47.0%) of a white solid. MS Calcd for $C_{14}H_{23}GdN_4O_6 [M - H^+]$: Gd isotope pattern centered at 499.6, found Gd isotope pattern centered at 499.7; Anal. Calcd for $C_{14}H_{23}GdN_4O_6$: C, 33.59; H, 4.63; N, 11.19. Found: C, 33.41; H, 4.99; N, 11.00.

Europium(III) 1,4,7,10-tetraazacyclododecane-1,4,7-triacetic acid (11): 1,4,7-tris-*tert*-butoxycarbonylmethyl-1,4,7,10-tetraazacyclododecane (0.313 g, 0.609 mmol) was dissolved in trifluoroacetic acid (25 mL) and stirred for two hours. The trifluoroacetic acid was removed and the residue washed with cold MTBE. The resulting residue was taken up in water (10 mL) and **12** (0.162 g, 0.731 mmol) was added. The reaction mixture was stirred at 80 °C for 12 hours cooled to ambient temperature. The pH of the reaction mixture was adjusted to 11 with ammonium hydroxide. The reaction mixture was then filtered through a 0.2 µm syringe filter and HPLC purification (Aquasil C-18 column (Keystone, PA)) yielded 0.439 g (36.5%) of a white solid. MS Calcd for $C_{14}H_{23}EuN_4O_6 [M - H^+]$: Eu isotope pattern centered at 494.6, found Eu isotope pattern centered at 494.7; Anal. Calcd for $C_{14}H_{23}EuN_4O_6 \cdot H_2O$: C, 32.76; H, 4.91; N, 10.91. Found: C, 32.50; H, 5.15; N, 10.71.

Europium(III) hydroxide pentahydrate (12): To a solution of $EuCl_3$ (10.00 g, 0.0387 mol) in water (100 mL) was added a saturated solution of sodium hydroxide until

the pH of the solution was 14. The resulting white precipitate was filtered, washed with water and dried under reduced pressure to yield 7.54 g (65.9%). Anal. Calcd for $\text{EuH}_3\text{O}_3 \cdot 5\text{H}_2\text{O}$: Eu, 51.85. Found: Eu, 51.48.

References

- (1) T. Haraguchi, *Cell Struct. Funct.* **2002**, *27*, 333-334.
- (2) K.-i. Morimoto, T. Shimizu, K. Furukawa, H. Morio, H. Kurosawa, and T. Shirasawa, *Biochem. Biophys. Res. Commun.* **2002**, *292*, 999-1009.
- (3) S. R. Cherry, *J. Clin. Pharmacol.* **2001**, *41*, 482-491.
- (4) S. W. Ruffins, R. E. Jacobs, and S. E. Fraser, *Curr. Opin. Neurobiol.* **2002**, *12*, 580-586.
- (5) J. Zhang, E. Campbell Robert, Y. Ting Alice, and Y. Tsien Roger, *Nat. Rev. Mol. Cell Biol.* **2002**, *3*, 906-918.
- (6) A. Miyawaki and R. Y. Tsien, *Methods Enzymol.* **2000**, *327*, 472-500.
- (7) A. E. Merbach and E. Toth, *The Chemistry of Contrast Agents in Medical Magnetic Resonance Imaging*; John Wiley & Sons, Ltd., New York, 2001.
- (8) R. E. Jacobs, E. T. Ahrens, T. J. Meade, and S. E. Fraser, *Trends Cell Biol* **1999**, *9*, 73-76.
- (9) M. M. Hueber, A. B. Staubli, K. Kustedjo, M. H. B. Gray, J. Shih, S. E. Fraser, R. E. Jacobs, and T. J. Meade, *Bioconjugate Chem* **1998**, *9*, 242-249.
- (10) P. Wunderbaldinger, L. Josephson, and R. Weissleder, *Bioconjugate Chem.* **2002**, *13*, 264-268.
- (11) R. Bhorade, R. Weissleder, T. Nakakoshi, A. Moore, and C.-H. Tung, *Bioconjugate Chem.* **2000**, *11*, 301-305.
- (12) M. Lewin, N. Carlesso, C.-H. Tung, X.-W. Tang, D. Cory, D. T. Scadden, and R. Weissleder, *Nature Biotechnol.* **2000**, *18*, 410-414.
- (13) L. Josephson, C.-H. Tung, A. Moore, and R. Weissleder, *Bioconjugate Chem.* **1999**, *10*, 186-191.
- (14) C. H. Dodd, H. C. Hsu, W. J. Chu, P. Yang, H. G. Zhang, J. D. Mountz, K. Zinn, J. Forder, L. Josephson, R. Weissleder, and J. M. Mountz, *J. Immunol. Meth.* **2001**, *256*, 89-105.

- (15) J. F. Kayyem, R. M. Kumar, S. E. Fraser, and T. J. Meade, *Chem. Biol.* **1995**, *2*, 615-620.
- (16) S. Heckl, J. Debus, J. Jenne, R. Pipkorn, W. Waldeck, H. Spring, R. Rastert, C. W. Von der Lieth, and K. Braun, *Cancer Res.* **2002**, *62*, 7018-7024.
- (17) J. F. Kayyem, R. M. Kumar, S. E. Fraser, and T. J. Meade, *Chem Biol* **1995**, *2*, 615-620.
- (18) D. J. Mitchell, D. T. Kim, L. Steinman, C. G. Fathman, and J. B. Rothbard, *J Peptide Res* **2000**, *56*, 318-325.
- (19) S. Futaki, T. Suzuki, W. Ohashi, T. Yagami, S. Tanaka, K. Ueda, and Y. Sugiura, *J Biol Chem* **2001**, *276*, 5836-5840.
- (20) J. S. Wadia and S. F. Dowdy, *Curr. Opin. Biotechnol.* **2002**, *13*, 52-56.
- (21) J. B. Rothbard, E. Kreider, C. L. VanDeusen, L. Wright, B. L. Wylie, and P. A. Wender, *J. Med. Chem.* **2002**, *45*, 3612-3618.
- (22) J. B. Rothbard, S. Garlington, Q. Lin, T. Kirschberg, E. Kreider, L. P. McGrane, P. A. Wender, and P. A. Khavari, *Nature Med.* **2000**, *6*, 1253-1257.
- (23) J. C. Mai, H. Shen, S. C. Watkins, T. Cheng, and P. D. Robbins, *J. Biol. Chem.* **2002**, *277*, 30208-30218.
- (24) S. A. Kates and F. Albericio, *Solid-Phase Synthesis: A Practical Guide*; Marcel Dekker, Inc., New York, 2000.
- (25) T. F. Gabriel, *Int. J. Pept. Protein Res.* **1987**, *30*, 40-43.
- (26) J. Cornish, K. E. Callon, C. Q. X. Lin, C. L. Xiao, T. B. Mulvey, G. J. S. Cooper, and I. R. Reid, *Am. J. Physiol.* **1999**, *277*, E779-E783.
- (27) R. I. Freshney, *Culture of Animal Cells: A Manual of Basic Technique, Fourth Edition*; John Wiley & Sons, Inc., New York, 2000.
- (28) J. T. Goodwin, R. A. Conradi, N. F. H. Ho, and P. S. Burton, *J. Med. Chem.* **2001**, *44*, 3721-3729.
- (29) S. D. Kramer, *Pharm. Sci. Tech. Today* **1999**, *2*, 373-380.
- (30) R. A. Conradi, A. R. Hilgers, N. F. H. Ho, and P. S. Burton, *Pharm. Res.* **1991**, *8*, 1453-1460.
- (31) S. M. Potter, *Curr. Biol.* **1996**, *6*, 1595-1598.

- (32) Image attained on 09/02/03 from
<http://www.bris.ac.uk/Depts/Anatomy/research/neuro/OneTwoPhoton/TwoPhoton.htm>.
- (33) D. C. Harris, *Quantitative Chemical Analysis, Fourth Edition*; W. H. Freeman and Company, New York, 1995.
- (34) D. A. Skoog, F. J. Holler, and T. A. Nieman, *Principles of Instrumental Analysis*; Saunders College Pub., Philadelphia, 1998.
- (35) Image attained on 08/21/03 from
<http://www.hpl.hp.com/hpjournal/97aug/aug97a9.pdf>.

Chapter 3

An MR Contrast Agent to Cross Cell Membranes, the Blood Brain Barrier, and Label Ab Plaques

Introduction

Alzheimer's disease (AD) affects over four million Americans.¹ This disease is defined based on severe memory loss and other cognitive deficits along with the presence of plaques and tangles upon microscopic examination of the brain.² The plaques and tangles are composed of naturally occurring, transmembrane amyloid proteins that have become incorrectly folded.³ The role that amyloid (A β) plaques take in the advancement of AD is uncertain.⁴ Regardless of the exact role of the plaques in Alzheimer progression, their presence is one of the two necessary factors for definitive diagnosis of the disease. Definitive diagnosis of AD requires both a psychological evaluation and identification of plaques upon postmortem examination.⁵

AD is difficult to distinguish from normal aging and other ailments such as Pick's disease and Huntington's disease until very late stages of the disease.^{2,5} The difficulty in diagnosing AD is evident upon postmortem examination when over twenty percent of cases are found to have conditions other than AD.⁶ Because of poor diagnosis techniques, the study of AD and search for potential treatments, preventions, or a cure remain a daunting task. Early detection of the plaques responsible for AD would make the disease easier to diagnose and study.

Magnetic Resonance Imaging (MRI) is a powerful tool for noninvasive clinical and biological imaging. MRI offers a noninvasive means to map structure and function by sampling the amount, flow, and environment of water protons in vivo. Images are produced from the relaxation times of water protons where the intensity in a given volume element is a function of the water concentration and relaxation times (T_1 and T_2). Intrinsic contrast can be augmented by the use of paramagnetic contrast agents.

Typically, the paramagnetic ion gadolinium(III) is used in MRI agents to decrease the local T_1 of water protons and therefore provide increased contrast.⁷ One major limitation of current clinically approved contrast agents is their lack of biological specificity. The systemic delivery of these agents to specific sites in vivo represents an enormous challenge.

If contrast agent aided MRI is to be used as a diagnostic method for AD, the contrast agents used will need to bind specifically to A β plaques. Since A β plaques are located in the brain, a key obstacle of in vivo detection of the plaques is the delivery of contrast agents across the blood-brain barrier (BBB). The BBB is a highly advanced defense system composed of special cells and membranes that controls the flow of material into and out of the brain. Many invasive techniques have been used to bypass the BBB but are not viable for use with human patients.⁸ One recent, noninvasive method used to deliver molecules via conjugation to other molecules that facilitate transport through the BBB.⁹⁻¹²

Various research groups are attempting to image AD plaques in vivo using imaging techniques other than MRI such as two-photon laser microscopy, fluorescence microscopy, positron emission tomography (PET), and single-photon emission computerized tomography (SPECT).¹³⁻²⁶ These methods are extremely invasive, involve the use of ionizing radiation, or offer poor spatial resolution. However, Benveniste and coworkers have used high-resolution MRI to visualize AD plaques. Unfortunately, their method requires extremely long scan times that are unacceptable for use on humans.²⁶

An MRI contrast agent for the diagnosis of AD would offer significant advantages over other methods in that repeated non-harmful scans could be acquired to diagnose and

monitor the progress of the disease. The use of an MRI contrast-agent would allow for faster scans which would lead to shorter amounts of time needed to identify AD plaques.

Recently, Poduslo and coworkers have used contrast agent aided MRI to image AD plaques.²⁷ Conjugated gadolinium(III) diethylenetriaminepentaacetic acid (DTPA) to a putrescine modified A β peptide was able to cross the BBB with the aid of the putrescine moieties although the mechanism of the delivery is unknown. Targeting of A β peptides in vivo is achieved because of the tendency of A β plaques to aggregate. Although the gadolinium(III)-labeled, putrescine-modified A β peptide is promising, this compound is quite large (MW 4976), the synthesis involves multiple purification steps, and the final product is not easily characterized because of its large size. A small molecule based contrast agent would be an improvement over the A β peptide agent because of the relative ease with which it could be synthesized, purified, and characterized.

Many small organic compounds have been found to possess high binding affinities for the A β aggregates associated with AD. These compounds include Congo Red, Chrysamine G, Thioflavin S, (*trans, trans*)-1-bromo-2,5-bis-(3-hydroxycarbonyl-4-hydroxy)styrylbenzene (BSB), and smaller styrylbenzenes shown in **Figure 3.1**. Some of these compounds are capable of crossing the BBB in addition to labeling A β plaques. Recently the *N,N*-dimethylamino modified stilbene, **5**, has been shown to both label A β aggregates and permeate the BBB.²⁸ The mechanism for uptake across the BBB is unknown. The selective binding of these compounds to A β plaques is unknown but believed to involve a chemical mechanism similar to that operative in the direct labeling of cellulose fibers in which the dyes align within linear portions of the plaques.²⁹ In this

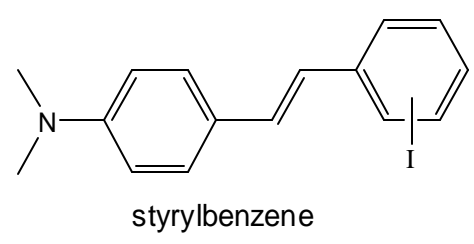
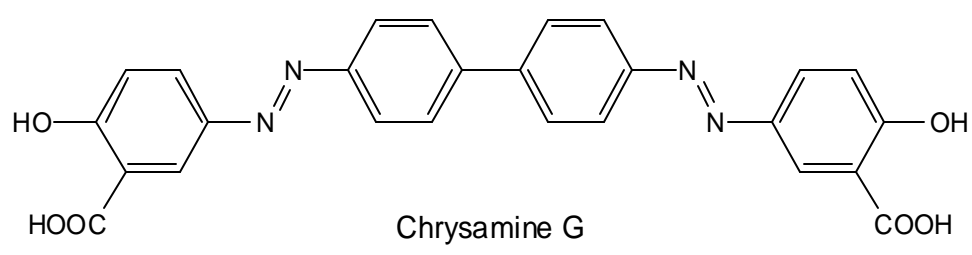
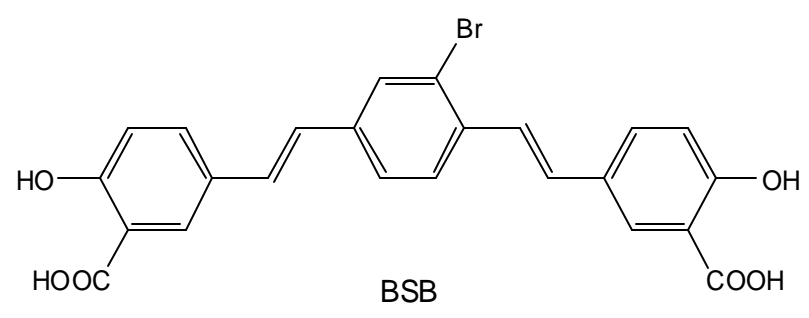
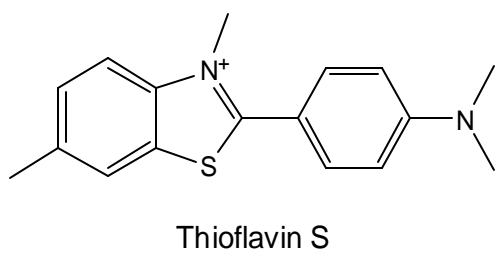
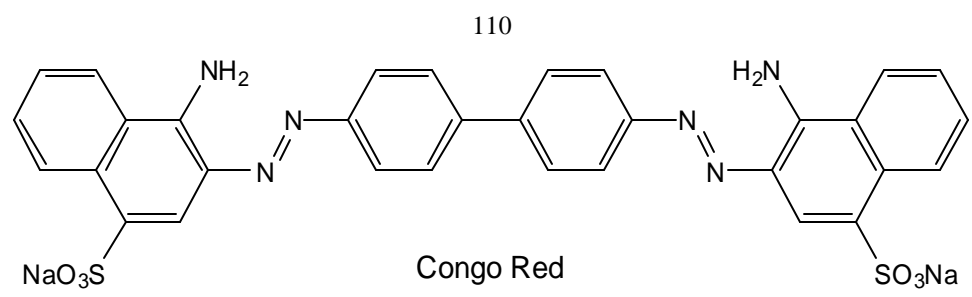


Figure 3.1: Chemical structures of compounds that bind to A β plaques: Congo Red, Chrysamine G, Thioflavin S, BSB, and styrylbenzenes.

binding model, the spacing between each peptide backbone aligns charged residues on the plaques with the acidic or basic groups of dyes.³⁰

In an attempt to deliver MRI contrast agents across the BBB and label A β plaques using small complexes (MW ~1000 Daltons), compounds **1-3** shown in **Figure 3.2** were synthesized. The compounds were characterized and tested in vitro. Because of the inability to accurately diagnosis AD, these compounds hold great potential for aiding early, accurate diagnosis of AD.

Results

Synthesis

The syntheses of **1-3** are shown in **Scheme 1**. The isothiocyanide derivative of the modified stilbene, **4**, was synthesized via reaction of the amino derivative with thiophosgene. Ligands were generated through the reaction of **4** with the aniline derivative of the appropriate chelate to give a thiourea linkage. The ligands were metalated using gadolinium(III) chloride hexahydrate and purified on a Sephadex G-25 size exclusion column. Final gadolinium(III) complexes were characterized by electrospray mass spectrometry and elemental analysis.

Partition Coefficients

Octanol-water partition coefficients ($P_{\text{oct/wat}}$) were measured by dissolving 7-10 mg of each compound in one milliliter of a 1:1 mixture of octanol and water. The resulting biphasic solution was shaken vigorously for two hours at which point 400 μL of the octanol layer and 400 μL of the water layer were removed. The solvent from each sample was removed under reduced pressure and the mass of the compound in the octanol sample was divided by the mass of the compound in the water sample. This

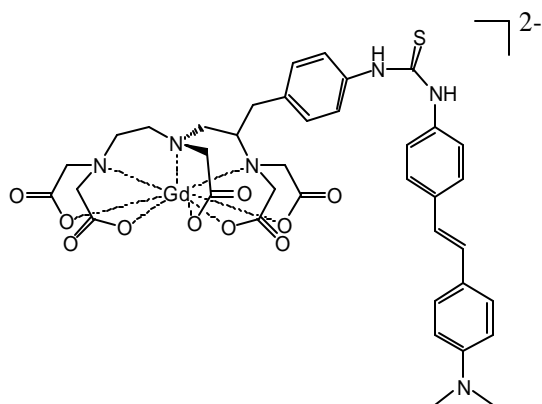
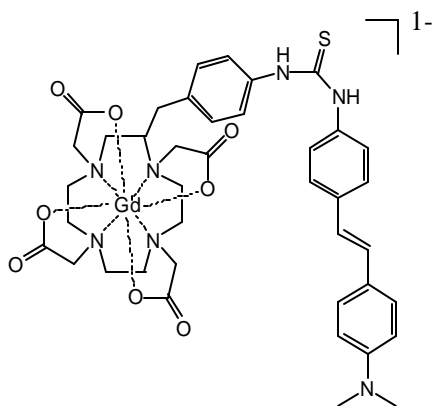
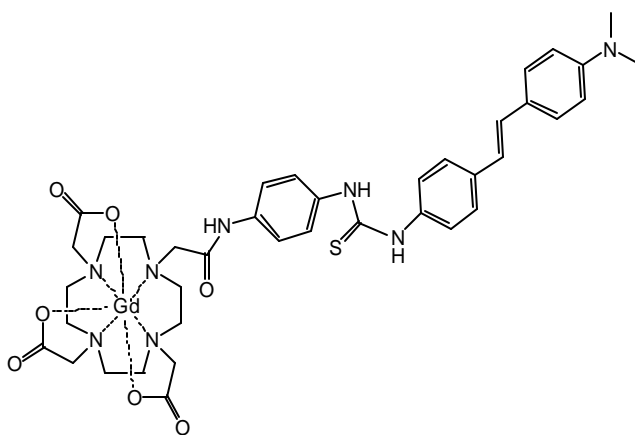
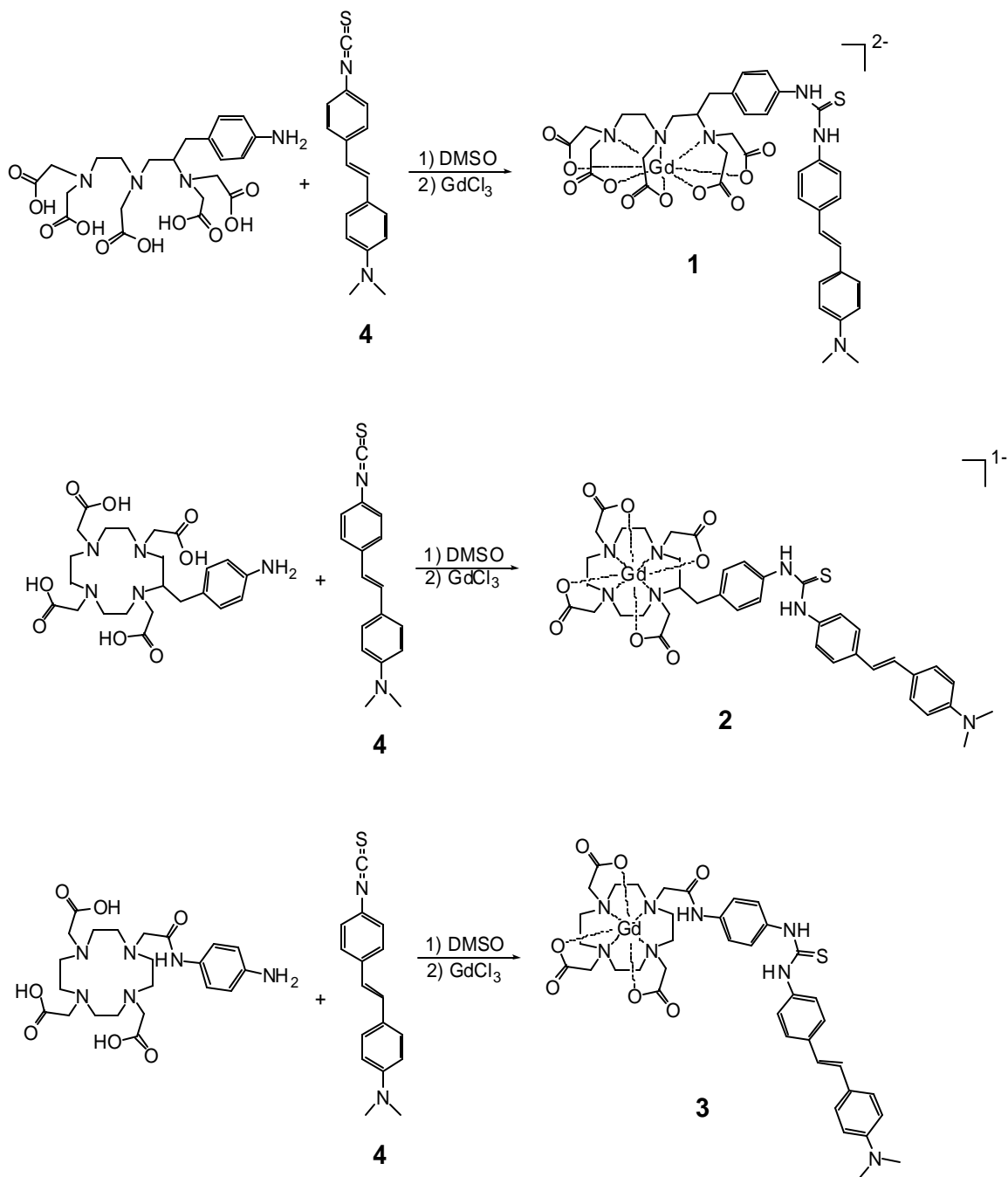
**1****2****3**

Figure 3.2: Dianionic (**1**), monoanionic (**2**), and neutral (**3**) versions of the amyloid targeting MRI contrast agent.



Scheme 3.1: Synthetic route to the dianionic (**1**), monoanionic (**2**), and neutral (**3**) versions of A β targeting MRI contrast agents.

experiment was repeated in triplicate, and the results were averaged to give the $P_{\text{oct/wat}}$ values shown in **Table 3.1**. Complex **3** was not completely soluble in the mixture of octanol and water. A portion of **3** remained at the interface of the octanol and water layers. Undissolved material was avoided when sampling at the end of the experiments involving **3**.

Relaxivities

The relaxivity (r_1) values for compounds **1-3** are shown in **Table 3.1**. Values were obtained by calculating the slope of a plot of T_1^{-1} versus concentration. The measurements were acquired in a pH 7.41 3-(*N*-morpholino)propanesulfonic acid (MOPS) buffer or in 10% Pluronic F-127. Additionally, the relaxivity of **1** was determined to be 22 and 27 $\text{mM}^{-1}\text{s}^{-1}$ when measured at pH 4.99 and 2.96, respectively.

UV-Visible and Fluorescence Spectroscopy

UV-Visible Absorption

UV-visible spectra for compounds **1-3** were acquired and the maximum absorption wavelengths (λ_{EX}) are listed in **Table 3.2**. Spectra were obtained in the MOPS buffer used for relaxivity measurements and also in a 10% solution of Pluronic F-127. Molar absorptivity values were calculated by calculating the slope of a plot of absorbance versus concentration. Five concentrations were used for the calculations and the results are shown in **Table 3.2**.

Fluorescence Spectroscopy

Fluorescence excitation and emission spectra for complexes **1-3** were acquired and are shown in **Figure 3.3**. The maximum excitation (λ_{EX}) and emission (λ_{EM}) wavelengths are listed in **Table 3.2**. Fluorescence quantum yields (Φ) for **1-3** were

Complex	Charge	$P_{\text{oct/wat}}$	r_1 ($\text{mM}^{-1}\text{s}^{-1}$)	r_1 ($\text{mM}^{-1}\text{s}^{-1}$)
			MOPS	Pluronic
1	-2	0.01	24.9	21.4
2	-1	0.02	23.9	20.1
3	neutral	0.8	16.8	16.9

Table 3.1: Physical properties of **1-3** including molecular charge, $P_{\text{oct/wat}}$, and r_1 in pH 7.41 MOPS buffer and 10% Pluronic F-127.

Complex	Charge	λ_{EM} (nm)	λ_{EX} (nm)	$\epsilon_{Pluronic}$ ($M^{-1}cm^{-1}$)	ϵ_{MOPS} ($M^{-1}cm^{-1}$)	Φ
1	-2	491	343	34,000	18,000	0.240
2	-1	448	399	37,000	23,000	0.279
3	neutral	470	354	58,000	22,000	0.255

Table 3.2: UV-visible and fluorescence properties of **1-3** including molar absorptivity (ϵ) in 10% Pluronic F-127 and MOPS buffer, fluorescence quantum yield (Φ), λ_{EM} , and λ_{EX} .

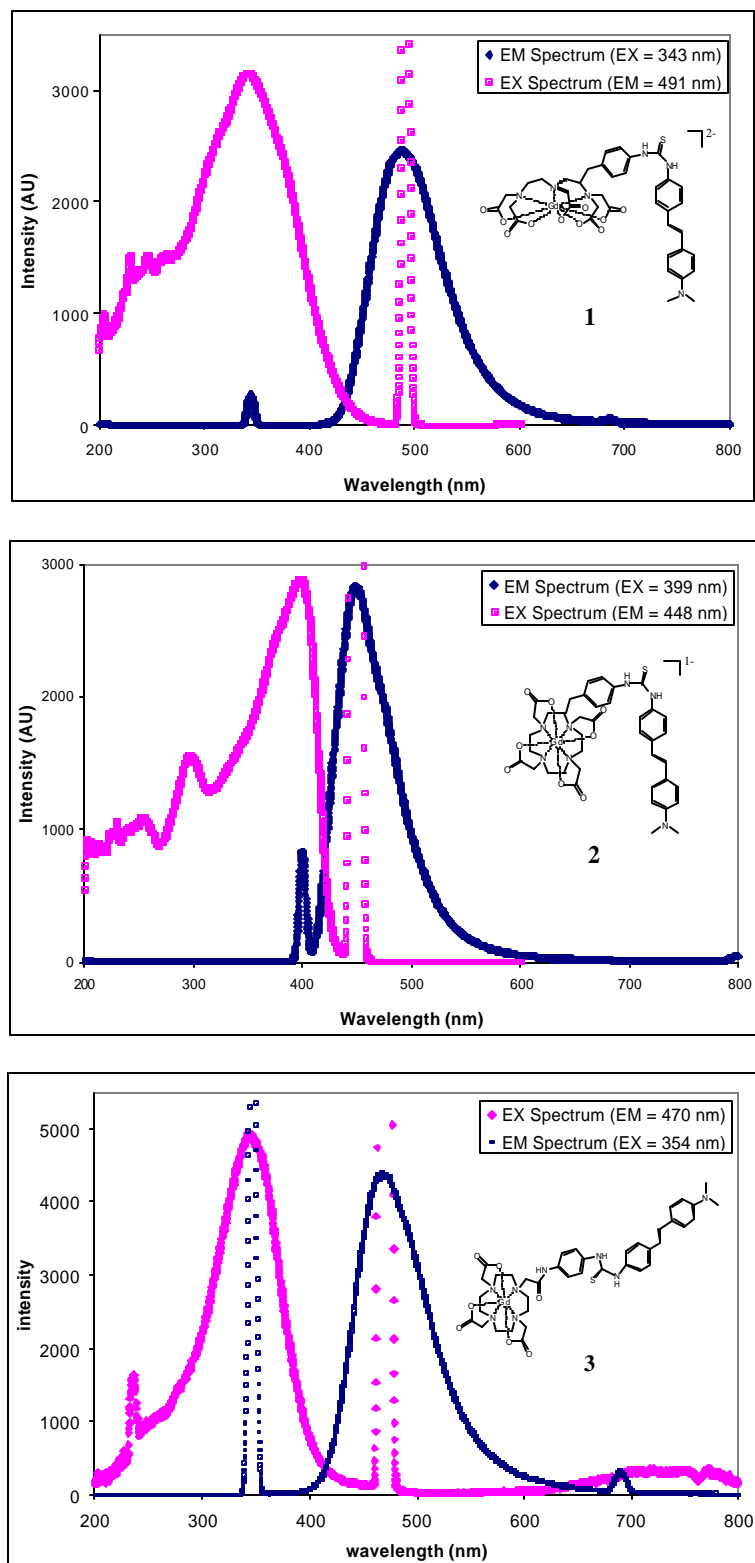


Figure 3.3: Excitation and emission spectra for 1-3.

measured using the same method as Damrauer and coworkers (**Equation 3.1**).³¹ The absorption spectrum of a solution of **1**, **2**, or **3** in 10% Pluronic F-127 was acquired and fluorescence emission spectra of the same solutions were acquired using the maximum absorbance wavelength for excitation. The intensity value for the absorption was used for the value of A_{unk} , and the area under the fluorescence emission peak was used for I_{unk} . Absorbance and emission measurements were repeated for fluorescein in 0.1 N aqueous sodium hydroxide and rhodamine 6G in ethanol, and the acquired values were used for A_{std} and I_{std} . The refractive indexes of 10% Pluronic F-127, 0.1 N aqueous sodium hydroxide and ethanol were measured and used for η_{unk} and η_{std} as appropriate. Values for Φ_{std} for fluorescein and rhodamine 6G were taken from reference.³² Values for Φ_{unk} were calculated for **1-3** using **Equation 3.1** and the measured values. Calculations using fluorescein and rhodamine 6G values were averaged to determine the Φ values for **1-3** that are listed in **Table 3.2**.

$$\text{Equation 3.1: } \Phi_{unk} = \Phi_{std} \left(\frac{I_{unk}}{A_{unk}} \right) \left(\frac{A_{std}}{I_{std}} \right) \left(\frac{h_{unk}}{h_{std}} \right)^2$$

Dynamic Light Scattering

Dynamic light scattering was used to examine the behavior of compounds **1-3** in solution. Solutions of **1-3** were prepared by serial dilution using 0.2 μm filtered 10% Pluronic F-127 or MOPS buffer. The measured concentrations ranged from 1 mg/mL to 2 ng/mL. Acquired data was analyzed using the cumulants algorithm. A representative

autocorrelation function for the compounds is shown in **Figure 3.4**. Results of the light scattering experiments are shown in **Figure 3.5** and **Figure 3.6**.

Cell Studies

Viability Assays

All cell experiments described were repeated in at least triplicate. To determine the toxicity of **1**, trypan blue assays were performed as a part of all subsequent experiments involving mouse fibroblast (NIH/3T3) cells. One drop of a trypsin suspension of NIH/3T3 cells was mixed with one drop of trypan blue. Viable cells will not take up the blue dye whereas unviable cells will be stained a dark blue with the dye. The number of blue cells is divided by the total number of cells to determine the percent of viable cells.³³ In the concentration ranges tested, cells treated with **1** were greater than 95% viable.

Concentration Effects

To examine the effect of contrast agent concentration on cellular uptake, inductively coupled plasma mass spectrometry (ICP-MS) was utilized. NIH/3T3 cells were grown in Costar 12 well plates (polystyrene, tissue culture treated) in a 5% carbon dioxide incubator at 37 °C with modified Dulbecco's modified Eagle's medium (DMEM) containing 10% bovine calf serum (BCS). Cells were incubated with **1** for one hour at 37 °C with concentrations of 0.1, 0.5, and 3 mM in modified DMEM containing 10% BCS in a 5% carbon dioxide incubator. At the end of the incubation period, the medium was removed and the cells were rinsed in triplicate with Dulbecco's phosphate buffered saline (DPBS) at ambient temperature. The cells were exposed to 500 µL of 0.25% trypsin and harvested at which point they were counted using a hemacytometer and examined for

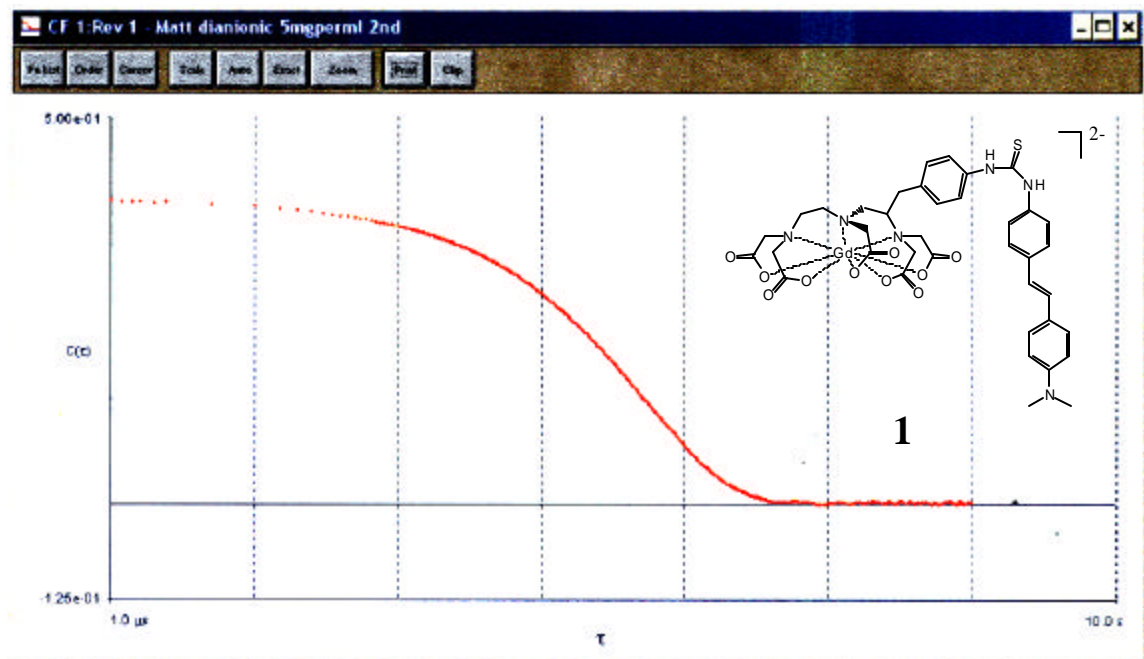


Figure 3.4: A representative autocorrelation function from dynamic light scattering of **1** in MOPS buffer.

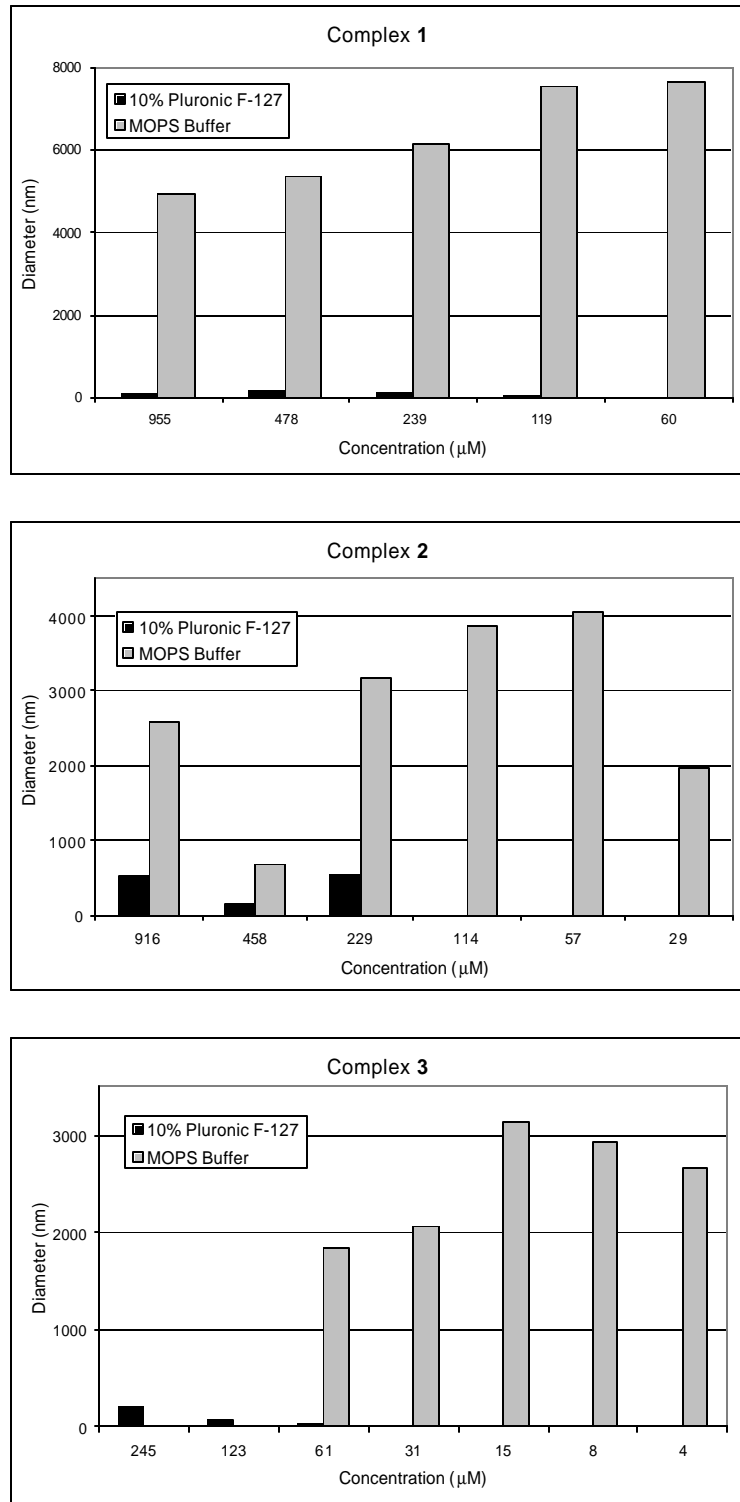


Figure 3.5: Dynamic light scattering results showing the size of aggregates at various concentrations in 10% Pluronic F-127 and MOPS buffer.

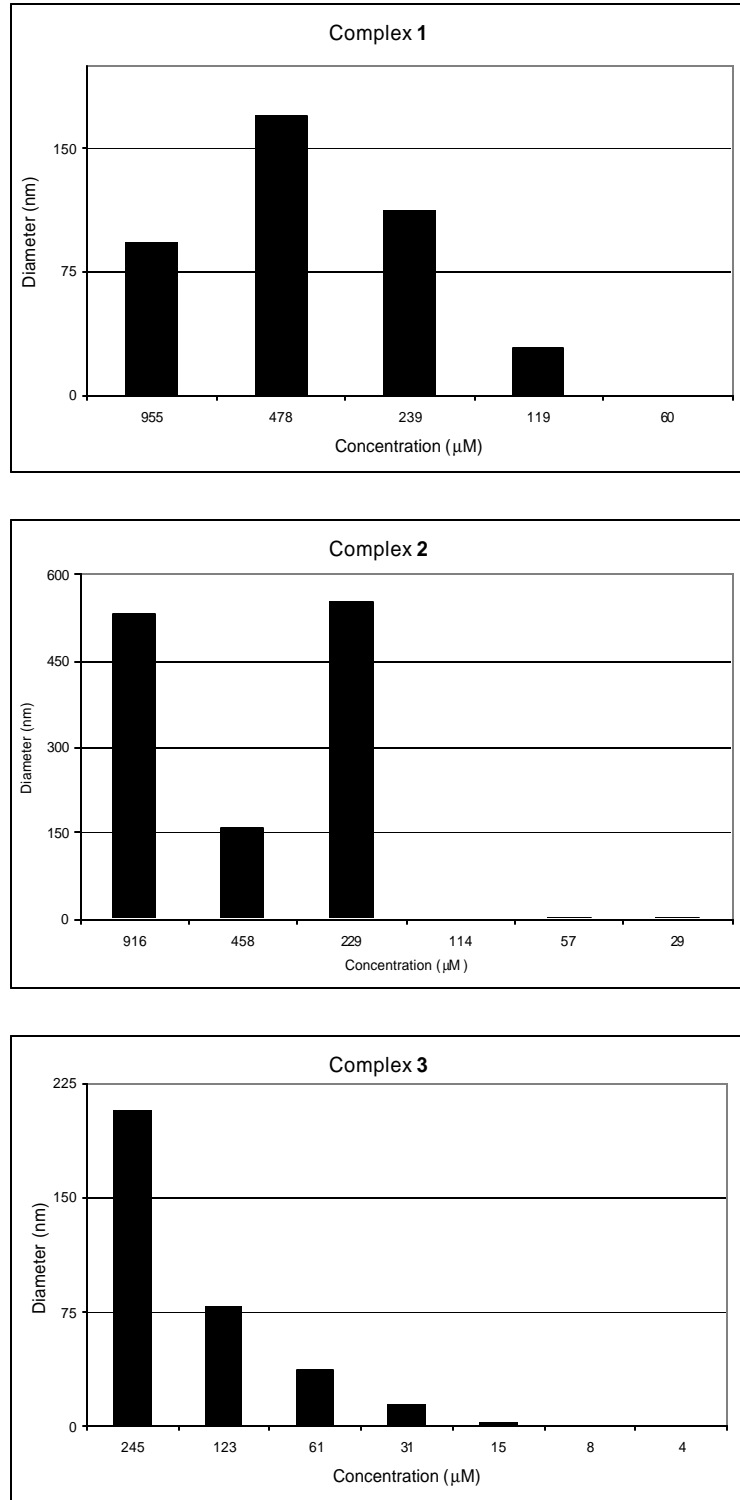


Figure 3.6: Dynamic light scattering results showing the size of aggregates at various concentrations in 10% Pluronic F-127.

viability using a trypan blue assay. There was an average of 1,010,000 cells per well. The trypsin/cell suspensions were incubated with concentrated nitric acid at 80 °C for four hours. Dissolved cells were diluted to a final volume of 10 mL. Final cell solutions were in 3% nitric acid with 5 ppb of indium as an internal standard. The samples were analyzed by ICP-MS, and the amount of gadolinium per cell was calculated and is shown in **Figure 3.7**.

Incubation Time

ICP-MS was used in determining the effect of incubation time on uptake of **1**. NIH/3T3 cells were grown in CorningTM brand tissue culture flasks (25 cm² with vent cap) with modified DMEM containing 10% BCS in a 5% carbon dioxide incubator. Cells were incubated with **1** (0.3 mM in modified DMEM containing 10% BCS) for periods of one-half, one, two, four, ten, or twenty-four hours at 37 °C in a 5% carbon dioxide incubator. At the end of the incubation period, the medium was removed and the cells were rinsed in triplicate with DPBS at ambient temperature. The cells were exposed to 500 µL of 0.25% trypsin and harvested at which point they were counted using a hemacytometer and checked for viability using a trypan blue assay. The trypsin/cell suspensions were incubated with 500 µL of concentrated nitric acid at 80 °C for four hours. The dissolved cells were diluted to 10 mL. The final cell solutions were in 3% nitric acid with 5 ppb of indium as an internal standard. The samples were analyzed by ICP-MS. The amount of gadolinium per dish was calculated and is shown in **Figure 3.8**.

Washout Studies

In studying the rate at which **1** leaches from cells, ICP-MS was used. NIH/3T3 cells were grown in CorningTM brand tissue culture flasks (25 cm² with vent cap) with

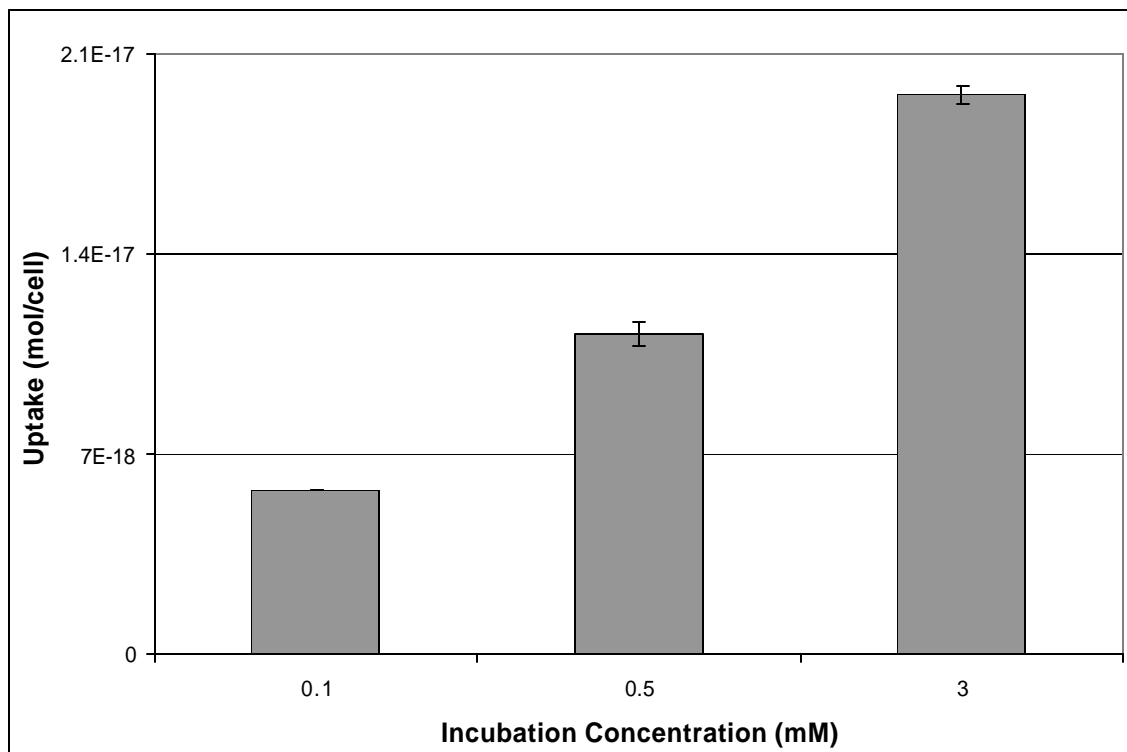


Figure 3.7: Demonstration of the dependence of uptake of **1** on incubation concentration. After incubation, NIH/3T3 cells were rinsed with DPBS, treated with trypsin, dissolved in nitric acid, and analyzed with ICP-MS. The graph shows uptake per cell plotted against incubation concentration. Error bars represent one standard deviation.

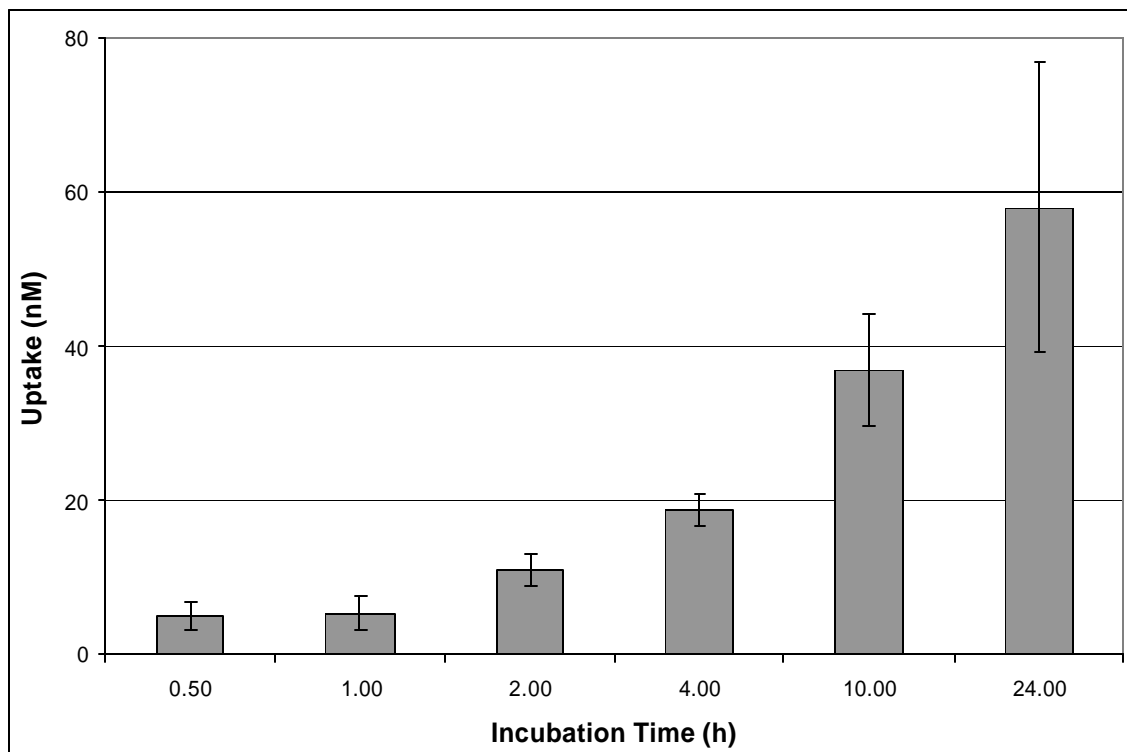


Figure 3.8: Demonstration of the dependence of uptake of **1** on incubation time. After incubation, NIH/3T3 cells were rinsed with DPBS, treated with trypsin, dissolved in nitric acid, and analyzed with ICP-MS. The graph shows uptake per dish plotted against incubation concentration. Error bars represent one standard deviation.

modified DMEM containing 10% BCS in a 5% carbon dioxide incubator. Cells were incubated with **1** (0.3 mM in modified DMEM) for one hour at 37 °C in a 5% carbon dioxide incubator. At the end of the incubation period, the medium was removed and the cells were rinsed in triplicate with DPBS at ambient temperature. Fresh medium was applied to the cells and they were returned to the incubator. After periods of 24 and 48 hours, the medium was removed and replaced with fresh medium (5 mL) after triplicate rinsing with DPBS. The removed medium was analyzed for gadolinium concentration using ICP-MS. This experiment was repeated with shorter sampling times of 1, 3, and 6 hours. The results of these experiments are shown in **Figure 3.9**.

Blood Brain Barrier Model

To examine the ability of **1-3** to permeate the BBB, the Clonetics[®] bovine brain microvascular endothelial cell system (bMVEC-B) was used. Cryopreserved bMVEC-B cells were thawed and plated at 50,000 cells/cm² onto Biocoat[®] cell culture inserts for use with 24-well plates. The bottom of the insert consisted of a 0.45 µm filter coated with type 1 rat tail collagen (**Figure 3.10**). Cells were grown in a 5% carbon dioxide incubator at 37 °C with EBM-2 basal medium modified to contain ascorbic acid, β-ECGF, platelet poor horse serum, heparin, penicillin, streptomycin, and fungizone. Cells were allowed to grow for 11 days with a medium change every 48 hours as described by the bMVEC-B instructions. On the eleventh day, a 3 mM solution of **1** in modified EBM-2 basal medium was applied to the insert containing a monolayer of bMVEC-B cells. The cells were incubated at 37 °C in a 5% carbon dioxide incubator and samples of the medium from the bottom of the dish were taken at 30, 60, and 180 minutes; dissolved

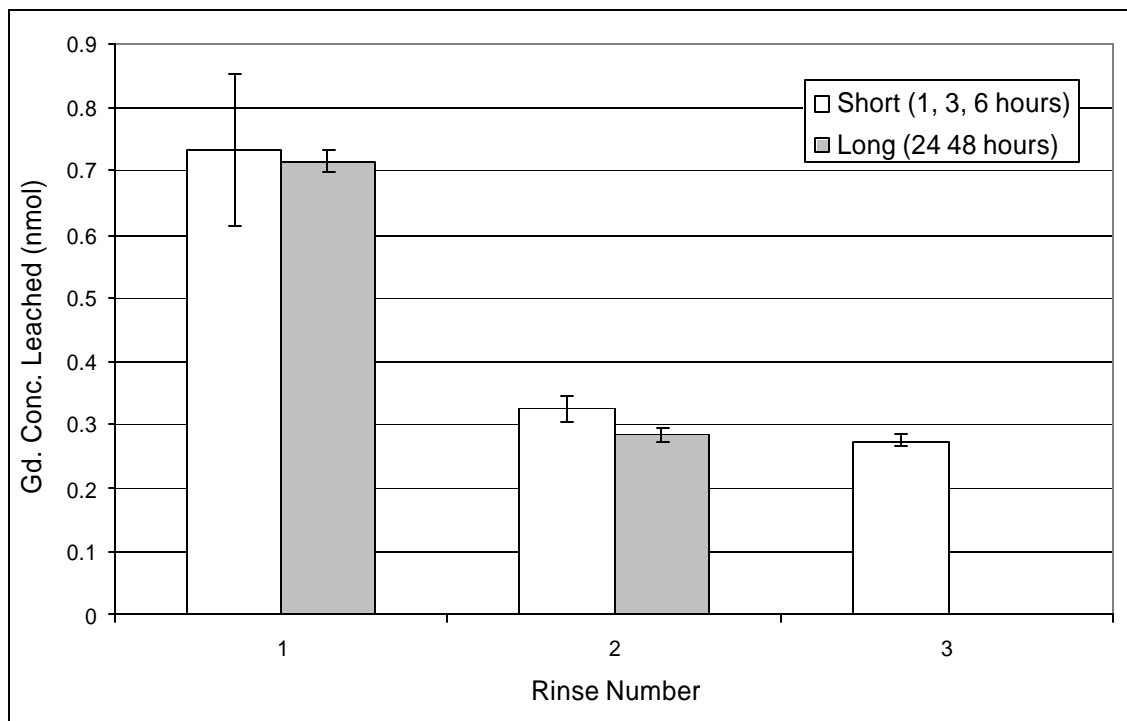


Figure 3.9: Washout rate of **1** from NIH/3T3 cells as a function of the number of rinses. Cells were incubated for one hour and the medium was changed. After each rinse period the medium was removed and analyzed using ICP-MS. Long incubation times were 24 and 48 hours. Short incubation times were 1, 3, and 6 hours. Error bars represent one standard deviation.

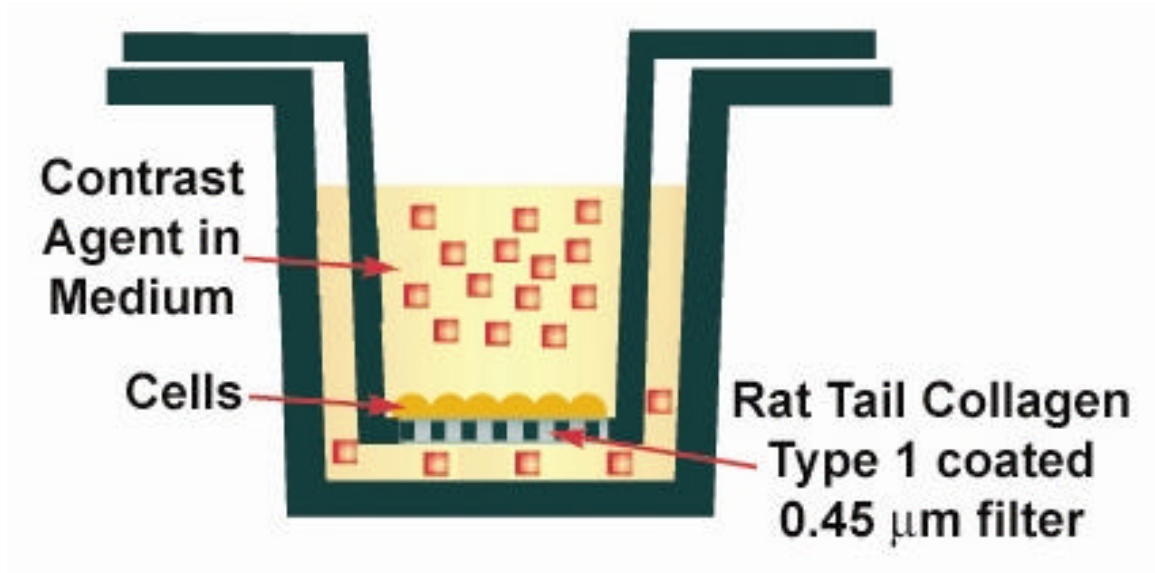


Figure 3.10: Schematic of cell culture well and insert used in BBB model experiment. The base of the insert is a 0.45 μm filter coated with type 1 rat tail collagen. bMVEC-B cells formed a monolayer over the filter. Contrast agent was added to the insert, and samples of medium were taken from the bottom chamber and analyzed for gadolinium content using ICP-MS.³⁴

in 3% nitric acid with 5 ppb of indium as an internal standard; and analyzed by ICP-MS. This procedure was repeated with 3 mM solutions of **2** and a saturated solution of **3** in modified EBM-2 basal medium. These experiments were repeated using 0.01 mM solutions of **1-3**. All six experiments were performed using modified EBM-2 basal medium saturated with Pluronic F-127. Control experiments with gadolinium(III) 1,4,7,10-tetraazacyclododecane-1,4,7,10-tetraacetic acid (DOTA), **6**, were carried out under identical conditions. All experiments were repeated in triplicate, and the results of the 3 mM experiments are shown in **Figure 3.11**. A detectable amount of gadolinium did not cross the membrane in the experiments using 0.01 mM solutions of **1-3**.

Brain Slices

To examine the ability of **1** and **2** to label A β plaques, brain slices from a PDAPP mouse were used. Histology was done by John F. Reilly at Neurome, Inc., San Diego, CA. In treating the brain slices, the protocol of Trojanowski and coworkers was used.³⁵ Brain sections were obtained at autopsy and treated with a solution of **1** or **2** in 50% ethanol for 30 minutes, washed in saturated lithium carbonate, and differentiated in 50% ethanol before examination by fluorescent microscopy. Staining using **1** and **2** was verified by and compared with staining with Congo Red and Thioflavin S. Additionally, a simplified protocol in which staining and washing was performed in phosphate buffered saline (PBS) in place of 50% ethanol was performed and worked well with both **1** and **2** at 0.01%. Fluorescence microscopy images showing the presence of A β plaques in the hippocampus but not the midbrain, and the relative staining ability of **1** and **2** are shown in **Figure 3.12**.

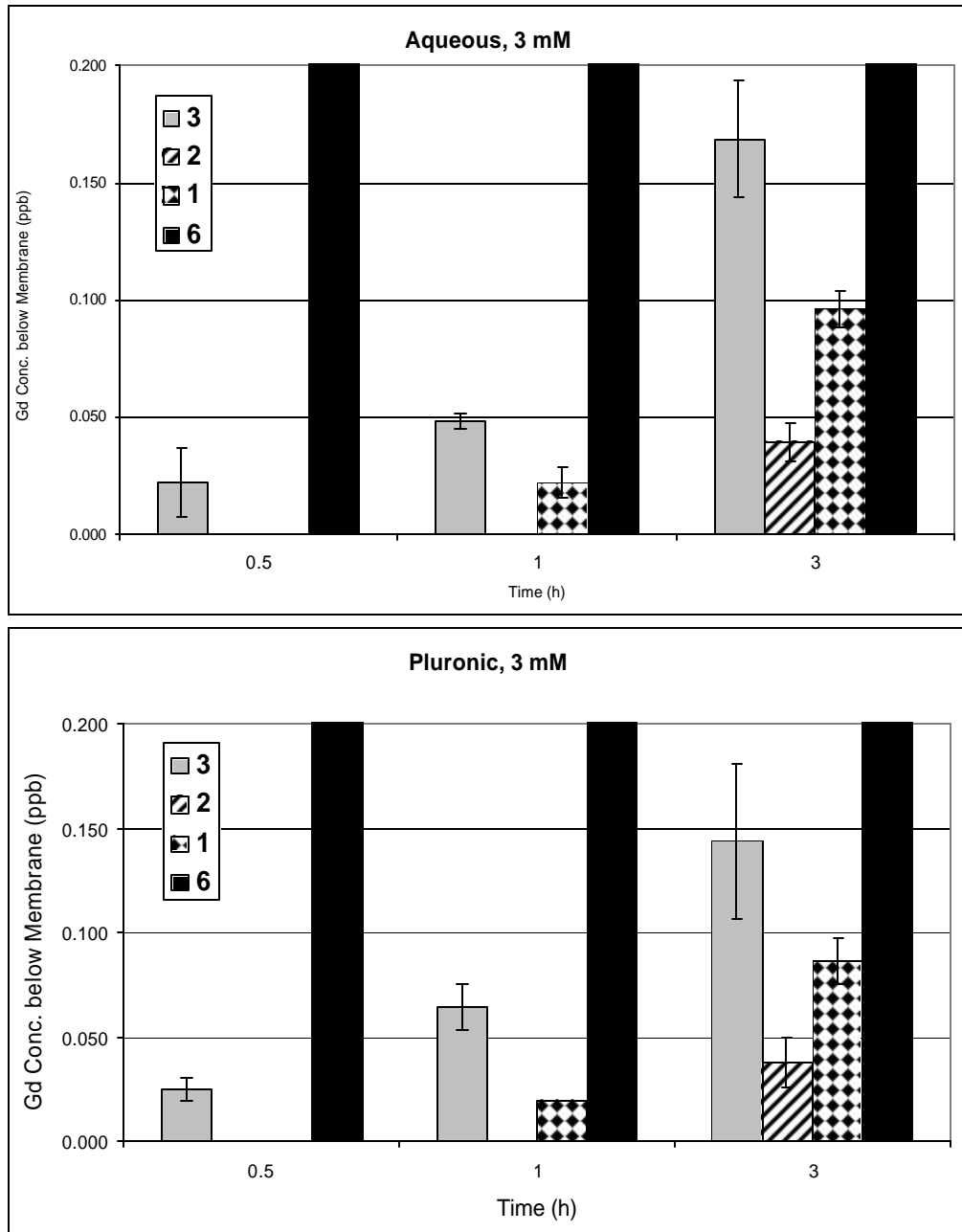


Figure 3.11: Results of BBB model experiment testing the ability of compounds **1-3**, and **6** to permeate the BBB. The graphs depict the concentration of gadolinium that had crossed the BBB model versus time. Cells were incubated with 3 mM compound in modified EBM-2 medium (top) and modified EBM-2 medium saturated with Pluronic F-127 (bottom).

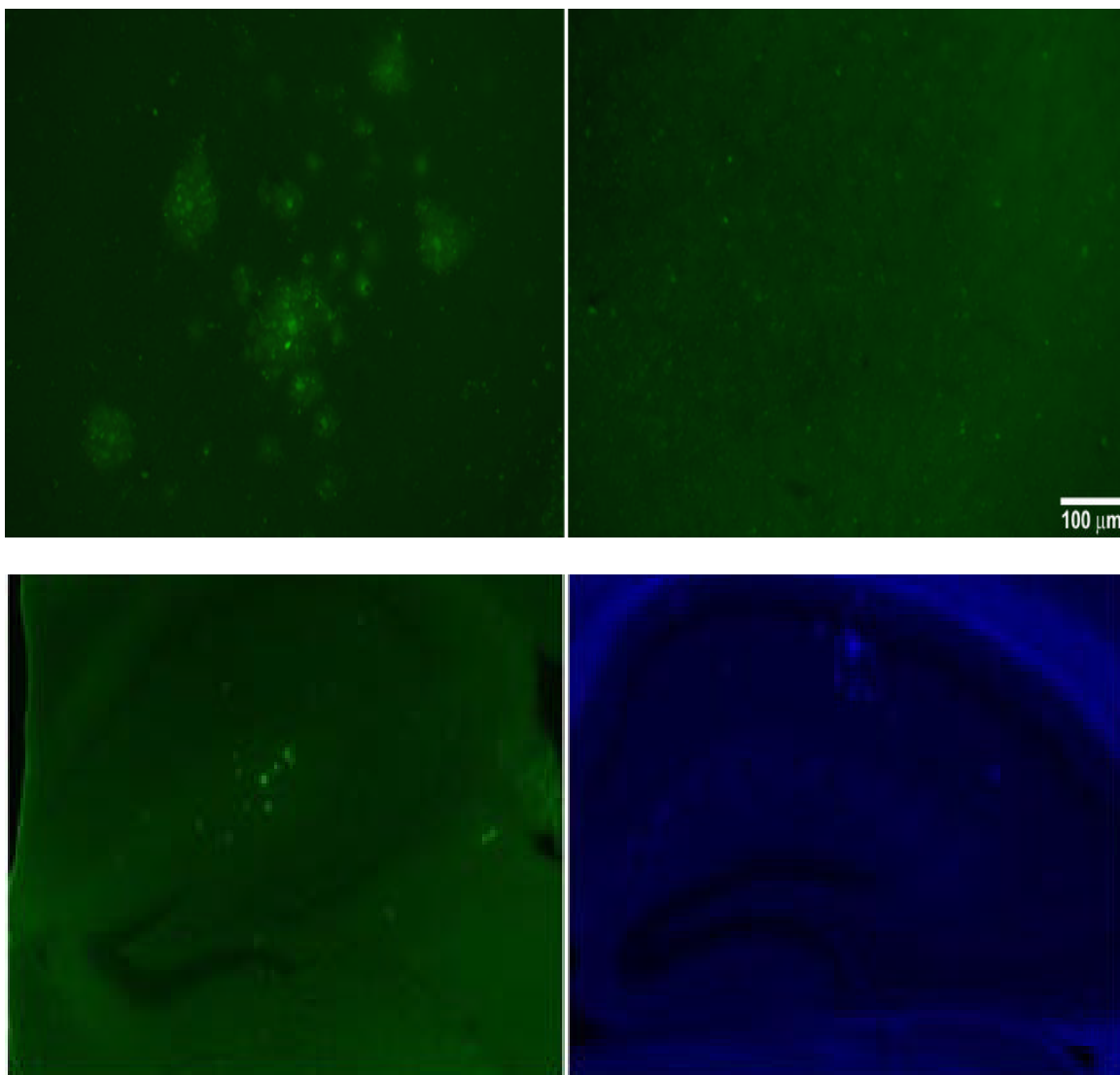


Figure 3.12: Fluorescence microscopy images of brain slices exposed to complexes **1** and **2**. Top: Sections of hippocampus (left) and midbrain (right) from a PDAPP mouse that were treated with **1**. Bottom: Sections of a PDAPP mouse brain that were treated with **1** (left) or **2** (right).

Discussion

Synthesis and Physical Properties

A series of contrast agents covalently conjugated to styrylbenzene was synthesized with the goal of delivering these agents through the BBB and to the A β plaques (**Figure 3.2**). The lanthanide chelates used to synthesize complexes **1-3** (two derivatives of DOTA: 1,4,7,10-tetraazacyclododecane-*N,N,N',N''*-tetraacetic acid and one derivative of DTPA) were chosen because they are clinically approved, and after conjugation to **5**, each possesses a different molecular charge (dianionic - **1**, monoanionic - **2**, and neutral - **3**). Variation in charge is critical because it is one factor believed to contribute to the ability of a molecule to penetrate the BBB.⁸ Other factors influencing BBB permeability include lipophilicity and molecular weight.⁸

The gadolinium(III) chelates were conjugated to the modified stilbene shown in **Figure 3.1** at the position of the iodo moiety because Kung and coworkers noted that binding affinity was not sensitive to the position of the iodo group.²⁸ Complexes **1-3** are much smaller (5 times) than the A β peptide containing agent of Poduslo and coworkers.²⁷ The small size leads to simplified synthesis, purification, and characterization compared to the larger A β containing complex.

The small size of complexes **1-3** makes them closer to the predicted maximum molecular weight for lipid-mediated transport across the BBB of 600 Daltons than the A β agent.³⁶ Compounds **1-3** have molecular weights of (930 – 942 Daltons) which are larger than the 600 Dalton cutoff. They are probably too large for lipid-mediated transport across the BBB; however, this may not be important because even large molecules, such

as the A β agent of Poduslo, can be transported across the BBB utilizing compounds such as putrescine that are known to cross the BBB.²⁷

A common measure of lipophilicity for predicting lipid-mediated BBB permeability is the octanol water partition coefficient ($P_{\text{oct/wat}}$).³⁷ The values for $P_{\text{oct/wat}}$ for the two charged complexes, **1** and **2**, are an order of magnitude smaller than the value for the neutral complex, **3**. These values are reflected in the water solubility of the three complexes. Complexes **1** and **2** are extremely water soluble (> 10 mM) while **3** is only slightly soluble (< 1 mM). The low water solubility of **3** contributed to its low yield because much of the complex precipitated on the Sephadex G-25 column during purification. According to published methods for correlating $P_{\text{oct/wat}}$ to BBB permeability, the predicted brain uptake of **1** and **2** should be similar to that of ethylene glycol and formamide and much less than the predicted uptake of **3**, which should be similar to that of caffeine.³⁷⁻³⁹

Relaxivities

The relaxivity values of **1-3** are remarkably high when compared to clinical MRI contrasts agents. For instance, the r_1 of gadolinium(III) 1,4,7,10-tetraazacyclododecane-1-hydroxypropyl-3,7,10-trisacetic acid, ProhanceTM, at same field strength, temperature, and pH is $3.1 \text{ mM}^{-1}\text{s}^{-1}$. The high relaxivity values were first thought to be due to pH affects similar to pH sensitive agent of Hovland and coworkers in which the protonation of an amine regulates the formation of aggregates resulting in a pH dependence of relaxivity.⁴⁰ To test this hypothesis, the relaxivity of **1** was measured at pH values above (7.41), below (2.96), and near (4.99) the pKa of dimethylaniline (5.20). While the measurement at pH 2.96 was slightly higher, most likely due to increased prototropic

exchange similar to that seen in similar gadolinium(III) complexes,^{41,42} there was not a large enough difference between the measurements to account for the high relaxivity values.

Without an explanation for the high relaxivity values based on a pH dependence, it was hypothesized that the hydrophobic nature of the stilbene made the complex amphiphilic enough to aggregate in solution and that this aggregation was independent of pH. The formation of aggregates would result in an increase in the rotational correlation time and subsequently an increase in relaxivity (**Figure 3.13**).

Aggregate Sizing

Dynamic light scattering was used to examine the aggregation properties of complexes **1-3** in solution. Dynamic light scattering, also known as quasi-elastic light scattering and photon correlation spectroscopy, is a technique used to characterize particles ranging in size from nanometers to a few microns.⁴³ When a beam of light passes through a colloidal dispersion, the particles scatter light. Particles in this size range exhibit significant random motion that produces fluctuations in light scattered. If a laser beam is passed through a solution of macromolecules, at a wavelength not absorbed by the sample, it is possible to observe these temporal fluctuations in the intensity of the scattered light using a photomultiplier tube. The time dependence of the intensity fluctuation can be analyzed and used to calculate the diameter of the particles if the viscosity and refractive index of the medium are known. One assumption that must be made in order to calculate particle diameter using the algorithms supplied with the instrument software is that all particles are spherical.

The dynamic light scattering experiments showed that complexes **1-3** form polydisperse aggregates in aqueous solution (**Figure 3.5**). If the aggregates are micelle-like, the modified stilbene moieties of **1-3** could be hindered or prevented from displaying the same, desirable properties as styrylbenzene (**Figure 3.13**). The biocompatible surfactant Pluronic F-127 was used in an attempt to increase the solubility of complexes **1-3** and prevent aggregation thus exposing the hydrophobic stilbene moieties. Pluronic F-127 is a nonionic surfactant polyol that has been found to facilitate the solubilization of water-insoluble dyes and other materials in physiological media.⁴⁴ The surfactant has a molecular weight of approximately 12,500 Daltons and the structure shown in **Figure 3.14**.

Aggregate size diminished greatly in the presence of 10% Pluronic F-127 (**Figure 3.5**). Aggregates of complexes **1-3** in 10% Pluronic F-127 were not detectable at low concentrations where aggregates in aqueous MOPS buffer at the same concentrations were still observed (**Figure 3.5** and **Figure 3.6**). Specifically, the aggregation of **1**, **2**, and **3** in 10% Pluronic F-127 was not observed below 119 μM , 229 μM , and 31 μM , respectively. Additionally, the presence of 10% Pluronic F-127 increased the solubility of complex **3** relative to aqueous MOPS buffer as shown in the bottom of **Figure 3.5**.

The affect of Pluronic F-127 on the relaxivity values of complexes **1-3** was examined. To accomplish this, the relaxivity values of **1-3** were measured in 10% Pluronic F-127. The measured values were not much smaller than those measure in MOPS buffer (**Table 3.1**). This is most likely due to a large rotational correlation time caused by the six fold increase in viscosity of Pluronic F-127 over MOPS buffer.⁴⁵ These

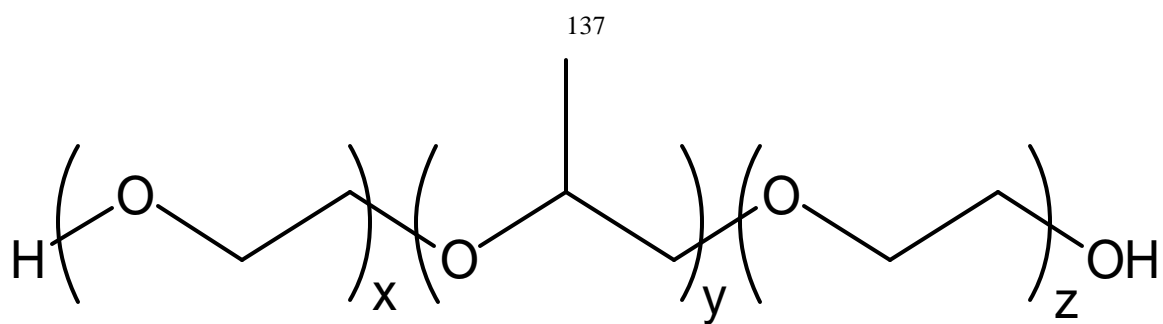


Figure 3.14: Structure of Pluronic F-127.

data demonstrate that the smaller aggregates formed in Pluronic F-127 have higher relaxivity values than monodisperse gadolinium(III) based agents.

UV-Visible and Fluorescence Spectroscopy

In addition to having high relaxivities, complexes **1-3** possess fluorescent properties which enable them to be used as dyes for fluorescence microscopy. This property allows for the verification of MR images using a secondary means which is extremely desirable. The excitation and emission spectra of **1-3** are shown in **Figure 3.3** and λ_{EX} and λ_{EM} maximums are listed in **Table 3.2**. There is no correlation between molecular charge and λ_{EX} or λ_{EM} for compounds **1-3**. The dianionic complex, **1**, has the largest λ_{EM} and smallest λ_{EX} , while the monoanionic complex, **2**, has the smallest λ_{EM} and largest λ_{EX} . The neutral complex, **3**, lies between the other two complexes in λ_{EX} and λ_{EM} values.

The molar absorptivities, ϵ , of **1-3** in MOPS buffer and 10% Pluronic F-127 are shown in **Table 3.2**. The values of ϵ in 10% Pluronic F-127 are approximately double the values acquired in MOPS buffer. This data support the results of the dynamic light scattering experiments that show that the formation of aggregates is hindered by the presence of Pluronic F-127. Smaller aggregates would probably have more of the stilbene moiety exposed leading to larger absorptions at all concentrations.

The molar absorptivity of **1** was measured in other solvents to examine the affect that they would have on ϵ . The other solvents used included 50% dimethylsulfoxide (DMSO), 5 mM tris(hydroxymethyl)aminomethane (TRIS) buffer, and the previously described MOPS buffer modified to contain 1 M NaCl. The molar absorptivities were $18,000 \text{ M}^{-1}\text{cm}^{-1}$, $19,000 \text{ M}^{-1}\text{cm}^{-1}$, and $13,000 \text{ M}^{-1}\text{cm}^{-1}$ in 50% DMSO, 5 mM TRIS buffer,

and 1 M NaCl MOPS buffer, respectively. The absorptivities in DMSO and TRIS solutions did not vary greatly from ϵ measured in the original MOPS buffer; however, the value of ϵ in the presence of increased NaCl concentration was much lower than the value in the unmodified MOPS buffer. The decreased ϵ value is likely due to quenching from the high ionic strength of the buffer. These experiments demonstrate that of the solvents examined, 10% Pluronic F-127 causes the largest increase in molar absorptivity.

Fluorescence quantum yields, Φ , for complexes **1-3** were measured and the determined values are reported in **Table 3.2**. The values of Φ for **1-3** ranged from 24% to 28%. These values are not high compared to commercially available fluorescent dyes such as rhodamine 6G and fluorescein, which have Φ values >90%, but they are high enough to be used in fluorescence microscopy. The multimodal property of these complexes is an extremely beneficial property because it allows for verification of the presence of complexes **1-3** by an orthogonal method.

Cell Studies

Viability Assays

To determine the toxicity of **1**, trypan blue assays were performed on all cell experiments discussed in this paper. All cells incubated with **1** at concentrations up to 3 mM for all incubation times studied were at least 98% viable. The viability assays justify further testing of the properties of **1** for use as an MRI contrast agent.

Concentration Effects

ICP-MS utilizes a plasma nebulizer as an atomizer and ionizer.⁴⁶ The technique has a high degree of selectivity, good precision and accuracy and low detection limits (parts per billion (ppb)). Additionally this method can be automated to facilitate analysis

of a large number of samples (hundreds) in a relatively short time period (hours). This high throughput, sensitive method lends itself perfectly to studying the cell culture properties of **1**. ICP-MS was used in this and subsequent studies because of the facile manner with which it allows for extreme accuracy and precision in measuring a large quantity of samples quickly.

A range of concentrations from 0.1 mM to 3 mM was tested to determine the amount of material taken up by NIH/3T3 cells as a function of concentration (**Figure 3.7**). From 0.1 mM to 3 mM a dramatic increase in uptake occurred corresponding to increasing incubation concentration. This study demonstrates that uptake of **1** is concentration dependant between 0.1 and 3 mM.

Incubation Time and Washout Studies

The amount of contrast agent taken up per cell was found to be dependent on the length of incubation when monitored from 0.5 - 24 hours (**Figure 3.8**). The washout rate of **1** was dependent on time and the number of rinses (**Figure 3.9**). For both long time medium changes (24 and 48 hours) and short time medium changes (1, 3, and 6 hours) more compound leached from the cells on the first rinse (24 hours or 1 hour) than on subsequent rinses. Washout from the cells for subsequent rinses remained constant. The difference in the amount released between the first and subsequent rinses was the same for the long and short times. These results demonstrate that there is a time dependence for uptake of **1**, and a dependence on the number of rinses for the washout of **1**.

Blood Brain Barrier Model

The bMVEC-B system used to model the BBB is composed of cryopreserved primary bovine brain microvascular endothelial cells from a pool of multiple donor brains

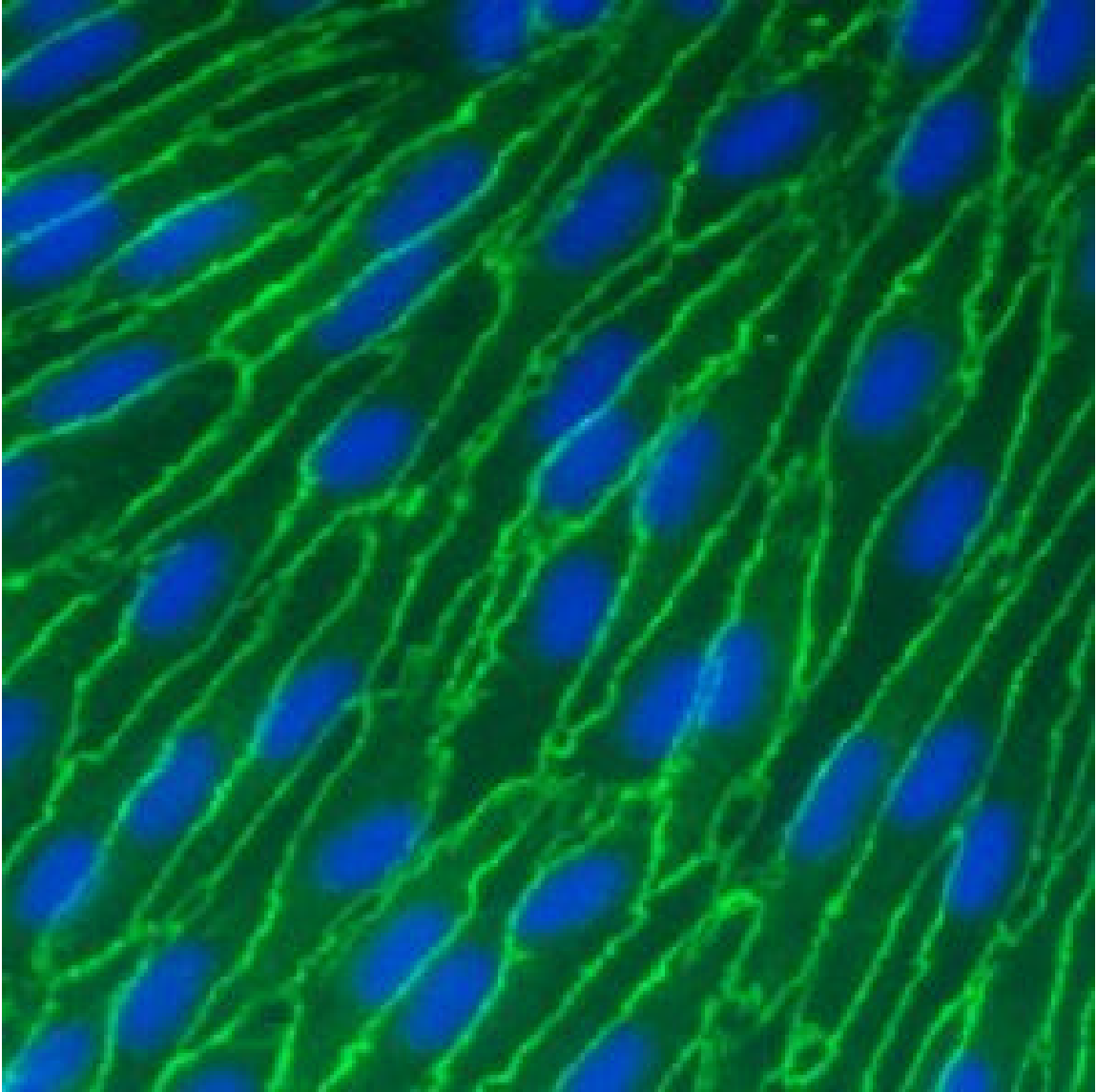


Figure 3.15: bMVEC-B cells day 3-4 after confluence that have been stained with anti ZO-1 to label tight junctions (bright green). Blue is the nuclear stain DAPI.⁴⁷

and medium that is optimized for growth into confluent monolayers. The bMVEC-B cells express cellular tight junctions and transport characteristics common to the blood brain barrier (**Figure 3.15**). The system is a commercially available tool for the study of active and passive transport across the BBB, brain endothelial cell tight junctions, and the basic biology of brain microvascular endothelial cells.

The results of the BBB model experiment are shown in **Figure 3.11**. Unfortunately, the control compound, **5**, was able to permeate the BBB model at a significantly higher rate than compounds **1-3**. This demonstrates that the bMVEC-B model did not serve its purpose of mimicking the BBB in this instance because the strictly extravascular contrast agent, **5**, was able to permeate the BBB model.

Comparison with Polyarginine Cell Culture Properties

The ability of the dimethylamino modified stilbenes to facilitate the transport of gadolinium(III) chelates across cell membranes can be compared to the ability of the polyarginine containing agents from Chapter 2. The uptake of **1** and the polyarginine complexes increases with increasing concentration of agent from 0.1-3 mM. While uptake of the arginine complexes is not time dependent, uptake of **1** increases with incubation time. The washout rate of both types of complexes is dependent on the number of rinses; however, the washout rate of the polyarginine series is additionally dependent on the duration of the rinses, while the washout rate of **1** is independent of the duration of the rinses. Finally, the polyarginine agents quickly exit cells while **1** remains in cells longer.

The delivery properties of the two agents are complementary to each other. If a quick loading of cells is needed, polyarginine based agents should be used. If cells need

to retain contrast for a longer period of time, complex **1** should be used. To increase the loading of both types of complexes, higher concentrations can be used, and longer incubation times can also be used for complex **1**. With the properties of the two types of agents, intercellular delivery of contrast agents is possible in a variety of circumstances.

Brain Slices

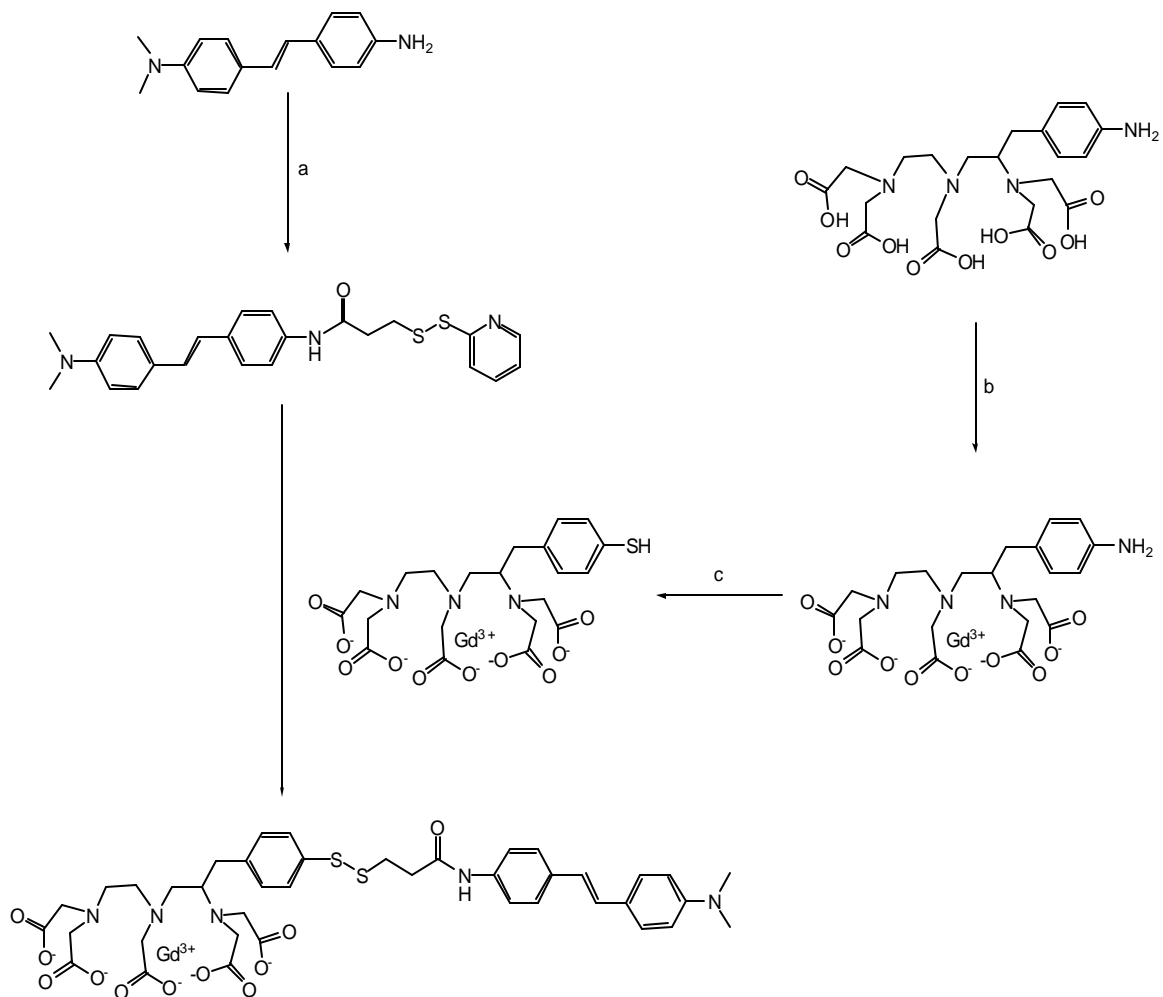
In assessing the ability of agents **1** and **2** to label A β plaques, brain slices from a PDAPP mouse were used. The PDAPP mouse is a model of familial Alzheimer's disease in which mice express the human V717F mutation in the amyloid precursor protein (APP) gene under the control of the platelet derived (PD) growth factor-beta promoter. Brain slices treated with **1** or **2** were subsequently stained with Congo Red or Thioflavin S to confirm the presence of plaques. As can be seen from **Figure 3.12**, complex **1** labeled plaques in the hippocampus, but nothing was labeled in the midbrain where no plaques would be expected. Both **1** and **2** were more sensitive at staining plaques than Congo Red and slightly less sensitive than Thioflavin S. Complex **2** gave a higher background signal, especially in white matter, while **1** had a higher signal-to-noise ratio. The optimal staining of plaques with agents **1** and **2** occurred at concentrations of 0.1% and 0.005%, respectively. Since staining in 50% ethanol is not feasible in vivo, a simplified protocol consisting of staining and washing with phosphate buffered saline (PBS) was used and worked well with both compounds at 0.01%. These experiments demonstrate that A β plaques can be labeled and visualized by fluorescence microscopy using complexes **1** and **2**.

Conclusion

Contrast agents able to permeate the BBB and label A β plaques would make the diagnosis of AD possible antemortem. Detection early enough would allow the disease to be more easily studied. A series of MRI contrast agents has been synthesized that are able to label A β plaques and have the potential to cross the BBB. Additionally, these agents display favorable cellular delivery properties that complement the properties of the polyarginine based agents described in Chapter 2. These agents were shown to aggregate in solution, possess high relaxivity values, and allow for secondary verification of their presence by fluorescence microscopy. Additionally, the presence of Pluronic F-127 has a favorable affect on the fluorescence properties of **1-3** and decreases aggregate size but does not greatly affect the high relaxivity values. The contrast agents presented in this chapter hold great promise as diagnostic tools.

Future Work

There are many avenues to explore in advancing the research of complexes **1-3**. Extensive biological testing could be performed including in vivo testing with mouse models of Alzheimer's disease to further explore the ability of complexes **1-3** to permeate the BBB and label A β plaques. The lanthanide chelate portion of **1-3** could be replaced with an enzymatically activatable contrast agent in order to monitor intercellular enzymatic activity. Finally, the intercellular delivery properties of complexes **1-3** could be altered by inserting a dithiol linker between the gadolinium(III) chelate and the modified stilbene (**Scheme 3.2**). The dithiol would be cleaved in the reducing environment inside the cell leading to a separation of the lanthanide chelate from the stilbene, thus increasing the lifetime of the chelate inside of the cell.³



Scheme 3.2: Proposed synthesis of a contrast agent conjugated to styrylbenzene via a dithiol linker for extending intercellular lifetime. (a) *N*-succinimidyl-3-(2-pyridyldithio)propionate, 0.1 M pH 7.4 phosphate buffer, DMSO; (b) $\text{Gd}(\text{OH})_3$, 80 °C; (c) (1) NaNO_2 , HCl , 0 °C, (2) KS_2COEt , 65 °C, (3) NaOH , 65 °C.

Experimental Procedures

All reagents and solvents were the highest commercially available grades and used without further purification unless otherwise noted. 2-*p*-aminobenzyl-1,4,7,10-tetraazacyclododecane-1,4,7,10-tetraacetic acid (*p*-NH₂-Bz-DOTA), *p*-aminobenzyl-diethylenetriaminepentaacetic acid (*p*-NH₂-Bz-DTPA), 1,4,7,10-tetraazacyclododecane-1,4,7,10-tetraacetic acid (DOTA), and 1,4,7,10-tetraazacyclododecane-1,4,7,10-tetraacetic acid [mono(*p*-aminoanilide) (DOTA-*p*-NH₂-anilide)] were purchased from Macrocyclics (Dallas, TX) and used without further purification. 4-amino-4'-(*N,N*-dimethylamino)stilbene was purchased from TCI America (Portland, OR) and purified using silica gel chromatography (ethyl acetate/hexanes, 1:5 followed by 1:1). Gadolinium(III) hydroxide hydrate and gadolinium(III) chloride hexahydrate was purchased from Strem Chemicals (Newburyport, MA). NIH/3T3 cells and Dulbecco's Modified Eagle's Medium (DMEM) with 4 mM L-glutamine modified to contain 4.5 g/L glucose and 1.5 g/L sodium bicarbonate were purchased from American Type Culture Collection (ATCC) (Manassas, VA). Dulbecco's Phosphate Buffered Saline (DPBS) w/o calcium and magnesium, bovine calf serum (BCS), 0.25% trypsin, trypan blue, vent-cap flasks, and multiwell plates were purchased from Fisher Scientific. bMVEC-B cells; EBM-2 basal medium; and EMVB BulletKit[®] containing ascorbic acid, β-ECGF, platelet poor horse serum, heparin, penicillin, streptomycin, and fungizone were purchased from Cambrex (East Rutherford, NJ). Biocoat[®] cell culture inserts coated with type 1 rat tail collagen were purchased from Becton Dickinson (Bedford, MA). Pluronic F-127 was purchased from Molecular Probes (Eugene, OR). All other solvents and reagents were purchased from Aldrich (Milwaukee, WI).

^1H and ^{13}C NMR spectra were obtained on a Varian mercury spectrometer at 300 and 75.5 MHz, respectively. Samples were run in CDCl_3 , with values of 7.27 and 77.23 ppm used as internal references for the ^1H and ^{13}C spectra, respectively. Mass spectrometry samples were analyzed using electrospray ionization (ESI), quadrupole mass spectrometry in the PPMAL – Protein/Peptide MicroAnalytical Laboratory, California Institute of Technology, Beckman Institute. Results reported for m/z are for $[\text{M} + \text{H}]^+$ or $[\text{M} - \text{H}]^-$. Elemental analyses were performed at Desert Analytics Laboratory, Tucson, AZ.

The longitudinal water proton relaxation rate at 59.97 MHz was measured by using a Bruker mq60 NMR Analyzer (Bruker Canada, Milton, Ont. Canada) operating at 1.5 T, by means of the standard inversion-recovery technique (20 data points, 8 scans each). A typical 90° -pulse length was 6.16 μs and the reproducibility of the T_1 data was $\pm 0.3\%$. Temperature was maintained by the instrument at 37 $^\circ\text{C}$, and samples were prepared in a buffer composed of 10 mM 3-(*N*-morpholino)propanesulfonic acid (MOPS), 100 mM sodium chloride, 20 mM sodium bicarbonate, and 4 mM sodium phosphate monobasic at pH 7.41.

UV-visible absorption measurements were acquired using a Hewlett Packard 8452A diode array spectrophotometer. Fluorescence measurements were acquired on a Hitachi F-4500 Fluorescence Spectrophotometer. Refractive indexes were measured using a Misco Digital Probe Refractometer Model Number DFR 123. Viscosity values were measured with a Gilmont Instruments Falling Ball Viscometer.

Dynamic light scattering data were collected using a Brookhaven Instruments dynamic light scattering apparatus including a BI-9000AT autocorrelator, a BI-300SM

goniometer, and a Lexel Laser Inc. Model 95 argon ion laser at the Keck Biophysics Facility at Northwestern University. The laser was operated at 514.5nm at a power of 300 mW. Measurements were conducted at 22 °C. Samples were filtered through a 0.2 μm filter to remove particulates prior to measurements. Measurements were acquired using a first delay time of 2.0 μs, a last delay time of 100.0 ms, and an elapsed time of 10 min. Data were analyzed using the cumulants algorithm supplied with the instrument software.

Cells were counted using a Bright-Line hemacytometer. Inductively Coupled Plasma Mass Spectrometry (ICP-MS) was performed either at Desert Analytics Laboratory (Tucson, AZ), or at Northwestern University's Analytical Services Laboratory (ASL) on a PQ ExCell Inductively Coupled Plasma Mass Spectrometer.

Gadolinium(III) {[2-({2-(biscarboxymethylamino)-3-[4-(3-{4-[2-(4-dimethylaminophenyl)vinyl]phenyl}-thioureido)phenyl]propyl}-carboxymethylamino)ethyl}-carboxymethylamino}-acetic acid (1): A solution of *p*-NH₂-Bz-DTPA·4HCl (1.00 g, 1.55 mmol) and **4** (0.435 g, 1.55 mmol) in dimethylsulfoxide (DMSO) (10 mL) was heated at 80 °C for six hours and then the DMSO was removed under reduced pressure. The resulting residue was taken up in water (10 mL) and GdCl₃ hexahydrate (0.287 g, 0.772 mmol) was added as a solid. The pH was adjusted to seven with 1 N sodium hydroxide and the resulting mixture was stirred for 12 hours. The pH was adjusted to 11 with 1 N sodium hydroxide. The mixture was then filtered through a 0.2 μm syringe filter and purified using Sephadex G-25 size exclusion chromatography. The water was removed under reduced pressure to yield 0.814 g (56.2%) of a yellow solid. MS Calcd for C₃₈H₄₁GdN₆O₁₀S [M - H⁺]: Gd isotope pattern centered at 930.2, found Gd isotope

pattern centered at 930.2; Anal. Calcd for $C_{38}H_{42}GdN_6NaO_{10}S$: C, 48.23; H, 4.77; N, 8.65. Found: C, 48.50; H, 4.54; N, 8.20.

Gadolinium(III) {4,7,10-triscarboxymethyl-6-[4-(3-{4-[2-(4-dimethylamino-phenyl)vinyl]phenyl}-thioureido)benzyl]-1,4,7,10-tetraazacyclododec-1-yl}-acetic acid (2): A solution of *p*-NH₂-Bz-DOTA·4HCl (0.506 g, 0.772 mmol) and **4** (0.238 g, 0.849 mmol) in DMSO (10 mL) was heated at 80 °C for six hours and then the DMSO was removed under reduced pressure. The resulting residue was taken up in water (10 mL) and GdCl₃ hexahydrate (0.287 g, 0.772 mmol) was added. The pH was adjusted to seven with 1 N sodium hydroxide and the resulting mixture was stirred for 12 hours. The pH was adjusted to 11 with 1 N sodium hydroxide. The mixture was then filtered through a 0.2 μm syringe filter and purified using Sephadex G-25 size exclusion chromatography. The water was removed under reduced pressure to yield 0.477 g (65.1%) of a yellow solid. MS Calcd for $C_{40}H_{47}GdN_7O_8S$ [M - H⁺]: Gd isotope pattern centered at 942.2, found Gd isotope pattern centered at 942.4; Anal. Calcd for $C_{40}H_{47}GdN_7NaO_8S \cdot 2H_2O$: C, 47.94; H, 5.13; N, 9.78. Found: C, 48.34; H, 4.89; N, 8.88.

Gadolinium(III) (4,10-biscarboxymethyl-7-{[4-(3-{4-[2-(4-dimethylamino-phenyl)vinyl]phenyl}-thioureido)-phenylcarbamoyl]methyl}-1,4,7,10-tetraazacyclododec-1-yl)-acetic acid (3): A solution of mono(*p*-aminoanilide) (DOTA-*p*-NH₂-anilide)·4HCl (0.500 g, 0.763 mmol) and **4** (0.214 g, 0.763 mmol) in DMSO (10 mL) was heated at 80 °C for six hours and then the DMSO was removed under reduced pressure. The resulting residue was taken up in water (10 mL) and GdCl₃ hexahydrate (0.287 g, 0.772 mmol) was added. The pH was adjusted to seven with 1 N sodium hydroxide and the resulting mixture was stirred for 12 hours. The pH was adjusted to 11 with 1 N sodium hydroxide.

The mixture was then filtered through a 0.2 μm syringe purified using Sephadex G25 size exclusion chromatography. The water was removed under reduced pressure to yield 0.120 g (17.0%) of a yellow solid. MS Calcd for $\text{C}_{40}\text{H}_{51}\text{GdN}_8\text{O}_7\text{S}$ $[\text{M} + \text{H}^+]^+$: Gd isotope pattern centered at 930.3, found Gd isotope pattern centered at 930.2; Anal. Calcd for $\text{C}_{40}\text{H}_{51}\text{GdN}_8\text{O}_7\text{S}$: C, 50.41; H, 5.10; N, 12.06. Found: C, 50.80; H, 5.12; N, 11.60.

4-isothiocyanato-4'-(N,N-dimethylamino)stilbene (4): To a solution of 4-amino-4'-(N,N-dimethylamino)stilbene (1.00 g, 4.20 mmol) in chloroform (50 mL) at 0 °C were added simultaneously a solution of potassium carbonate (1.16 g, 8.39 mmol) in water (30 mL) and a solution of thiophosgene (0.640 mL, 0.00839 mol) in chloroform (30 mL). The reaction was allowed to warm to ambient temperature for four hours. The organic layer was then separated and washed with water, dried over magnesium sulfate, filtered, and the solvent was removed under reduced pressure to yield 0.87 g (83.9%) of a yellow solid. ^1H NMR (CDCl_3): δ = 3.01 (s, 6H), 6.72 (d, J = 8.7 Hz, 2H), 6.86 (d, J = 16.4 Hz, 1H), 7.04 (d, J = 16.4 Hz, 1H), 7.19 (d, J = 8.7 Hz, 2H), 7.43 (dd, J = 8.7 Hz, 6.9 Hz, 4H); ^{13}C NMR (CDCl_3): δ = 40.68, 112.47, 122.75, 125.18, 126.12, 126.92, 127.90, 128.83, 130.35, 134.85, 137.65, 150.38; MS Calcd for $\text{C}_{17}\text{H}_{16}\text{N}_2\text{S}$ $[\text{M} + \text{H}^+]^+$: 281.4, found 281.2; Anal. Calcd for $\text{C}_{17}\text{H}_{16}\text{N}_2\text{S}$: C, 72.82; H, 5.75; N, 9.99. Found: C, 73.03; H, 5.74; N, 9.77.

Gadolinium(III) 1,4,7,10-tetraazacyclododecane-1,4,7,10-tetraacetic acid (5): To a solution of DOTA \cdot 7H $_2$ O (0.115 g, 0.234 mmol) in water (10 mL) was added gadolinium(III) hydroxide hydrate (53.0 mg, 0.234 mmol). The resulting mixture was stirred at 80 °C for 12 hours, cooled to ambient temperature, and the pH was adjusted to 12 using ammonium hydroxide. The resulting suspension was filtered through a 0.2 μm

filter and freeze dried to yield 0.145 g of a white solid. MS Calcd for C₁₆H₂₅GdN₄O₈ [M - H⁺]: Gd isotope pattern centered at 558.1, found Gd isotope pattern centered at 558.1.

References

- (1) K. Shoghi-Jadid, W. Small Gary, D. Agdeppa Eric, V. Kepe, M. Ercoli Linda, P. Siddarth, S. Read, N. Satyamurthy, A. Petric, S.-C. Huang, and R. Barrio Jorge, *Am. J. Geriatr. Psychiatry* **2002**, *10*, 24-35.
- (2) A. Frazer, P. B. Molinoff, and A. Winokur, *Biological Bases of Brain Function and Disease*; Raven Press, New York, 1994.
- (3) H. Lodish, A. Berk, S. L. Zipursky, P. Matsudaira, D. Baltimore, and J. E. Darnell, *Molecular cell biology*; W.H. Freeman, New York, 2000.
- (4) P. F. Chapman, A. M. Falinska, S. G. Knevet, and M. F. Ramsay, *Trends Genet.* **2001**, *17*, 254-261.
- (5) Z. S. Khachaturian, *Arch. Neurol.* **1985**, *42*, 1097-1105.
- (6) G. McKhann, D. Drachman, M. Folstein, R. Katzman, D. Price, and E. M. Stadlan, *Neurology* **1984**, *34*, 939-944.
- (7) A. E. Merbach and E. Toth, *The Chemistry of Contrast Agents in Medical Magnetic Resonance Imaging*; John Wiley & Sons, Ltd., New York, 2001.
- (8) D. F. Emerich, *Expert Opin. Ther. Pat.* **2000**, *10*, 279-287.
- (9) J. F. Poduslo and G. L. Curran, *J. Neurochem.* **1996**, *66*, 1599-1609.
- (10) J. F. Poduslo and G. L. Curran, *J. Neurochem.* **1996**, *67*, 734-741.
- (11) J. F. Poduslo, G. L. Curran, and J. S. Gill, *J. Neurochem.* **1998**, *71*, 1651-1660.
- (12) J. F. Poduslo, S. L. Whelan, G. L. Curran, and T. M. Wengenack, *Ann. Neurol.* **2000**, *48*, 943-947.
- (13) B. J. Bacskai, S. T. Kajdasz, R. H. Christie, C. Carter, D. Games, P. Seubert, D. Schenk, and B. T. Hyman, *Nature Med.* **2001**, *7*, 369-372.
- (14) T. M. Wengenack, G. L. Curran, and J. F. Poduslo, *Nature Biotechnol.* **2000**, *18*, 868-872.
- (15) T. M. Wengenack, S. Whelan, G. L. Curran, K. E. Duff, and J. F. Poduslo, *Neuroscience* **2000**, *101*, 939-944.

- (16) Y. Wang, W. E. Klunk, G.-F. Huang, M. L. Debnath, D. P. Holt, and C. A. Mathis, *J. Mol. Neurosci.* **2002**, *19*, 11-16.
- (17) C. A. Mathis, B. J. Bacskai, S. T. Kajdasz, M. E. McLellan, M. P. Frosch, B. T. Hyman, D. P. Holt, Y. Wang, G.-F. Huang, M. L. Debnath, and W. E. Klunk, *Bioorg. Med. Chem. Lett.* **2002**, *12*, 295-298.
- (18) Z. P. Zhuang, M. P. Kung, C. Hou, D. M. Skovronsky, T. L. Gur, K. Ploessl, J. Q. Trojanowski, V. M. Y. Lee, and H. F. Kung, *J. Med. Chem.* **2001**, *44*, 1905-1914.
- (19) A. Kurihara and W. M. Pardridge, *Bioconjugate Chem.* **2000**, *11*, 380-386.
- (20) R. P. Friedland, R. E. Majocha, J. M. Reno, L. R. Lyle, and C. A. Marotta, *Mol. Neurobiol.* **1994**, *9*, 107-113.
- (21) N. D. Volkow, Y. S. Ding, J. S. Fowler, and S. J. Gatley, *Biol. Psychiatry* **2001**, *49*, 211-220.
- (22) R. H. Christie, B. J. Bacskai, W. R. Zipfel, R. M. Williams, S. T. Kajdasz, W. W. Webb, and B. T. Hyman, *J. Neurosci.* **2001**, *21*, 858-864.
- (23) N. A. Dezutter, R. J. Dom, T. J. de Groot, G. M. Bormans, and A. M. Verbruggen, *Eur. J. Nucl. Med.* **1999**, *26*, 1392-1399.
- (24) J. R. Marshall, E. R. Stimson, J. R. Ghilardi, H. V. Vinters, P. W. Mantyh, and J. E. Maggio, *Bioconjugate Chem.* **2002**, *13*, 276-284.
- (25) E. D. Agdeppa, V. Kepe, J. Liu, S. Flores-Torres, N. Satyamurthy, A. Petric, G. M. Cole, G. W. Small, S.-C. Huang, and J. R. Barrio, *J. Neurosci.* **2001**, *21*, RC189/181-RC189/185.
- (26) H. Benveniste, G. Einstein, K. R. Kim, C. Hulette, and G. A. Johnson, *Proc. Natl. Acad. Sci. U. S. A.* **1999**, *96*, 14079-14084.
- (27) J. F. Poduslo, T. M. Wengenack, G. L. Curran, T. Wisniewski, E. M. Sigurdsson, S. I. Macura, B. J. Borowski, and C. R. Jack, *Neurobiol. Dis.* **2002**, *11*, 315-329.
- (28) H. F. Kung, C.-W. Lee, Z.-P. Zhuang, M.-P. Kung, C. Hou, and K. Ploessl, *J. Am. Chem. Soc.* **2001**, *123*, 12740-12741.
- (29) H. Puchtler, F. Sweat, and M. Levine, *J. Histochem. Cytochem.* **1962**, *10*, 355-364.
- (30) W. E. Klunk, M. L. Debnath, and J. W. Pettegrew, *Neurobiol. Aging* **1995**, *16*, 541-548.
- (31) N. H. Damrauer, T. R. Boussie, M. Devenney, and J. K. McCusker, *J. Am. Chem. Soc.* **1997**, *119*, 8253-8268.

- (32) D. Magde, R. Wong, and P. G. Seybold, *Photochem. Photobiol.* **2002**, 75, 327-334.
- (33) R. I. Freshney, *Culture of Animal Cells: A Manual of Basic Technique, Fourth Edition*; John Wiley & Sons, Inc., New York, 2000.
- (34) Image modified from picture obtained on 10/09/03 from http://www.noabbiodescoveries.com/Technotes/applicationnotes_permeabilityassays.pdf.
- (35) D. M. Skovronsky, B. Zhang, M.-P. Kung, H. F. Kung, J. Q. Trojanowski, and V. M. Y. Lee, *Proc. Natl. Acad. Sci. U. S. A.* **2000**, 97, 7609-7614.
- (36) W. M. Pardridge, *J. Neurochem.* **1998**, 70, 1781-1792.
- (37) N. Bodor and P. Buchwald, *Adv. Drug Deliv. Rev.* **1999**, 36, 229-254.
- (38) S. Rim, K. L. Audus, and R. T. Borchardt, *Int. J. Pharm.* **1986**, 32, 79-84.
- (39) S. I. Rapoport, K. Ohno, and K. D. Pettigrew, *Brain Res.* **1979**, 172, 354-359.
- (40) R. Hovland, C. Glogard, A. J. Aasen, and J. Klaveness, *J. Chem. Soc., Perkin Trans. 2* **2001**, 929-933.
- (41) S. Zhang, K. Wu, and A. D. Sherry, *Angew. Chem. Int. Ed.* **1999**, 38, 3192-3194.
- (42) P. Caravan, J. J. Ellison, T. J. McMurry, and R. B. Lauffer, *Chem. Rev.* **1999**, 99, 2293-2352.
- (43) B. B. Weiner and W. W. Tscharnuter, *ACS Symposium Series* **1987**, 332, 48-61.
- (44) L. B. Cohen, B. M. Salzberg, H. V. Davila, W. N. Ross, D. Landowne, A. S. Waggoner, and C. H. Wang, *J. Membrane. Biol.* **1974**, 19, 1-36.
- (45) R. B. Lauffer, *Chem. Rev.* **1987**, 87, 901-927.
- (46) D. A. Skoog, F. J. Holler, and T. A. Nieman, *Principles of Instrumental Analysis*; Saunders College Pub., Philadelphia, 1998.
- (47) Image obtained on 10/09/03 from <http://www.cambrex.com/CatNav.asp?oid=884&prodoid=bBBB>.

Chapter 4

Towards a Matrix Metalloproteinase Sensitive Contrast Agent

Introduction

Matrix metalloproteinases (MMPs) are a family of structurally related zinc-containing enzymes that mediate the breakdown of connective tissue.¹ MMPs are capable of degradation of protein-containing tissues in the body and hence are crucial to normal physiology of connective tissue in development, morphogenesis, and wound healing.² The mammalian MMP family contains at least 20 enzymes (MMP-1, MMP-2, etc.) and is one of the five classes of endopeptidases (the other four being serine proteases, aspartic proteases, threonine proteases, and cysteine proteases).^{3,4}

While the presence of MMPs is critical to normal development, overexpression of MMPs is involved in numerous ailments such as arthritis, atherosclerosis, and tumor cell metastasis.^{2,4} MMPs are involved in the early stages of tumor progression at the beginning of metastasis, which is the major cause of mortality in cancer patients.⁵ Chemotherapy is only partially effective against metastatic cancer.⁶ Because of the ineffectiveness of chemotherapy, research is being focused on the mechanism of tumor cell metastasis. A large portion of this research is directed at slowing MMP activity in tumor cells, which would potentially limit growth of the primary tumor as well as metastasis of the tumor.⁶

If a tumor cell is to metastasize, it must move into the vasculature, survive circulation, move out of the vasculature, invade surrounding tissue, and grow. Tumor cells contain proteases that participate in many of these steps at primary and metastatic sites.⁵ If a method is developed for observing MMP activity or overexpression, many of the diseases associated with MMP over-expression could be detected at their earliest stages. This early detection would lead to quicker and more thorough assessments of

potential therapies. An MMP responsive contrast agent for magnetic resonance imaging (MRI) could be used as a non-invasive tool for this purpose.

MRI is a robust tool for the non-invasive acquisition of three-dimensional internal images in clinical and biological settings.⁷ It works using the same principles as NMR spectroscopy where the nuclear spins of the protons of water molecules are excited with radiofrequency pulses. The relaxation times (T_1 or T_2) are measured and used to produce an image. The intrinsic contrast offered by the variance of water concentration found in biological systems can be altered with the use of paramagnetic contrast agents. The paramagnetic ion gadolinium(III) is typically used to increase contrast because it has seven unpaired electrons making it the most stable paramagnetic metal ion.⁸ The free gadolinium(III) ion is toxic to biological systems, thus chelators such as 1,4,7,10-tetraazacyclododecane-1,4,7,10-tetraacetic acid (DOTA) are needed to bind the ion in order to reduce toxicity by preventing biological uptake. These chelators reduce the toxicity of gadolinium(III) enough to be approved for clinical use. One characteristic of all clinically approved MRI contrast agents is that they affect contrast in MR images at all times.

In the last several years, activatable contrast agents that have the ability to change the level of signal enhancement in the presence of a biological phenomena have been created.⁹⁻³⁰ These agents utilize a biological event such as the presence of an enzyme, a change in pH, or the presence of a biologically relevant metal ion to trigger a change in the relaxivity of the contrast agent, where relaxivity is a measure of the ability of a contrast agent to shorten T_1 or T_2 .

Zhao and coworkers have recently developed a protease sensitive MRI contrast agent.³¹ With this agent, the strong interaction between biotin and avidin is exploited through the use of aggregating, superparamagnetic iron oxide particles. A molecule of biotin is conjugated to each side of a peptide that is cleaved by proteases. Iron oxide particles coated with avidin are exposed to the bi-biotinylated peptides. In the presence of protease specific for the peptide, the particles will not aggregate; however, in the absence of protease, aggregation of the iron oxide particles occurs resulting in an increase in relaxivity. Currently, this agent is only used in vitro.

Our research group has pioneered the design of activatable agents that alter relaxivity through a biologically induced change in the number of inner sphere water molecules, q , that are directly coordinated to the lanthanide ion.^{22-24,27} These agents work because the relaxivity of a contrast agent is directly proportional to q .⁷ The first q modulated agent used a covalently attached galactose moiety to lower q and subsequently relaxivity (**Figure 4.1**).^{24,27} This agent had low relaxivity until exposed to β -galactosidase at which point the enzyme cleaved the pendant sugar causing an increase in q and relaxivity.

Results and Discussion

Design and Synthesis

The goal of this project was to design an MRI contrast agent to monitor MMP activity, specifically, an agent that is observable solely in the presence of MMPs. The design was based on that of the β -galactosidase responsive agent shown in **Figure 4.2**. In the proposed agent, an MMP peptide substrate would restrict water access to the metal center thus affecting q and relaxivity in a similar fashion to that of β -galactose. The

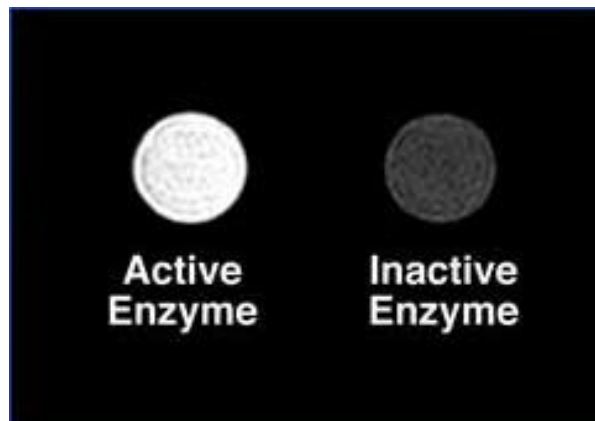
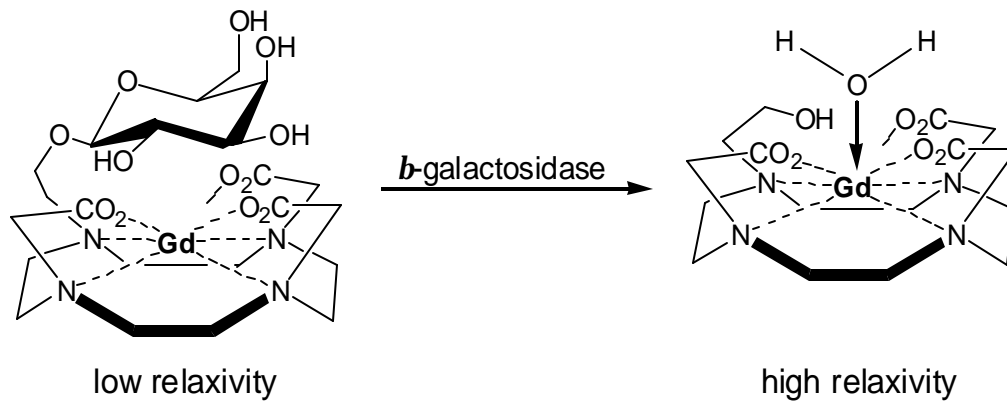


Figure 4.1: Structure of β -galactosidase responsive contrast agent (Top), and MRI of capillary tubes containing the contrast agent and either active or inactive enzyme (Bottom).^{24,27}

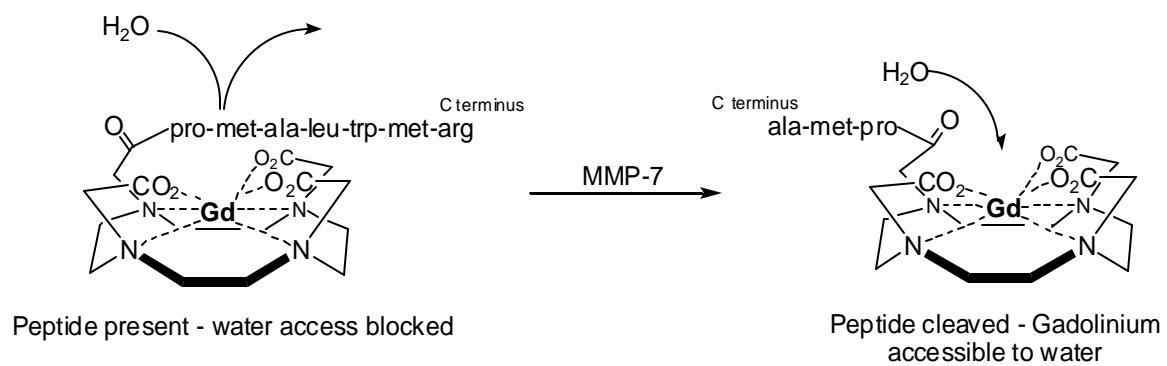


Figure 4.2: Structure of proposed MMP responsive MRI contrast agent.

peptide sequence pro-met-ala-leu-trp-met-arg is cleaved by MMP-7 between alanine and leucine.³² The peptide is even recognized when the fluorescent label dinitrophenyl (DNP) is covalently attached to the N-terminus.³² The ability to be recognized and cleaved with a pendant fluorophore suggests that if the label is replaced with a contrast agent, the peptide will still be recognized by MMP-7.

MMP-7 was chosen as a target for this project because of its correlation to cancer. It has been detected in breast and colon adenomas.^{33,34} The protease has been found in over 80% of spontaneous human colonic adenocarcinomas and is believed to contribute to early tumor development. MMP-7 is predominantly expressed in cancer cells and may play an important role in tumor metastasis.³⁵ Since MMP-7 plays a role in the development and metastasis of cancer, it is an excellent target candidate for activatable MRI contrast agents.

Upon cleavage of a peptide by an MMP, shorter peptide fragments are generated. When attached to a gadolinium(III) chelate, one of the peptides resulting from cleavage of the initial peptide may interact with the gadolinium(III) center. The difference in interaction between the gadolinium(III) ion and the pre- and post-cleavage peptides is the determining factor as to the viability of this attachment approach for peptides for activatable MRI contrast agents. To test the viability of the system, the contrast agents shown in **Figure 4.3** were synthesized and their q values were measured and compared. The contrast agents are models representative of before and after cleavage by MMP-7, and the length of the peptide was shortened from seven amino acids to examine the affect of the N-terminal amino acid on the efficacy of the agent.

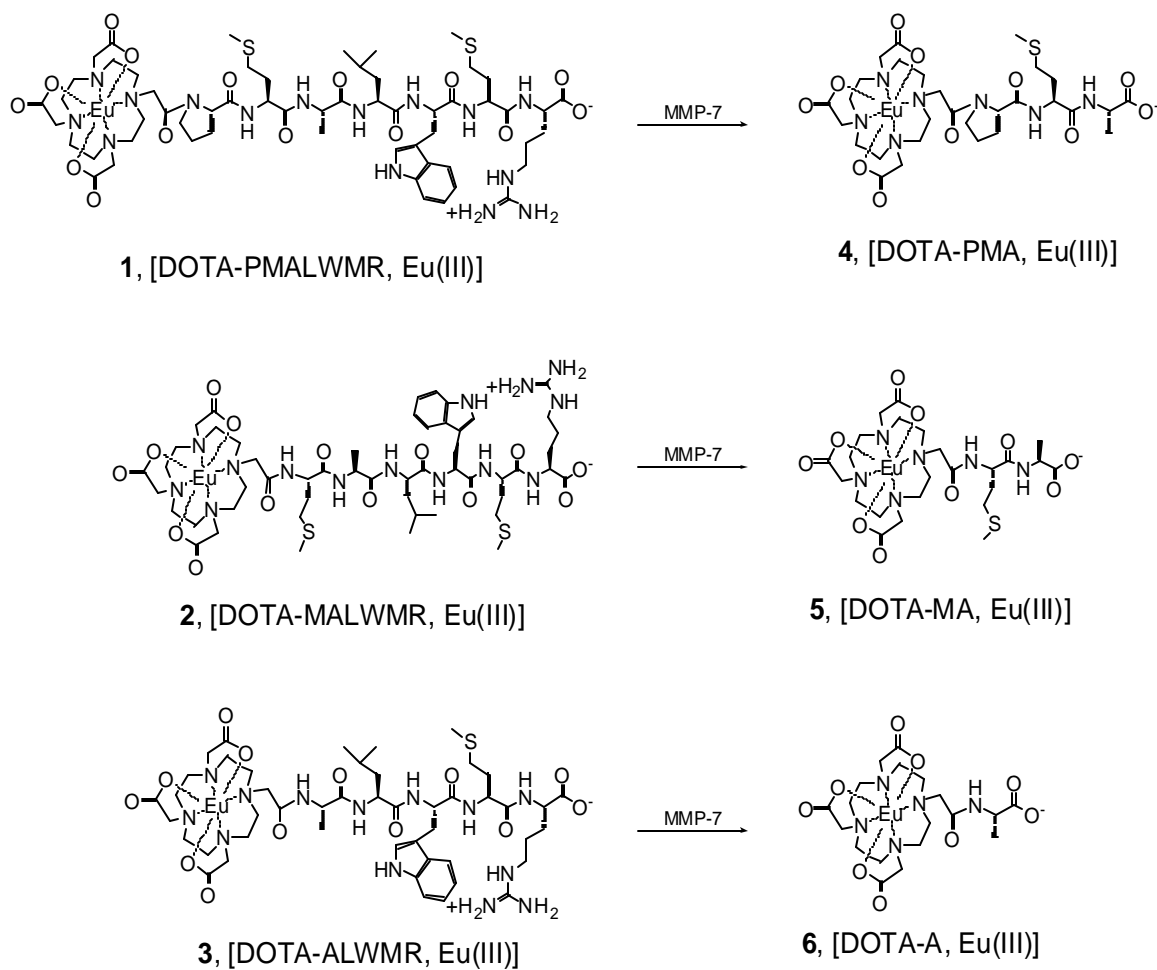


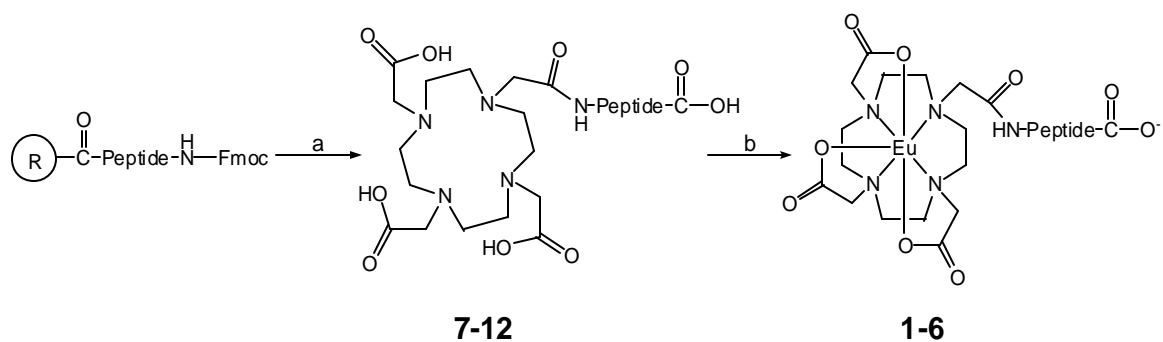
Figure 4.3: Model complexes representing MMP responsive contrast agent before and after exposure to MMP-7.

Although MRI contrast agents commonly contain gadolinium(III), europium(III) was used in these complexes because the two ions are extremely similar in size (atomic radii: gadolinium(III) = 1.08 Å, europium(III) = 1.09 Å); however, europium(III) has fluorescent properties that allow for the facile measurement of the number of coordinated water molecules in its inner coordination sphere (q).^{7,36}

Europium(III) complexes **1-6** and their corresponding free ligands, **7-12**, were synthesized as shown in **Scheme 4.1** using standard solid phase peptide synthesis techniques and the chelate 1,4,7,10-tetraazacyclododecane-1,4,7-tris(acetic acid-*tert*-butyl ester)-10-acetic acid [DOTA(*tris-t*-Bu ester)].³⁷ The conditions used to cleave the peptides from the resin simultaneously deprotected the *tert*-butyl esters on the chelate and the 2,2,4,6,7-pentamethyldihydrobenzofurane-5-sulfonyl (Pbf) protecting groups on the side chains of peptides to yield the free ligands **7-12**. The cleavage cocktail varied depending on the identity of the amino acids present, see experimental section for cocktails specific for each sequence. The corresponding europium(III) complexes, **1-6** were made using europium(III) hydroxide. Products were purified using either high performance liquid chromatography (Aquasil C-18 column (Keystone, PA)) or size exclusion chromatography (Sephedex G-25) and characterized by ¹H NMR spectroscopy, mass spectrometry, and elemental analysis.

Determination of q Values

Europium(III) ions are used in place of gadolinium(III) when measuring q values of lanthanide based contrast agents because gadolinium(III) complexes are not susceptible to OH or OD quenching because of their extremely large energy gaps between emissive and ground states. Europium(III) complexes, when excited from the



Scheme 4.1: Synthesis of europium(III) chelates modified with peptides: (a) i. Piperidine, DMF, ii. DOTA(tris-*t*-bu ester), HATU, DMF, DIPEA, iii. TFA cleavage cocktail; (b) $Eu(OH)_3$, H_2O , Δ .

7F_0 ground state to a higher state, undergo radiationless decay to a long-lived (>0.1 ms) 5D_0 state. Luminescence quenching can occur via a vibrational energy transfer involving high-energy vibrations of solvent molecules bound to the ligand (i.e. OH and OD) (**Figure 4.4**). Energy transfer to OD oscillators is about 200 times slower than for OH oscillators and is directly proportional to the number of oscillators associated with the lanthanide ion. Therefore, the number of water molecules can be calculated from the rate of luminescence decay in D_2O and H_2O and the empirically derived **Equation 4.1**.³⁸

$$\text{Equation 4.1: } q = 1.11(k_{H_2O} - k_{D_2O} - 0.235)$$

The q values for complexes **1-6** are shown in **Table 4.1** and range from 1.0 to 1.1 water molecules. A sample calculation is shown in **Figure 4.5**. No significant difference in the number of coordinated water molecules was observed between the six europium(III) complexes. Although no difference in q value was observed in the series of complexes **1-6**, a peptide controlled q modulating activatable contrast agent was still a desirable goal and inspired further investigation into the nature of the interaction between peptides and macrocyclic lanthanide chelates.

Aspartic Acid Model Complexes

To examine the effect of the N-terminal amino acid, a series of aspartic acid peptide-DOTA complexes were synthesized (**Figure 4.6**). The aspartic acid derivatives of DOTA, **16-18** and their corresponding free ligands **13-15** were synthesized as in **Scheme 4.1**. This series was chosen because aspartic acid contains two carboxylic acids between its C-terminus and its side chain. By spacing the aspartic acid residues from the

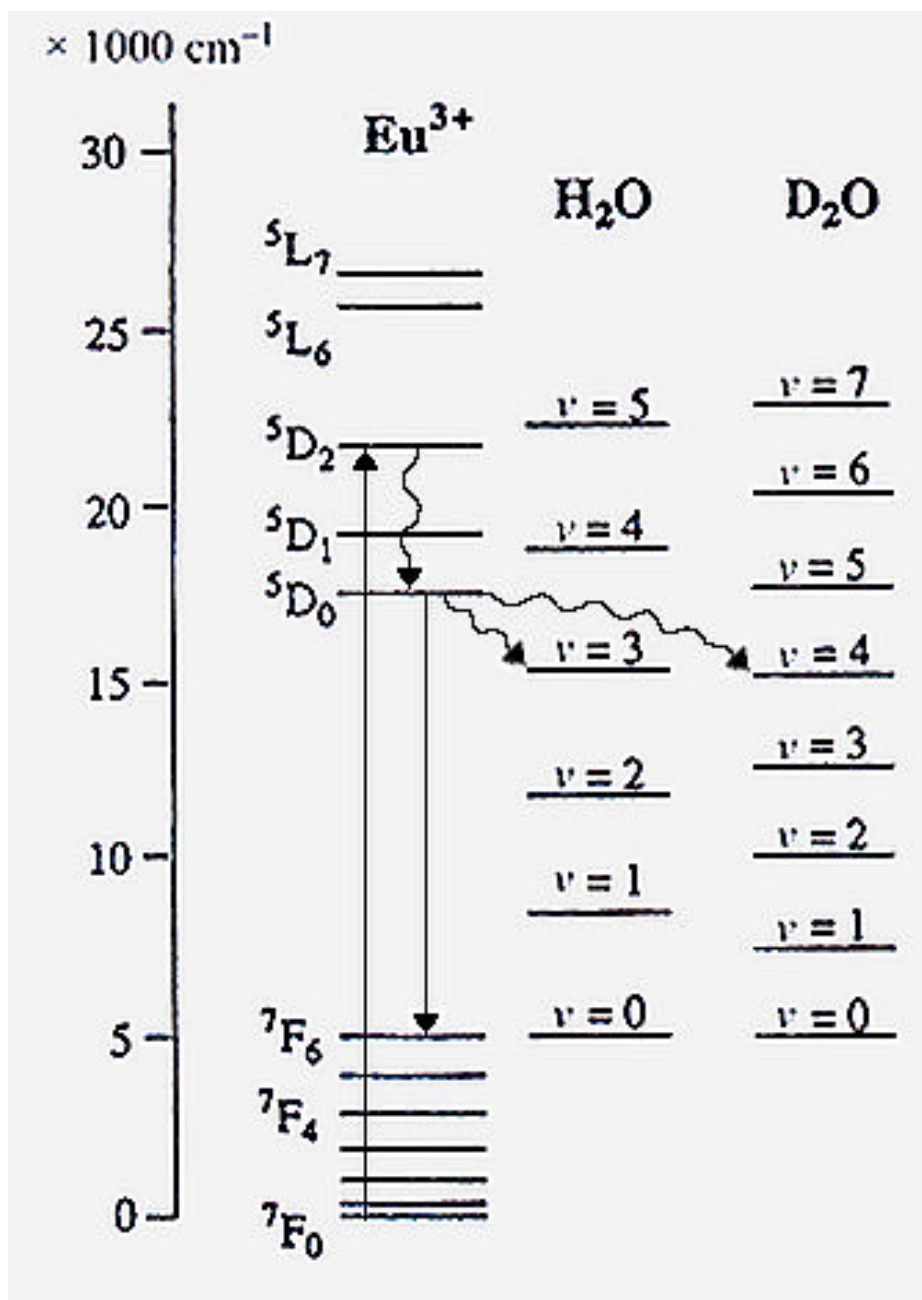


Figure 4.4: Vibrational quenching of europium(III) emissive state by water. An offset has been applied so that the lowest vibrational level of OH/OD is shown at the same energy as the highest level of the ground-state manifold of the europium(III) ion. No anharmonicity is assumed in the vibrational ladder, with $\nu_{\text{OH}} = 3405 \text{ cm}^{-1}$ and $\nu_{\text{OD}} = 2520 \text{ cm}^{-1}$. Figure modified from reference 7.

Eu Complex	$q (\pm 0.1)$
6	1.0
5	1.0
4	1.1
3	1.0
2	1.1
1	1.0

Table 4.1: Values of q measured for the peptide-contrast agent conjugates **1-6**.

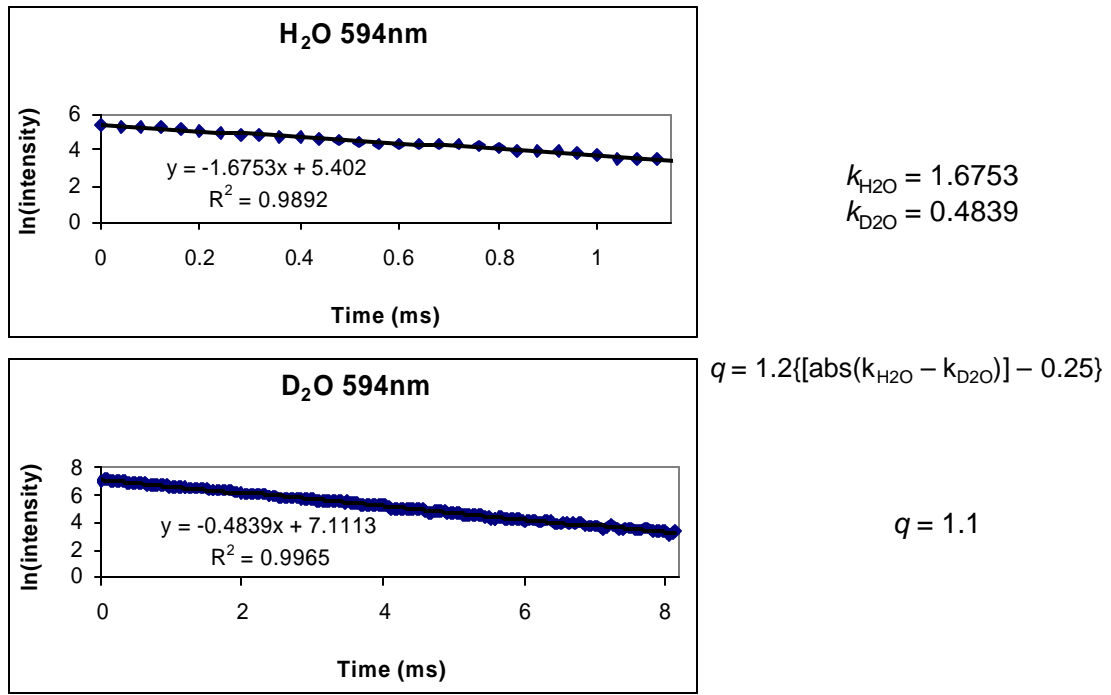
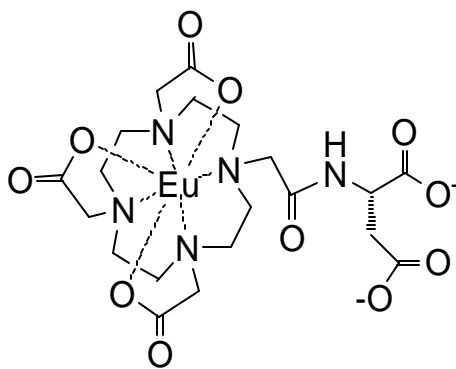
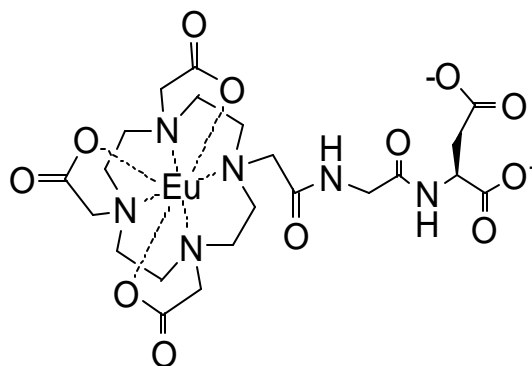


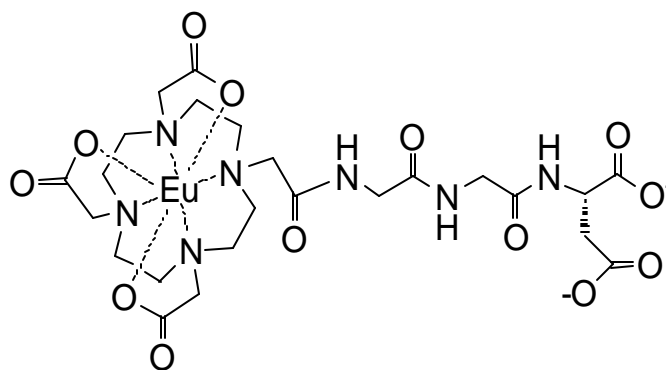
Figure 4.5: Sample fluorescence decay measurements used to determine values of q . Top graph: Fluorescence lifetime decay measurement in H₂O at 594 nm. Bottom graph: Fluorescence lifetime decay measurement in D₂O at 594 nm. Right: Sample calculation to determine value of q .



16



17



18

Figure 4.6: Chemical structures of a series of aspartic acid modified europium(III) chelates.

macrocycle with zero, one, or two glycine units, the ability of either of the carboxylic acids to bind the metal ion and alter q was tested. Carboxylic acids were chosen because they readily bind to lanthanides and aspartic acid is amenable to peptide synthesis.

After the synthesis of **16-18**, q values of the complexes were measured (**Table 4.2**). The q values were determined in an analogous fashion to those of **1-6** and the values ranged from 0.9-1.2 water molecules. This is not a dramatic range of q values and would most likely not affect relaxivity of the gadolinium(III) complexes.

Proposed Binding of Amide Carbonyl

The amino acid sequences contained in **1-6** and **16-18** varied greatly in their chemical properties which allowed for a comparison of the effect of these properties on q . Alanine is hydrophobic while aspartic acid is hydrophilic. Proline and glycine are special in that proline contains a secondary amine that restricts the conformation of the peptide while glycine has no side chain and is achiral. Methionine contains a thioether, tryptophan contains an indole, and aspartic acid contains an acetic acid; those groups may allow for coordination to the lanthanide ion. The series of aspartic acid containing complexes, **16-18**, was synthesized to explore the ability of the carboxylic acid side chain to coordinate to the metal ion.

The independence of q with respect to the identity of amino acid sequence leads to the hypothesis that the peptide is coordinated to the lanthanide ion via the amide oxygen of the N-terminal amino acid (**Figure 4.7**). This binding mechanism would account for the change in relaxivity seen in the β -galactosidase responsive agent, because there is no amide available for bonding to the lanthanide either before or after exposure to

Eu Complex	$q (\pm 0.1)$
16	0.9
17	1.0
18	1.2

Table 4.2: Values of q measured for the aspartic acid-contrast agent conjugates **16-18**.

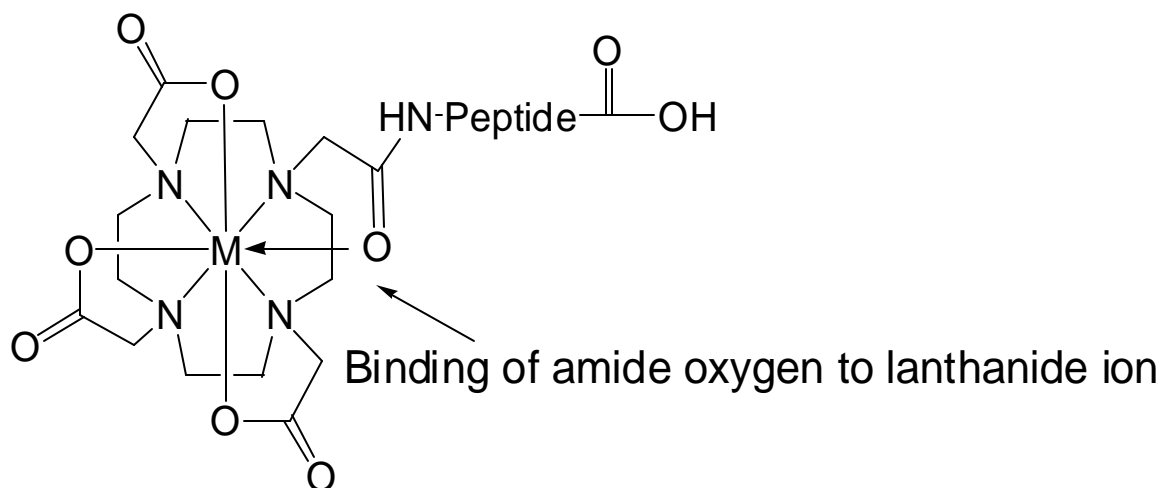


Figure 4.7: Proposed binding of peptide modified DOTA.

β -galactosidase. Many attempts towards crystallization of complexes **1-6** and **16-18** were attempted unsuccessfully.

Conclusion

A biologically responsive MRI contrast agent that utilizes the cleavage of short peptides would be an extremely useful diagnostic tool in experimental animals and humans. This chapter describes the synthesis and measurement of q values for a series of europium(III) derivatives of amino acid modified MRI contrast agents. A total of nine complexes with five different amino acids directly conjugated to DOTA through an amide bond were synthesized for this study. The five amino acids were alanine, methionine, proline, aspartic acid, and glycine. It was found that the identity of the amino acid directly attached to one of the carboxylic acids of DOTA through an amide bond did not influence the value of q nor does using amino acids with carboxylic acid side chain donors. Thus, attachment of a peptide at the N-terminus to the macrocyclic chelate DOTA via an amide bond does not affect the q value of the complex enough to be used as a q modulating activatable contrast agent.

Future Directions

While no changes in q were detected by varying the identity of the amino acids in this study, other means of conjugating the peptide to the macrocycle still hold promise. The preparation of a peptide based activatable gadolinium(III)-based MRI contrast agent would produce an extremely powerful tool for the study of in vivo enzyme activity. The synthesis of such an agent is the subject of ongoing work in the Meade laboratory.

A method that has the potential to be used as a peptide based, q modulating, activatable MRI contrast agent is shown in **Figure 4.8**. In this complex, a peptide is

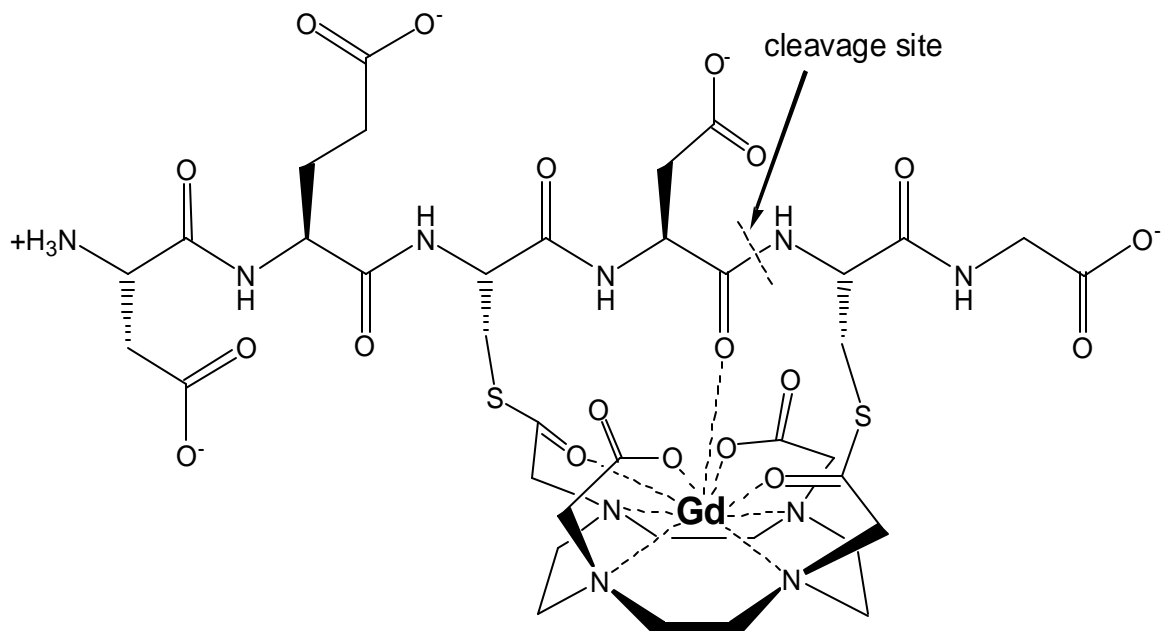


Figure 4.8: Structure of target bridged complex in which a caspase cleavable peptide is held over the free coordination sites of gadolinium(III). Upon exposure to caspase the peptide should be cleaved allowing for water access to the gadolinium(III) ion and a subsequent increase in q .

attached to DOTA in two positions through the side arms of the peptide. This conjugation method would force the peptide over the open coordination site of the lanthanide(III) ion which should produce a complex with a q value of zero. The peptide shown will theoretically be cleaved by class II caspases, which are proteases involved in apoptosis, between the modified cysteine and aspartic acid residues.^{39,40} Upon exposure to caspase the peptide should be cleaved allowing for water access to the gadolinium(III) ion and a subsequent increase in q .

Experimental Procedures

All reagents and solvents were the highest commercially available grades and used without further purification. 1,4,7,10-tetraazacyclododecane-1,4,7-tris(acetic acid-*tert*-butyl ester)-10-acetic acid [DOTA(*tris-t*-Bu ester)] and 1,4,7,10-tetraazacyclododecane-1,4,7,10-tetraacetic acid (DOTA) were purchased from Macrocylics (Dallas, TX). Resins with attached single amino acids and amino acids were purchased from Novabiochem (San Diego, CA). Resins with attached peptides used to synthesize compounds **2-7** were purchased from the Biopolymer Synthesis Facility of the Beckman Institute of the California Institute of Technology. All other starting materials were purchased from Aldrich (Milwaukee, WI). Europium(III) hydroxide was synthesized as in chapter 2.

¹H NMR spectra were obtained on a Varian mercury spectrometer at 300 MHz. Spectra were obtained in D₂O using a value of 4.80 ppm as an internal reference. Mass spectrometry samples were analyzed using electrospray ionization (ESI), quadrupole mass spectrometry or matrix-assisted laser desorption ionization time of flight (MALDI-TOF) mass spectrometry in the PPMAL – Protein/Peptide MicroAnalytical Laboratory,

California Institute of Technology, Beckman Institute or at the Northwestern University Chemistry Department Analytical Services Laboratory. Results reported for m/z are for $[M + H]^+$ or $[M - H]^+$. Fluorescence lifetime decay values were measured on a Hitachi F-4500 Fluorescence Spectrophotometer. High Performance Liquid Chromatography was performed on a Varian ProStar HPLC using an Aquasil C-18 reverse phase column (Keystone, PA).

Determination of q Values

Values for q were acquired using a Hitachi F-4500 Fluorescence Spectrophotometer in Time Scan mode using a Phosphorescence Life Time (Short) setting with an excitation wavelength of 394 nm and emission wavelengths of 594 nm and 614 nm. The average of 25 scans was taken at a 0.04 ms data interval. The natural log of the average intensity of the 25 scans was plotted against time and the slope was used as the decay rate. This was performed in water and D₂O. **Equation 4.1** was used to calculate q values at 614 nm and 594 nm which were averaged to give final q values (**Figure 4.5**).³⁸

General Europium(III) Complex Synthesis

To a solution of the free ligand in water (12-40 mM) was added Eu(OH)₃ (1.3 equiv.). The reaction mixture was heated to 80 °C and stirred for twelve hours. The reaction mixture was then cooled to ambient temperature and the pH of the reaction was brought to eleven with aqueous ammonium hydroxide. The mixture was then filtered through a 0.2 μm syringe filter, freeze dried, and purified using either HPLC or Sephadex G-25 size exclusion chromatography to yield a white solid.

Europium(III) *DOTA-(proline-methionine-alanine-leucine-tryptophan-methionine-arginine)* (**1**): Yield: 0.149 g (76.2%). ^1H NMR (D_2O): $\delta = -16.75, -15.94, -15.57, -14.19, -13.42, -12.96, -11.25, -10.70, -7.80, -6.86, -6.11, -5.68, -4.15, -2.96, -1.71, -0.01, 0.32, 0.44, 0.63, 1.20, 1.34, 1.65, 1.84, 2.02, 2.36, 3.16, 3.76, 6.62, 7.21, 7.56, 32.43, 33.00, 33.51, 34.56$; MS Calcd for $\text{C}_{58}\text{H}_{93}\text{EuN}_{14}\text{O}_{16}\text{S}_2$ $[\text{M} + \text{H}]^+$: Eu isotope pattern centered at 1458.6, found Eu isotope pattern centered at 1458.6; Anal. Calcd for $\text{C}_{58}\text{H}_{94}\text{EuN}_{14}\text{O}_{16}\text{S}_2 \cdot \text{C}_2\text{F}_3\text{O}_2 \cdot 5\text{H}_2\text{O}$: C, 43.11; H, 6.07; N, 12.78; S, 3.90. Found: C, 43.07; H, 5.78; N, 12.72; S, 4.05.

Europium(III) *DOTA-(methionine-alanine-leucine-tryptophan-methionine-arginine)* (**2**): Yield: 0.241 g (81.0%). ^1H NMR (D_2O): $\delta = -17.03, -16.12, -15.13, -14.55, -12.52, -11.83, -8.10, -7.52, -7.31, -5.82, -4.19, -3.22, -2.58, -0.17, 0.24, 0.29, 0.74, 0.97, 1.22, 1.39, 1.55, 1.72, 2.01, 2.21, 2.30, 2.40, 2.94, 3.06, 3.17, 3.36, 4.04, 4.28, 4.37, 6.07, 7.02, 7.15, 7.31, 7.57, 7.61, 7.63, 31.39, 32.12, 33.44$; MS Calcd for $\text{C}_{52}\text{H}_{81}\text{EuN}_{14}\text{O}_{14}\text{S}_2$ $[\text{M} - \text{H}]^-$: Eu isotope pattern centered at 1336.0, found Eu isotope pattern centered at 1336.1; Anal. Calcd for $\text{C}_{52}\text{H}_{82}\text{EuN}_{14}\text{O}_{14}\text{S}_2 \cdot \text{C}_2\text{F}_3\text{O}_2 \cdot 4\text{H}_2\text{O}$: C, 42.43; H, 5.94; N, 12.83. Found: C, 42.20; H, 5.87; N, 12.50.

Europium(III) *DOTA-(alanine-leucine-tryptophan-methionine-arginine)* (**3**): Yield: 0.105 g (75.7%). ^1H NMR (D_2O): $\delta = -17.19, -16.14, -15.07, -14.58, -14.42, -12.23, -11.99, -11.72, -11.22, -7.82, -7.67, -5.69, -3.98, -3.61, -2.78, -1.82, -0.46, 0.30, 0.59, 1.20, 1.53, 1.89, 2.75, 2.90, 3.89, 4.06, 6.27, 6.95, 7.34, 7.50, 7.59, 7.67, 30.24, 30.87, 31.37, 32.98$; MS Calcd for $\text{C}_{47}\text{H}_{72}\text{EuN}_{13}\text{O}_{13}\text{S}$ $[\text{M} + \text{H}]^+$: Eu isotope pattern centered at 1211.9, found Eu isotope pattern centered at 1212.1; Anal. Calcd for

$C_{47}H_{73}EuN_{13}O_{13}S \cdot C_2F_3O_2 \cdot 4H_2O$: C, 42.12; H, 5.84; N, 13.03. Found: C, 42.20; H, 5.87; N, 12.50.

Europium(III) DOTA-(proline-methionine-alanine) (4): Yield: 0.201 g (88.3%). 1H NMR (D_2O): $\delta = -16.66, -15.71, -15.45, -14.08, -13.46, -12.81, -11.17, -10.76, -7.96, -7.17, -6.16, -5.82, -3.96, -3.30, -1.99, -0.18, 0.17, 0.34, 0.61, 0.83, 1.01, 1.82, 2.13, 2.95, 3.22, 6.43, 31.50, 32.00, 32.60, 33.73$; MS Calcd for $C_{29}H_{46}EuN_7O_{11}S [M + H]^+$: Eu isotope pattern centered at 853.7, found Eu isotope pattern centered at 853.7; Anal. Calcd for $C_{29}H_{46}EuN_7O_{11}S \cdot 4H_2O$: C, 37.66; H, 5.89. Found: C, 37.35; H, 5.51.

Europium(III) DOTA-(methionine-alanine) (5): Yield: 0.145 g (90.4%). 1H NMR (D_2O): $\delta = -17.40, -16.27, -15.86, -15.38, -14.95, -12.76, -11.97, -8.15, -7.86, -5.83, -4.64, -3.61, -2.79, -2.39, -0.48, 0.13, 0.86, 1.27, 2.33, 30.98, 31.88, 33.62$; MS Calcd for $C_{24}H_{39}EuN_6O_{10}S [M - H]^-$: Eu isotope pattern centered at 754.7, found Eu isotope pattern centered at 754.9; Anal. Calcd for $C_{24}H_{39}EuN_6O_{10}S \cdot H_2O$: C, 37.26; H, 5.34. Found: C, 37.35; H, 5.51.

Europium(III) DOTA-(alanine) (6): Yield: 0.246 g (99.4%). 1H NMR (D_2O): $\delta = -16.82, -15.55, -15.08, -13.29, -15.52, -11.58, -10.47, -8.35, -7.25, -6.05, -5.54, -3.64, -1.99, -0.84, -0.65, 0.04, 30.69, 32.40, 32.79$; MS Calcd for $C_{19}H_{30}EuN_5O_9 [M - H]^-$: Eu isotope pattern centered at 625.6, found Eu isotope pattern centered at 625.7.

General Ligand Synthesis for Complexes 7-13

Polystyrene based Wang resin containing an Fmoc protected peptide (0.404 – 1.283 mmol) was swelled in dichloromethane and then washed four times with dimethylformamide (DMF). The resin was treated twice with a solution of 20% piperidine in DMF for ten minutes. The resin was washed four times with DMF. In a

separate vial DOTA(tris-*t*-bu ester) (2.2 equiv.), *O*-(7-azabenzotriazol-1-yl)-1,1,3,3-tetramethyluronium hexafluorophosphate (HATU), (2.1 equiv.), and DMF (5 mL) were combined and then diisopropylethylamine (DIPEA) (5.5 equiv.) was added. The resulting solution was added to the resin and sparged with argon for twelve hours. The resin was then drained and rinsed four times with DMF, four times with dichloromethane, four times with methanol, and then dried under vacuum. The appropriate cleavage cocktail was then added to the resin and the mixture was sparged with argon for one hour then drained. The resin was then rinsed with trifluoroacetic acid (TFA). The filtrate and rinse were combined and reduced in volume to ten milliliters under a stream of dry nitrogen. Forty milliliters of -20 °C methyl *tert*-butyl ether (MTBE) was added to precipitate a white solid. The solid was washed three times with cold MTBE, taken up in water and freeze dried to a white powder. The white powder was exposed to the TFA solution (2 – 7 hours) to deprotect the *tert*-butyl esters, washed with cold MTBE as above and freeze dried to yield a white powder.

DOTA-(proline-methionine-alanine-leucine-tryptophan-methionine-arginine) (**7**):

Cleavage cocktail: 81.5% trifluoroacetic acid (TFA), 5% thioanisole, 5% phenol, 5% water, 2.5% ethanedithiol, and 1% triisopropylsilane (TIS). Yield: 0.278 g (53.2%). ¹H NMR (D₂O): δ = 0.8-4.0 (m, 66H), 4.0-4.6 (m, 7H), 7.0-7.6 (m, 5H); MS Calcd for C₅₇H₉₁N₁₅O₁₅S₂ [M + H]⁺: 1290.6, found 1290.6.

DOTA-(methionine-alanine-leucine-tryptophan-methionine-arginine) (**8**):

Cleavage cocktail: 81.5% TFA, 5% thioanisole, 5% phenol, 5% water, 2.5% ethanedithiol, and 1% TIS. Yield: 0.496 g (73.6%). ¹H NMR (D₂O): δ = 0.8-4.0 (m,

58H), 4.0-4.7 (m, 6H), 7.0-7.6 (m, 5H); MS Calcd for $C_{52}H_{84}N_{14}O_{14}S_2$ $[M + H]^+$: 1193.6, found 1193.6.

DOTA-(alanine-leucine-tryptophan-methionine-arginine) (**9**): Cleavage cocktail: 81.5% TFA, 5% thioanisole, 5% phenol, 5% water, 2.5% ethanedithiol, and 1% TIS. Yield: 0.392 g (73.8%). 1H NMR (D_2O): δ = 0.8-4.0 (m, 51H), 4.0-4.7 (m, 5H), 7.0-7.6 (m, 5H); MS Calcd for $C_{47}H_{75}N_{13}O_{13}S$ $[M + H]^+$: 1062.5, found 1062.6.

DOTA-(proline-methionine-alanine) (**10**): Cleavage cocktail: 95% TFA, 2.5% water, and 2.5% TIS. Yield: 0.0496 g (83.3%). 1H NMR (D_2O): δ = 1.40 (d, J = 7.1 Hz, 3H), 1.9-2.0 (m, 4H), 2.07 (s, 3H), 2.2-2.3 (m, 2H), 2.57 (t, J = 7.4 Hz, 2H), 2.9-4.0 (m, 26H), 4.33 (q, J = 7.1 Hz, 1H), 4.45 (m, 2H); MS Calcd for $C_{29}H_{49}N_7O_{11}S$ $[M + H]^+$: 704.3, found 704.4.

DOTA-(methionine-alanine) (**11**): Cleavage cocktail: 95% TFA, 2.5% water, and 2.5% TIS. Yield: 0.232 g (70.1%). 1H NMR (D_2O): δ = 1.35 (d, J = 7.2 Hz, 3H), 1.9-2.0 (m, 2H), 2.02 (s, 3H), 2.53 (t, J = 7.4 Hz, 2H), 2.9-4.2 (m, 24H), 4.29 (q, J = 7.2 Hz, 1H), 4.38 (t, J = 6.9 Hz, 1H); MS Calcd for $C_{24}H_{42}N_6O_{10}S$ $[M + H]^+$: 607.3, found 607.2.

DOTA-(alanine) (**12**): Cleavage cocktail: 95% TFA, 2.5% water, and 2.5% TIS. Yield: 0.202 g (95.9%). 1H NMR (D_2O): δ = 1.33 (d, J = 7.2 Hz, 3H), 2.6-4.1 (m, 24H), 4.29 (q, J = 7.2 Hz, 1H); MS Calcd for $C_{19}H_{33}N_5O_9$ $[M + H]^+$: 476.2, found 476.2.

DOTA-(aspartic acid) (**13**): Cleavage cocktail: 95% TFA, 2.5% water, and 2.5% TIS. 1H NMR (D_2O): δ = 2.64 (d, J = 4.4 Hz, 2H), 2.6-3.8 (m, 24H), 4.74 (m, 1H).

DOTA-(glycine-aspartic acid) (**14**): Polystyrene based Wang resin containing an Fmoc protected aspartic acid residue with *tert*-butyl ester protected side chain (1.18 g,

0.708 mmol) was swelled in dichloromethane for 30 min then washed four times with peptide synthesis grade DMF. The resin was treated twice with a solution of 20% piperidine (20 mL) in DMF for ten minutes. The resin was washed four times with DMF. In a separate vial, Fmoc protected glycine (1.05 g, 3.54 mmol), HATU (1.28 g, 3.36 mmol), and DMF (5 mL) were combined and then DIPEA (1.17 mL, 6.72 mmol) was added. The resulting solution was added to the resin and allowed to react under argon for twelve hours. The resin was drained and rinsed four times with DMF. The resin was treated with piperidine and washed with DMF as described above. In a separate vial, [DOTA(tris-*t*-Bu ester)] (1.00 g, 1.77 mmol), HATU (0.605 g, 1.59 mmol), and DMF (5 mL) were combined and then DIPEA (0.617 mL, 3.54 mmol) was added. The resulting solution was added to the resin and allowed to react under argon for twelve hours. The solvent was removed and the resin was washed four times with DMF, four times with dichloromethane, four times with methanol, and then dried under vacuum. A 30 mL solution of 95% TFA, 2.5% TIS, and 2.5% water was then added to the resin and mixed for one hour then drained. The resin was then rinsed with 15 mL TFA. The filtrate and rinse were combined and reduced in volume to ten milliliters under a stream of dry nitrogen. Forty milliliters of -20 °C MTBE was added to precipitate a white solid. The solid was washed three times with cold MTBE, taken up in water and freeze dried to a white powder. The white powder was exposed to the TFA solution for five hours, washed with cold MTBE as above, and freeze dried to yield a white solid. ¹H NMR (D₂O): δ = 2.70 (d, J = 5.6 Hz, 2H), 2.6-3.8 (m, 24H), 3.75 (s, 2H), 4.54 (m, 1H).

DOTA-(glycine-glycine-aspartic acid) (15): Polystyrene based Wang resin containing an Fmoc protected aspartic acid residue with tert-butyl ester protected side

chain (1.18 g, 0.708 mmol) was swelled in dichloromethane for 30 min then washed four times with peptide synthesis grade DMF. The resin was treated twice with a solution of 20% piperidine (20 mL) in DMF for ten minutes. The resin was washed four times with DMF. In a separate vial, Fmoc protected glycine (1.05 g, 3.54 mmol), HATU (1.28 g, 3.36 mmol), and DMF (5 mL) were combined and then DIPEA (1.17 mL, 6.72 mmol) was added. The resulting solution was added to the resin and allowed to react under argon for twelve hours. The resin was drained and rinsed four times with DMF. The resin was treated with piperidine and washed with DMF as described above. In a separate vial, Fmoc protected glycine (1.05 g, 3.54 mmol), HATU (1.28 g, 3.36 mmol), and DMF (5 mL) were combined and then DIPEA (1.17 mL, 6.72 mmol) was added. The resulting solution was added to the resin and allowed to react under argon for twelve hours. The resin was drained and rinsed four times with DMF. The resin was treated with piperidine and washed with DMF as described above. In a separate vial, [DOTA(tris-*t*-Bu ester)] (0.70 g, 1.2 mmol), HATU (0.45 g, 1.2 mmol), and DMF (5 mL) were combined and then DIPEA (0.42 mL, 2.4 mmol) was added. The resulting solution was added to the resin and allowed to react under argon for twelve hours. The solvent was removed and the resin was washed four times with DMF, four times with dichloromethane, four times with methanol, and then dried under vacuum. A 30 mL solution of 95% TFA, 2.5% TIS, and 2.5% water was then added to the resin and mixed for one hour then drained. The resin was then rinsed with 15 mL TFA. The filtrate and rinse were combined and reduced in volume to ten milliliters under a stream of dry nitrogen. Forty milliliters of -20 °C MTBE was added to precipitate a white solid. The solid was washed three times with cold MTBE, taken up in water and freeze dried to a

white powder. The white powder was exposed to the TFA solution for six hours, washed with cold MTBE as above, and freeze dried to yield a white solid. ^1H NMR (D_2O): $\delta = 2.84$ (d, $J = 6.0$ Hz, 2H), 2.6-3.8 (m, 24H), 3.87 (s, 4H), 4.68 (m, 1H).

Europium(III) DOTA-(aspartic acid) (16): Yield: 0.339 g (71.5%). MS Calcd for $\text{C}_{20}\text{H}_{30}\text{EuN}_5\text{O}_{11}$ [M - H] $^-$: Eu isotope pattern centered at 667.4, found Eu isotope pattern centered at 667.8; Anal. Calcd for $\text{C}_{20}\text{H}_{30}\text{EuN}_5\text{O}_{11}\cdot 18\text{H}_2\text{O}$: C, 31.70; H, 5.44. Found: C, 31.38; H, 5.19.

Europium(III) DOTA-(glycine-aspartic acid) (17): Yield: 0.214 g (41.7%). MS Calcd for $\text{C}_{22}\text{H}_{33}\text{EuN}_6\text{O}_{12}$ [M - H] $^-$: Eu isotope pattern centered at 724.5, found Eu isotope pattern centered at 724.6; Anal. Calcd for $\text{C}_{22}\text{H}_{33}\text{EuN}_6\text{O}_{12}\cdot 14\text{H}_2\text{O}$: C, 32.64; H, 5.27. Found: C, 32.61; H, 5.29.

Europium(III) DOTA-(glycine-glycine-aspartic acid) (18): Yield: 0.273 g (49.3%). MS Calcd for $\text{C}_{24}\text{H}_{36}\text{EuN}_7\text{O}_{13}$ [M - H] $^-$: Eu isotope pattern centered at 781.5, found Eu isotope pattern centered at 781.7; Anal. Calcd for $\text{C}_{24}\text{H}_{36}\text{EuN}_7\text{O}_{13}\cdot 3\text{H}_2\text{O}$: C, 34.46; H, 5.06; N, 11.72. Found: C, 34.12; H, 5.09; N, 11.87.

References

- (1) J. Kos and T. T. Lah, *Oncol. Rep.* **1998**, *5*, 1349-1361.
- (2) K. Brew, D. Dinakarandian, and H. Nagase, *Biochim. Biophys. Acta* **2000**, *1477*, 267-283.
- (3) M. Whittaker, C. D. Floyd, P. Brown, and A. J. H. Gearing, *Chem. Rev.* **1999**, *99*, 2735-2776.
- (4) J. Mai, D. M. Waisman, and B. F. Sloane, *Biochim. Biophys. Acta* **2000**, *1477*, 215-230.
- (5) J. E. Koblinski, M. Ahram, and B. F. Sloane, *Clin. Chim. Acta* **2000**, *291*, 113-135.
- (6) J. L. Lauer-Fields and G. B. Fields, *Expert Opin. Ther. Pat.* **2000**, *10*, 1873-1884.

- (7) A. E. Merbach and E. Toth, *The Chemistry of Contrast Agents in Medical Magnetic Resonance Imaging*; John Wiley & Sons, Ltd., New York, 2001.
- (8) T. D. Mody and J. L. Sessler, *Perspect. Supramol. Chem.* **1999**, *4*, 245-294.
- (9) S. Aime, M. Botta, M. Fasano, and E. Terreno, *Spectrochimica Acta* **1993**, *49A*, 1315-1322.
- (10) S. Aime, G. Digilio, M. Fasano, S. Paoletti, A. Arnelli, and P. Ascenzi, *Biophys. J.* **1999**, *76*, 2735-2743.
- (11) S. Aime, S. G. Crich, M. Botta, G. Giovenzana, G. Palmisano, and M. Sisti, *Chem. Commun.* **1999**, 1577-1578.
- (12) S. Aime, M. Botta, E. Gianolio, and E. Terreno, *Angew. Chem. Int. Ed.* **2000**, *39*, 747-750.
- (13) S. Aime, D. Delli Castelli, F. Fedeli, and E. Terreno, *J. Am. Chem. Soc.* **2002**, *124*, 9364-9365.
- (14) S. Aime, A. Barge, D. D. Castelli, F. Fedeli, A. Mortillaro, F. U. Nielsen, and E. Terreno, *Magn. Reson. Med.* **2002**, *47*, 639-648.
- (15) P. L. Anelli, I. Bertini, M. Fragai, L. Lattuada, C. Luchinat, and G. Parigi, *Eur. J. Inorg. Chem.* **2000**, 625-630.
- (16) A. Bogdanov, Jr., L. Matuszewski, C. Bremer, A. Petrovsky, and R. Weissleder, *Molecular Imaging* **2002**, *1*, 16-23.
- (17) V. Comblin, D. Gilsoul, M. Hermann, V. Humblet, V. Jacques, M. Mesbahi, C. Sauvage, and J. F. Desreux, *Coord. Chem. Rev.* **1999**, *185-186*, 451-470.
- (18) K. Hanaoka, K. Kikuchi, Y. Urano, and T. Nagano, *J. Chem. Soc., Perkin Trans. 2* **2001**, 1840-1843.
- (19) K. Hanaoka, K. Kikuchi, Y. Urano, M. Narazaki, T. Yokawa, S. Sakamoto, K. Yamaguchi, and T. Nagano, *Chem. Biol.* **2002**, *9*, 1027-1032.
- (20) R. Hovland, C. Glogard, A. J. Aasen, and J. Klaveness, *J. Chem. Soc., Perkin Trans. 2* **2001**, 929-933.
- (21) L. Josephson, J. M. Perez, and R. Weissleder, *Angew. Chem. Int. Ed.* **2001**, *40*, 3204-3206.
- (22) W.-h. Li, S. E. Fraser, and T. J. Meade, *J. Am. Chem. Soc.* **1999**, *121*, 1413-1414.
- (23) W.-h. Li, G. Parigi, M. Fragai, C. Luchinat, and T. J. Meade, *Inorg. Chem.* **2002**, *41*, 4018-4024.

- (24) A. Y. Louie, M. M. Huber, E. T. Ahrens, U. Rothbacher, R. Moats, R. E. Jacobs, S. E. Fraser, and T. J. Meade, *Nat. Biotechnol.* **2000**, *18*, 321-325.
- (25) M. Mikawa, N. Miwa, M. Brautigam, T. Akaike, and A. Maruyama, *Chem. Lett.* **1998**, 693-694.
- (26) M. Mikawa, N. Miwa, T. Akaike, and A. Maruyama, *Proceedings of the International Symposium on Controlled Release of Bioactive Materials* **1999**, *26th*, 1158-1159.
- (27) R. A. Moats, S. E. Fraser, and T. J. Meade, *Angew. Chem., Int. Ed. Engl.* **1997**, *36*, 726-728.
- (28) A. L. Nivorozhkin, A. F. Kolodziej, P. Caravan, M. T. Greenfield, R. B. Lauffer, and T. J. McMurry, *Angew. Chem. Int. Ed.* **2001**, *40*, 2903-2906.
- (29) J. M. Perez, T. O'Loughin, F. J. Simeone, R. Weissleder, and L. Josephson, *J. Am. Chem. Soc.* **2002**, *124*, 2856-2857.
- (30) S. Zhang, K. Wu, and A. D. Sherry, *Angew. Chem. Int. Ed.* **1999**, *38*, 3192-3194.
- (31) M. Zhao, L. Josephson, Y. Tang, and R. Weissleder, *Angew. Chem. Int. Ed.* **2003**, *42*, 1375-1378.
- (32) S. Netzel-Arnett, Q. X. Sang, W. G. I. Moore, M. Navre, H. Birkedal-Hansen, and H. E. Van Wart, *Biochemistry* **1993**, *32*, 6427-6432.
- (33) C. L. Wilson, K. J. Heppner, P. A. Labosky, B. L. M. Hogan, and L. M. Matrisian, *Proc. Natl. Acad. Sci. U. S. A.* **1997**, *94*, 1402-1407.
- (34) J. Cha and D. S. Auld, *Biochemistry* **1997**, *36*, 16019-16024.
- (35) M. Honda, M. Mori, H. Ueo, K. Sugimachi, and T. Akiyoshi, *Gut* **1996**, *39*, 444-448.
- (36) F. A. Cotton and G. Wilkinson, *Advanced Inorganic Chemistry*; Wiley, New York, 1988.
- (37) S. A. Kates and F. Albericio, *Solid-Phase Synthesis: A Practical Guide*; Marcel Dekker, Inc., New York, 2000.
- (38) R. M. Supkowski and W. D. Horrocks, Jr., *Inorg. Chim. Acta* **2002**, *340*, 44-48.
- (39) N. A. Thornberry, T. A. Rano, E. P. Peterson, D. M. Rasper, T. Timkey, M. Garcia-Calvo, V. M. Houtzager, P. A. Nordstrom, S. Roy, J. P. Vaillancourt, K. T. Chapman, and D. W. Nicholson, *J. Biol. Chem.* **1997**, *272*, 17907-17911.
- (40) H. Blanchard, M. Donepudi, M. Tschopp, L. Kodandapani, J. C. Wu, and M. G. Grutter, *J. Mol. Biol.* **2000**, *302*, 9-16.